PALEOENVIRONMENTAL AND PALEOCLIMATIC RECONSTRUCTION OF A PLEISTOCENE CATENA USING PALEOPEDOLOGY AND GEOCHEMISTRY OF LAKE MARGIN PALEO-VERTISOLS, OLDUVAI GORGE, TANZANIA

by

EMILY JANE BEVERLY

A Thesis submitted to the

Graduate School-New Brunswick

Rutgers, The State University of New Jersey

in partial fulfillment of the requirements

for the degree of

Master of Science

Graduate Program in Geological Sciences

written under the direction of

Dr. Gail M. Ashley

and approved by

_____

_____

_____

New Brunswick, New Jersey

[January 2012]

ABSTRACT OF THE THESIS

Paleoenvironmental and paleoclimatic reconstruction of a Pleistocene catena using paleopedology and geochemistry of lake margin paleo-Vertisols, Olduvai Gorge, Tanzania

by EMILY JANE BEVERLY

Thesis Director:
Dr. Gail M. Ashley

Olduvai Gorge, Tanzania (3°S) contains a rich record of Pleistocene paleoclimates and paleoenvironments, as well as an abundance of paleontological and archaeological data. The 2.2 Ma of volcaniclastic infill can be divided into time-slices using dated tuffs. Until ~1.75 Ma the sediments were deposited in a semi-arid, closed rift basin that contained a shallow saline-alkaline lake that fluctuated periodically with climate, depositing sediment on the lake margin. Four trenches that range in thickness from 2 to 2.5 m in a ~1 km transect of the lake margin flat were described and sampled. This ~20 ka time-slice between Ng'eju Tuff and Tuff IF (~1.785 Ma) contains both stacked and cumulative paleosols that are interpreted as a heterogeneous paleocatena. Closer to the lake, these paleosols are thinner, vertically stacked, and separated by thin tuffs or tufa. Further from the lake margin, there is additional volcaniclastic input, and the paleosols are thicker and cumulative. Macroscale and micromorphological features identify these clay-rich paleosols as paleo-Vertisols. Abundant pedogenic slickensides and a variety of ped shapes were observed in the field as well as micro-ped structures and

stress cutans in thin section. Although weakly developed, these paleo-Vertisols also have distinct horizons defined by soil color changes, differing ped shapes, and bulk geochemistry.

Eighty samples from the paleosols and parent materials were analyzed for bulk geochemistry of major, rare, and trace elements. Geochemical proxies reveal a climosequence not definitively identifiable in the field or in the micromorphology. Molecular weathering ratios show increased weathering, and mass-balance calculations indicate greater translocations (positive and negative) through time. It is likely that lower soil moisture due to a drier climate created better-drained conditions allowing for increased pedogenesis. Mg oxides and zeolites precipitating in rhizoliths are further evidence for changing redox conditions and water chemistry, likely due to increased aridity. The drying trend in this climosequence is consistent with faunal, stable isotope, and lithostratigraphic records within Olduvai Gorge and with marine dust records from northern Africa. The paleocatena identified within this time-slice also provides additional paleoenvironmental and paleoclimatic data, coinciding with the first hominin migrations out of Africa at ~1.8 Ma.

ACKOWLEDGMENTS

The successful completion of this thesis would not have been possible without the help of numerous people. I particularly would like to thank my advisor Dr. Gail Ashley, who made all this possible, with her infinite energy, knowledge, and advice. Thank you also to my committee members, Dr. Craig Feibel and especially Dr. Steve Driese who went above and beyond the requirements of a committee member throughout this process. I would like to thank all the field assistants who worked with me in Tanzania, specifically Titus Ombori and Bonamax Mbasa. I would also like to thank Dr. Jim Wright and Richard Mortlock, who taught my first graduate class and helped me run my stable isotope samples. Thank you to the entire faculty who taught me so much over the past two years, and to the staff who keep everything running so smoothly. I would also like to thank all of the graduate students especially those exiled to the Doolittle Building for putting up with all my jokes. I would specifically like to thank Catherine Beck, Jon LaCarruba, and Linda Martin for their support, edits, and comedic relief. Thank you to my parents Jane and Rex Beverly who offered continuous support from afar for their daughter's desire to study dirt and rocks. I could not have done it without any of them.

I would like to acknowledge support from the Evolving Earth Foundation, Rutgers University Department of Earth and Planetary Sciences, The Geological Society of America Graduate Student Research Grant, and the Olduvai Paleoanthropology and Paleoecology Project (TOPPP). The data presented here were collected under permits from the Tanzania Commission for Science and Technology and the Tanzanian Antiquities Department to TOPPP, PIs M. Domínguez-Rodrigo, A.Z.P. Mabulla, H.T. Bunn and E. Baquedano.

TABLE OF CONTENTS

LISTS OF TABLES

LIST OF FIGURES

1. INTRODUCTION

Paleosols are increasingly being recognized as an important aspect of terrestrial environments (NRC, 2001; NSF Advisory Committee, 2009; SEPM-NSF, 2010). Valuable paleoenvironmental and paleoclimatic information recorded in soils and paleosols is often overlooked because soils do not have the same temporal resolution as marine proxies. Soils form at the surface where they directly interact with organisms, atmosphere, and climate. These soils have the potential to record much more accurate paleoenvironmental and paleoclimatic information than marine proxies far removed from the study site. Recent research has combined qualitative descriptions using modern soils as analogs and quantitative proxies using clay mineralogy and whole rock and isotopic geochemistry (Sheldon and Tabor, 2009, and references therein). Here new data are presented from paleosols identified along the margin of paleo Lake Olduvai, Tanzania. Previous research has demonstrated that the Pleistocene sediments of Olduvai Gorge contain a rich record of the paleolandscape as well as an abundance of paleontological and archaeological data (Leakey, 1971; Hay, 1990; Dominguez-Rodrigo et al., 2007).

Olduvai Gorge is located on the western margin of the East African Rift where incision during the Late Pleistocene exposed 100 m of basin infill (Hay, 1976). The 2.2 Ma of volcanic and fluvio-lacustrine infill can be divided into time-slices using dated tuffs (Gromme and Hay, 1971; Berggren et al., 1995; Tamrat et al., 1995; McHenry, 2004, 2005), and have been used to reconstruct the paleoenvironment and paleoclimate of the basin (e.g. Ashley and Driese, 2000; Hay and Kyser, 2001; Deocampo et al., 2002; Sikes and Ashley, 2007; Ashley et al., 2009, 2010a, b, c; Barboni et al., 2010). The sediments were deposited in semi-arid, closed rift basin containing a shallow saline-

alkaline lake which expanded and contracted with Milankovitch cycles until ~1.75 Ma (Kappelman, 1986; Hay and Kyser, 2001; Ashley and Hay, 2002; Ashley, 2007). Olduvai Gorge is well known for the hominins and associated cultural material and an abundance of faunal remains. Hay (1976) and Leakey (1971) mention numerous pedogenically modified beds found throughout the Olduvai stratigraphy, but few paleosols within the 100 m thick sediment package have been studied in high-resolution.

The sediments are well exposed and beds can be physically traced, making Olduvai Gorge an ideal locality to study paleosols in a paleolandscape context. Previous research on paleosols has focused on the calcium carbonate rich Aridisols forming on the well-drained fluvial environment west of paleo Lake Olduvai (Sikes and Ashley, 2007) and red Andisols forming on the volcaniclastic alluvial fan on the eastern margin of the basin (Ashley and Driese, 2000). This research focuses on a ~20 ka time-slice in uppermost Bed I (~1.8 Ma) where the lake periodically flooded and deposited sediment that was subsequently pedogenically modified. The time-slice is defined by Ng'eju Tuff (base) and Tuff IF (top) and contains both stacked and cumulative paleosols.

Olduvai Gorge has also been extremely productive site for hominins and their associated cultural remains and an abundance of faunal remains. Most of the archaeological sites are located on the eastern lake margin in the "junction" between the Main and Side Gorges (Leakey, 1971; Hay, 1976) where no high-resolution analysis of paleosols has been conducted. In upper Bed I, the focus of this research, two species of hominin were living near paleo Lake Olduvai: 1) *Homo habilis*, an ancestor of modern *Homo sapiens*, and 2) the now extinct *Australopithecus bosei* (Leakey, 1971; Dominguez-Rodrigo et al., 2007). Upper Bed I also coincides with the time of first

migrations of genus *Homo* out of Africa at ~1.8 Ma. The earliest evidence for genus *Homo* outside of Africa appears at the Dmanisi site in Georgia between 1.85 and 1.77 Ma (Gabunia et al., 2000; Lordkipanidze et al., 2007). High-resolution study of this Olduvai time-slice from 1.79 to 1.81 Ma between Tuff IF and Ng'eju Tuff where genus *Homo* was living may lead to a better understanding of the reasons for this migration. The objectives of this study are to 1) use field description, micromorphology of paleosols, and bulk geochemistry (specifically constitutive mass-balance calculations) to characterize the soil-forming processes and reconstruct the paleoenvironment and paleoclimate, 2) integrate the paleocatena forming on the eastern lake margin within the overall paleolandscape of the Olduvai Basin, and 3) use stacked paleosols to interpret climate change over a ~20 ka time-slice coinciding with the first migrations out of Africa at ~1.8 Ma.

2. BACKGROUND

Geologic Setting

Olduvai Gorge is located on the western margin of the East Africa (Gregory) Rift in northern Tanzania (Fig. 2.1A; Hay, 1976). The Olduvai basin was infilled with volcanics and volcaniclastics beginning at ~ 2.2 Ma, and a playa lake formed in the center of the basin (Hay, 1976; Hay and Kyser, 2001). A pulse of rift-related (extensional) tectonics in the Late Pleistocene tilted the basin eastward, draining the lake and creating a fluvial system that dissected the Serengeti Plain and exposed a 100 m thick sediment package (Hay, 1976). The Pleistocene deposits are divided into six units, from Bed I to the Ndutu Beds, and are composed of fluvio-lacustrine sediments interbedded with tuffs (Fig. 2.2; Hay, 1976; Ashley and Hay, 2002). The basin-wide stratigraphy of Olduvai Gorge has been previously determined using paleomagnetic studies and field mapping (Gromme and Hay, 1971; Tamrat et al., 1995; Hay, 1976) as well as mineral chemistry and $^{40}Ar/^{39}Ar$ dating (McHenry, 2004, 2005; Mollel et al., 2009).

Paleo Lake Olduvai was the major feature on the landscape between 1.92 and 1.7 Ma and is recorded in Beds I and lowermost Bed II (Hay, 1976; Hay and Kyser, 2001). The hydrologically closed system covered an area of approximately 3500 km^2, draining into paleo Lake Olduvai (Ashley and Hay, 2002). Clay mineralogical analysis determined that this was a non-potable saline-alkaline lake (Hay and Kyser, 2001; Hover and Ashley, 2003; Deocampo et al., 2009). The lake was bounded to the south and east by the Ngorongoro Volcanic Complex (NVC), a group of at least seven volcanoes within the East African Rift, and bounded to the north and west by Precambrian igneous and

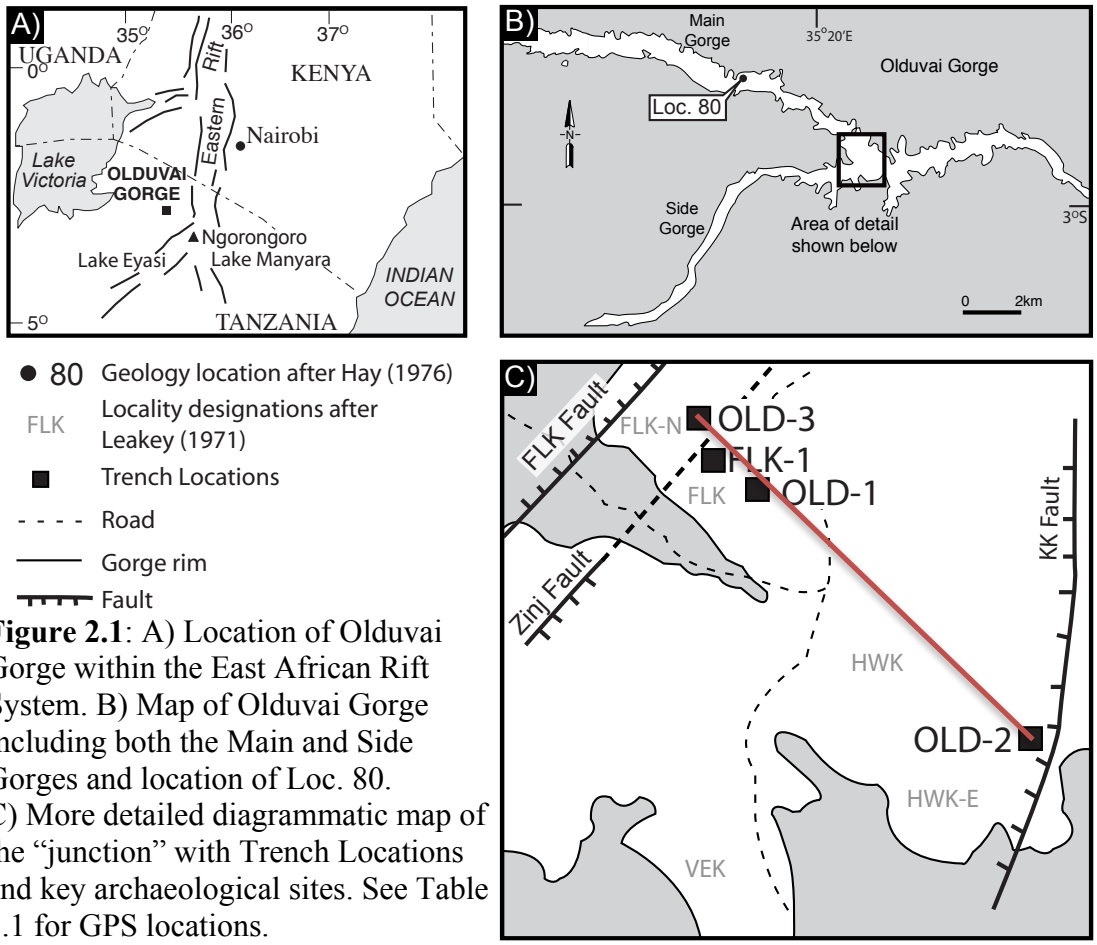

Figure 2.1: A) Location of Olduvai Gorge within the East African Rift System. B) Map of Olduvai Gorge including both the Main and Side Gorges and location of Loc. 80. C) More detailed diagrammatic map of the "junction" with Trench Locations and key archaeological sites. See Table 3.1 for GPS locations.

metamorphic basement. The shallow lake basin created large fluctuations in both depth and surface area with only minor changes in precipitation (Hay, 1976).

Tephrostratigraphic Correlation

The seven volcanic sources in the nearby NVC deposited an abundance of tuffs in the Olduvai basin allowing for accurate time constraints and enabling high-resolution reconstructions of the environment (e.g. Ashley and Driese, 2000; Hay and Kyser, 2001; Deocampo et al., 2002; Sikes and Ashley, 2007; Ashley et al., 2009, 2010a, b, c; Barboni et al., 2010). This research is focused on a 2 to 2.5 m thick time-slice of uppermost Bed I between the Ng'eju Tuff and Tuff IF, the boundary that divides Beds I and II (Fig. 2.2).

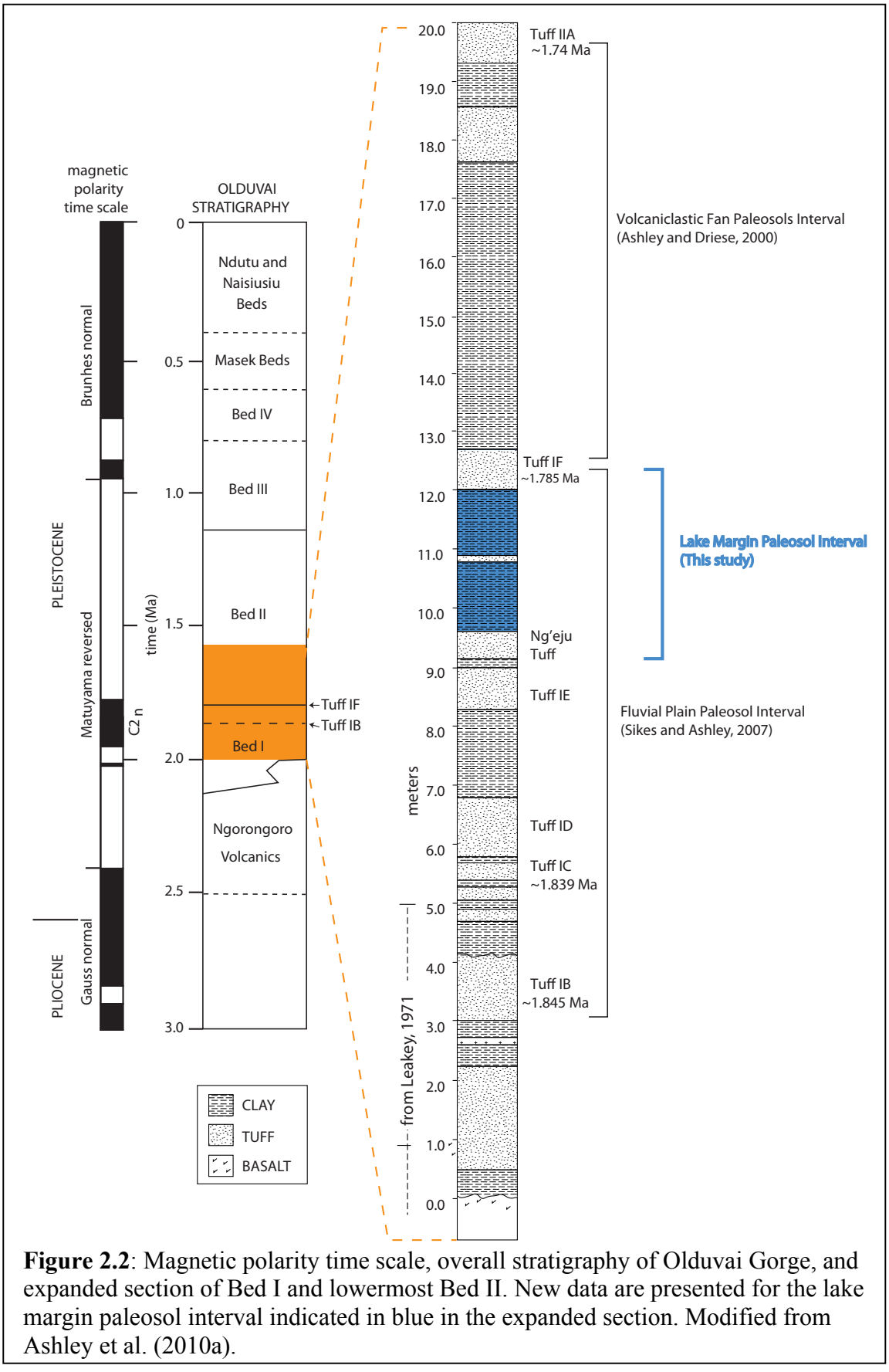

Figure 2.2: Magnetic polarity time scale, overall stratigraphy of Olduvai Gorge, and expanded section of Bed I and lowermost Bed II. New data are presented for the lake margin paleosol interval indicated in blue in the expanded section. Modified from Ashley et al. (2010a).

Extensive alteration (divitrification) of volcanic glass in the Olduvai tuffs has prevented the use of glass geochemistry in identifying and correlating tuffs throughout the basin (Hay, 1976). A multi-component approach using phenocryst composition successfully demonstrated that Tuff IF and Ng'eju Tuff are laterally extensive and distinct "marker" beds throughout Olduvai Gorge (McHenry, 2004, 2005, 2010).

Whereas the Ng'eju Tuff is classified as a trachyte and Tuff IF as a phonolite, both are interpreted to have erupted from Olmoti (McHenry, 2004, 2005; McHenry et al., 2008). Tuff IF is essentially at the top of the Olduvai subchron (CN2) dated at 1.785 Ma (Berggren et al., 1995) and the age of 1.79 Ma is used (Hay and Kyser, 2001), but no date is currently available for the Ng'eju Tuff. Using sedimentation rates of 0.1 mm/yr and 0.12 mm/yr established by Ashley (2007) and Hay (1976), respectively, time can be estimated until a date for the Ng'eju Tuff is published. The time-slice is 2 m at the thickest point when tuffs are excluded because they can be deposited very rapidly on the landscape. A 2 m thick package of sediment would represent ~ 20 ka interval of time from 1.79 to 1.81 Ma.

In addition, there are many other tuffs that are poorly preserved basin-wide and which have not been studied in detail, but locally these tuffs can be useful for correlation using stratigraphic position and chemistry. Between Tuff IF and the Ng'eju Tuff, a thin discontinuous tuff was identified in the FLK region (Ashley et al., 2010a). Following the multi-component approach established by McHenry (2004, 2005) for Olduvai tephra correlation, Baluyot (2011) analyzed feldspar phenocrysts using the electron microprobe at Rutgers University. The previously uncharacterized tuff in these three locations has similar average compositions of albite, anorthite, and orthoclase (Table 2.1). Samples

were analyzed from trenches FLK-1 and FLK-2 (Ashley et al., 2010a, c) and a new trench OLD-1 located in the area referred to as Maiko Gully by Hay (1976). Combined with a similar stratigraphic relationship and lithologic characteristics, this suggests that the tuffs identified at FLK-1 and OLD-1 are in fact the same tuff, greatly enhancing correlation between the two trenches (Baluyot, 2011). In addition, a tuff of similar lithology and stratigraphy height was identified at OLD-3 that has been tentatively correlated with the tuff identified at FLK-1, FLK-2, and OLD-1 until phenocryst composition can be analyzed (Fig. 2.3).

Table 2.1: Modified from Baluyot (2011).

	Average Values		
	Albite	Anorthite	Orthoclase
FLK-1	70.37	20.17	9.46
FLK-2	65.65	25.65	9.44
OLD-1	69.86	22.91	7.24

Paleoclimatic and Hydrologic Setting

The Olduvai Gorge region currently experiences a semi-arid environment due to the rain shadow created by the NVC, and an evaporation rate (estimated to be between 2000 and 3000 mm/yr) that greatly exceeds the amount of precipitation (Hay, 1976; Ashley et al., 2010a, c). Modern mean annual precipitation (MAP) is ~560 mm/yr with an average temperature of 23°C (Hay, 1976). Olduvai is located at ~3°S, near the equator where seasonal temperatures normally do not fluctuate significantly through time, but precipitation does vary. Multiple proxies have demonstrated that East Africa has experienced a general trend toward a more arid climate over the past 2 Ma (Feakins and deMenocal, 2010, and references therein). Stable isotopes of pedogenic carbonates from the Olduvai stratigraphy indicate a general drying trend (Cerling and Hay, 1986; Sikes and Ashley, 2007) as do paleosols in lowermost Bed II (Ashley and Driese, 2000) and marine eolian dust records from northern Africa (deMenocal, 1995). In addition, both

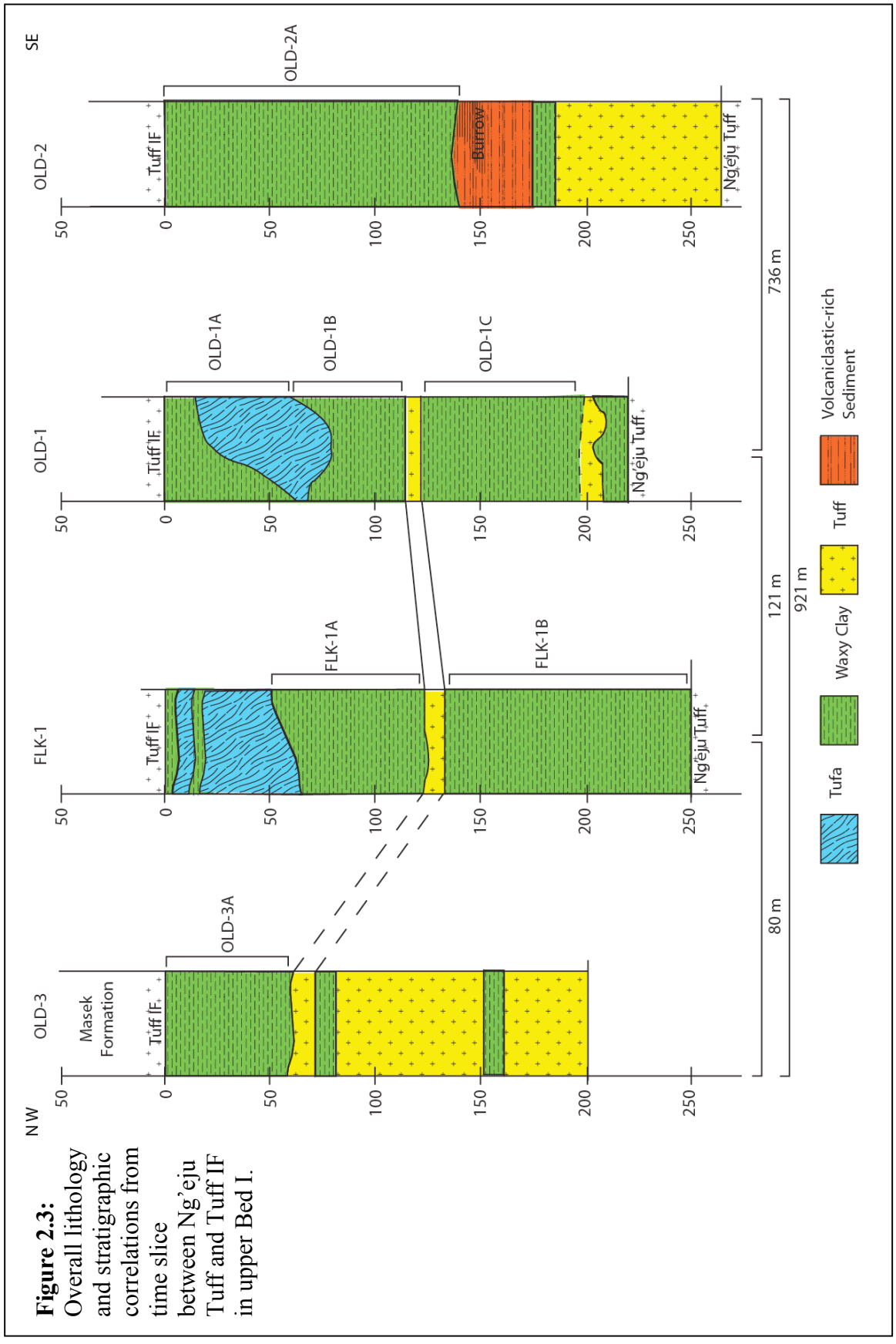

Figure 2.3: Overall lithology and stratigraphic correlations from time slice between Ng'eju Tuff and Tuff IF in upper Bed I.

macrofauna (Plummer and Bishop, 1994; Andrews and Humphrey, 1999) and microfauna (Fernandez-Jalvo et al., 1998) as well as pollen (Bonnefille, 1984) and phytoliths (Bamford et al., 2008; Barboni et al. 2010) all show a drying climate through the stratigraphic sequence.

Abundant time constraints have allowed for high-resolution reconstruction of the environmental changes between 1.84 to 1.74 Ma. The Olduvai region was heavily influenced by ~21 ka precession cycles that affect the amount of solar insolation (Ashley and Hay, 2002; Ashley, 2007). At the equator, changes in solar insolation cause stronger monsoons and therefore wetter climate, often referred to as the "orbital monsoon hypothesis" (Ruddiman, 2008). Over this 21 ka cycle, precipitation could potentially increase or decrease by approximately a third between the wet and dry portion of this cycle. This signal is recorded in the lithostratigraphy as the lake periodically expanded and contracted over the landscape depositing continuous beds of waxy clay at intervals consistent with wet periods of a 21 ka precession cycle and earthy claystones forming in lake margin wetlands during dry periods (Ashley, 2007).

Five complete cycles of lake expansion and contraction are identified from 1.84 and 1.74 Ma and between Tuffs IB an IIA (upper Bed I and lowermost Bed II) (Ashley, 2007). Sikes and Ashley (2007) estimated that MAP was ~800 mm/yr during wet periods in Bed I compared to the modern, which currently falls in a dry period with a MAP of ~560 mm/yr. During the time-slice between Tuff IF and the Ng'eju Tuff, there is likely one complete 21 ka cycle beginning with a dry period at ~1.81 Ma (Ashley, 2007).

Previous Paleosol Research at Olduvai Gorge

Only a few paleosols in upper Bed I and lowermost Bed II have been studied in high-resolution, but Hay (1976) and Leakey (1971) mention numerous pedogenically modified beds found throughout the Olduvai stratigraphy. Previous research has ranged from the study of calcium carbonate-rich silty Aridisols forming in the well-drained fluvial environment of middle to upper Bed I (Sikes and Ashley, 2007) to red Andisols forming in lowermost Bed II on the volcaniclastic alluvial fan (Fig. 2.2; Ashley and Driese, 2000).

The paleo-Aridisols formed on the interfluves and floodplain of the fluvial plain west of paleo Lake Olduvai during the ~60 ka time slice between Tuff IB and Tuff IF in Bed I and were at times forming simultaneously with those paleosols presented in this study on the eastern margin of the lake (Figs. 2.2 and 2.4). The parent material was eroded from a quartzofeldspathic metamorphic basement rocks and transported east in a fluvial system. These soils were well drained and above the influence of the water table. Stable isotopes of pedogenic carbonate within these soils recorded varying amounts of C_4 vs. C_3 grasses growing on the landscape due to changes in precipitation (Sikes and Ashley, 2007).

Paleo-Andisols also formed on the volcaniclastic fan to the east of paleo Lake Olduvai at ~1.75 Ma in lowermost Bed II in the time-slice between Tuff IF and IIA. The cumulative paleosols formed from a volcaniclastic parent material and probably received episodic contributions of pyroclastic material from the NVC throughout pedogenesis. The location of the soil on the volcaniclastic fan and the depth of the water table affected pedogenesis. Two distinct sets of pedogenic features sensitive to the moisture content

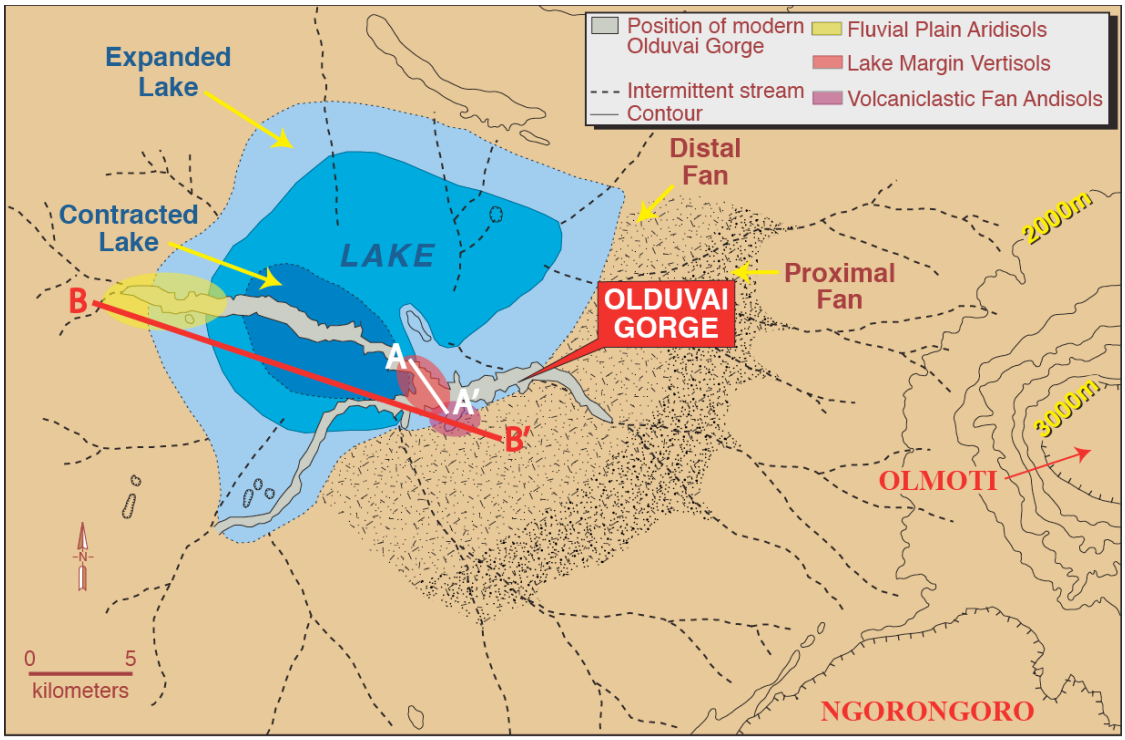

Figure 2.4: Paleogeographic map of Olduvai Gorge showing the distribution of paleoenvironments, the expansion and contraction of paleo Lake Olduvai during the Pleistocene, and the distribution of soil forming environments. Modified from Ashley et al. (2010c).

recorded changes in the water table depth. Higher lake levels (shallower water table) and an increase in volcaniclastic material may have slowed pedogenesis downslope but created a stacked paleosol upslope where the water table was lower and the soil was better drained (Ashley and Driese, 2000).

Paleontological, Archaeological, and Paleoecological Records

The focus of this research, upper Bed I, has a high density of artifacts and an abundance of large mammal bones (mostly bovids) clustered around sites FLK, FLK-N, and FLK-NN (Fig. 2.1C; Leakey, 1971). The time slice between the Ng'eju Tuff and Tuff IF at FLK-N contains one of the densest concentrations of these materials, but interpretation of this site has been highly controversial. This time slice is subdivided into 9 different archaeological levels. Levels 1 through 6 were originally excavated and

defined by Leaky (1971) and were reevaluated by Dominguez-Rodrigo et al. (2007). Levels 1-5 were originally interpreted as "living floors" where evidence of artifacts and bones indicated hominin occupation, and Level 6 was interpreted as an elephant butchery site (Leakey, 1971). After reassessment of Leakey's fossil assemblage with additional data collected by Bunn et al. (2010) from Levels 1 and 2, which added more than 1000 fossils to the collection, new hypotheses about site formation have been introduced. Dominguez-Rodrigo et al. (2007) suggested that Levels 1 through 5 are instead a result of carnivores (primarily felids and hyenas). Both the additional fossils (Bunn et al., 2010) from Levels 1 and 2 and the new Levels 7 through 9 (Dominguez-Rodrigo et al., 2010) suggested that hominin butchery was a secondary contributor to the site and that carnivores created most of the vertebrate record.

New data from FLK-N from the time-slice between the Ng'eju Tuff and Tuff IF suggest that the site was on a low ridge approximately 1 m above the surrounding landscape (Ashley et al., 2010a). Phytoliths indicate that palms grew on the ridge where the soil was better drained, while an abundance of woody plants and sedges grew in the surrounding lowlands, where seepage from groundwater-fed springs provided moisture in a semi-arid climate (Ashley et al., 2010a; Barboni et al., 2010). The lack of grass phytoliths is also indicative an abundance of water in the soil (Barboni et al., 2010) and called into question the overabundance of grass pollen found by Bonnefille (1984). A reevaluation of the original pollen data shows that 70% of the pollen came from woody plants such as thicket woodland, *Acacia*-groundwater woodland, gallery forest, and groundwater forests while only 30% matches swamp herbage and grasslands. Both the phytoliths and pollen data suggest that wetland surrounding FLK-N was similar to the

groundwater forest, thicket, and *Acacia*-woodland surrounding freshwater springs along Lake Manyara, Tanzania (Barboni et al., 2010). These new data suggest that the reason for the location of the archaeological site at FLK-N was a result of the FLK fault and Zinj Fault (related to rifting), which created fault-controlled springs (Fig. 2.1C). The horst between these two faults also created better-drained conditions allowing for woody vegetation to thrive and attract both hominins and carnivores (Ashley et al., 2010a; Barboni et al., 2010). The continued controversy and abundant archaeological record make this time-slice a priority for high-resolution reconstructions of the environment to aid in the interpretation of the site.

3. METHODOLOGY

Field Methods

Previous research demonstrates that the Ng'eju Tuff and Tuff IF are laterally extensive and distinct throughout Olduvai Gorge with 2 to 4 m of sediment between them (Hay, 1976; McHenry, 2004, 2005). A ~ 1 km transect was identified in uppermost Bed I, and three locations with known outcrops of the Ng'eju Tuff and Tuff IF were selected for excavation and detailed investigations. These three Trenches are designated as OLD-1, OLD-2, and OLD-3 (Figs. 2.1C and 2.3). Additional samples and descriptions by Gail M. Ashley in 2007 were used from Trench FLK-1, where previous research had focused on the tufa found beneath Tuff IF (Ashley et al., 2010a, c). These Trenches form a ~1 km cross-section of the lake margin in a NW-SE direction. Trench OLD-3 is closest to paleo Lake Olduvai and Trench OLD-2 is almost 1 km away nearest to the alluvial fan at the base of the NVC. Trenches FLK-1 and OLD-1 are located between (80 and 201 m, respectively) from Trench OLD-3 (Figs. 2.1C and 2.3).

All outcrops were documented using GPS (Table 3.1), stratigraphy was measured, macroscale features were logged in detail and photographed, and representative samples of each lithology collected. Additional samples for bulk geochemical analysis were collected from the paleosols for calculations of CIA-K and CALMAG estimations of

Table 3.1: GPS Locations of stratigraphic sections.

Year	Location	Trench	Latitude	Longitude
2007	FLK	FLK-1	2°59.387'S	35°20.927'E
2010	Maiko Gulley	OLD-1	2°59.415'S	35°20.978'E
2010	HWK-E	OLD-2	2°59.568'S	35°21.347'E
2010	FLK-N	OLD-3	2°59.338'S	35°20.905'E

mean annual precipitation, as well as for molecular weathering ratios and constitutive mass-balance calculations. Standard geochemical analysis of paleosols requires sampling every 10 cm in order to determine the geochemical signature of every soil horizon (Retallack, 2001). Whole soil clods were also collected at 10 cm intervals for bulk density analysis. Where possible, oriented samples were collected from each soil horizon for thin-section analysis of the micromorphology.

Laboratory Methods

Grain Size Analysis

Grain size analysis was conducted in order to determine the approximate amount of sand (>4ϕ) versus the clay/silt fraction (<4ϕ) (Folk, 1980). The smectitic composition of the clays prevented the removal of organics because the clays expand enormously when exposed to hydrogen peroxide added to remove any organic matter. Therefore the grain size was analyzed with both carbonate and organic matter present. This reaction to aqueous treatments also prevented the analysis of the silt/clay fraction using the pipette method. Twenty-one samples were analyzed in order to distinguish particle size changes between soil horizons. For each sample, approximately 30 g sample was weighed to 0.001 g and transferred to a beaker. Any large pieces of carbonate were avoided during sampling; however, finely disseminated matrix carbonate was not removed from samples. Approximately 100 ml of distilled water was added to the sample and left (for several days) to disaggregate. Samples were then wet-sieved using U.S. Standard Sieve Mesh no. 230 (63 μm screen), the boundary between very fine sand and coarse silt (Wentworth, 1922). The resulting separates were then oven-dried in pre-weighed beakers. Once dry, samples were then weighed and the percentage of sand was calculated and plotted against

depth. Samples were also visually characterized for sorting, range of grain sizes, and estimates of volcaniclastic contribution using a stereomicroscope.

Bulk Density Analysis

Bulk density analysis was conducted using the wax clod method (Blake and Hartge, 1986). Paleosol clods were dried in the oven at 60°C for 3-5 days. A 15-20 cm piece of monofilament fishing line was attached to the clod and then weighed. The clod was then dipped 2-3 times in paraffin heated to just above the melting point. If any areas were not completely coated with paraffin, a patch was applied to ensure the clod was waterproof. Once dry, the paraffin-coated clod was weighed in air and then suspended from the balance and weighed again while submerged in water. Any samples that bubbled, indicating that water had leaked into the clod, were discarded. Bulk density was then calculated:

$$\rho = (W_{od} \times 0.9) / [(W_p - W_{pw}) - (W_p - W_{od})] \quad (1)$$

Where

W_{od} = weight of oven dry sample

W_p = weight of sample with paraffin

W_{pw} = weight of sample with paraffin in water.

Whole-Rock Geochemical Analysis

Eighty samples were analyzed for bulk geochemistry. These samples were pulverized using a mortar and pestle and then sent for commercial analysis to ALS Chemex, Inc. (Minerals) for major, rare earth, and trace analyses using a combination of inductively coupled plasma atomic emission spectroscopy (ICP-AES) and inductively coupled plasma mass spectrometry (ICP-MS). The major oxides analyzed were SiO_2,

Al_2O_3, Fe_2O_3, CaO, MgO, Na_2O, K_2O, Cr_2O_3, TiO_2, MnO, P_2O_5, SrO, and BaO using ICP-AES. In addition, the following rare and trace elements were analyzed using ICP-MS: Ag, Ba, Ce, Co, Cr, Cs, Cu, Dy, Er, Eu, Ga, Gd, Hf, Ho, La, Lu, Mo, Nb, Nd, Nik, Pb, Pr, Rb, Sm, Sn, Sr, Ta, Tb, Th, Tl, Tm, U, V, W, Y, Yb, Zn, and Zr.

Mean Annual Precipitation Estimations

Previous research has shown that paleosols have the possibility to estimate mean annual precipitation (MAP) using depth to the Bk horizon (Retallack, 2001), Fe-Mn nodules in Vertisols (Stiles et al., 2001), and weathering indices (Sheldon et al., 2002; Nordt and Driese, 2010). Using the geochemical data, two weathering indices, the chemical index of alteration minus potassium (CIA-K) and CALMAG, were employed for the paleo-Vertisols identified at Olduvai Gorge. CIA-K was first introduced by Sheldon et al. (2002) for use on B horizons of all types of paleosols formed on sedimentary rocks and is calculated as follows:

$$\text{CIA-K} = [Al_2O_3/(Al_2O_3 + CaO + Na_2O) \times 100]. \quad (2)$$

The weight % of each oxide was divided by its molecular weight to normalize the oxide, and then values for each paleosol were averaged. The resulting values were then applied to a linear equation derived by (Sheldon et al., 2002):

$$y = 14.3x - 37.6 \quad (3)$$

Where x = CIA-K and y = mean annual precipitation in mm.

In addition, Nordt and Driese (2010) created a weathering index specifically for paleo-Vertisols. Of the four major base-forming oxides (CaO, MgO, Na_2O, and K_2O), the concentrations of CaO and MgO have a much better correlation for MAP in Vertisols than well-established CIA-K weathering index. The CALMAG method is defined as:

$$CALMAG = [Al_2O_3/ (Al_2O_3 + CaO + MgO) \times 100]. \quad (4)$$

The weight % of each oxide was normalized and then oxide values for each paleosol were averaged. The resulting values were then used in calculation using the linear equation developed by Nordt and Driese (2010):

$$y = 22.69x – 435.8 \quad (5)$$

Where x = CALMAG and y = mean annual precipitation in mm.

Molecular Weathering Ratios

Molecular weathering ratios were used to approximate the amount of hydrolysis, leaching, hydration, and salinization that occurred during the formation of the soil, following Retallack (2001), for comparison with constitutive mass-balance. The weight % of each oxide was normalized by dividing by its molecular weight prior to calculation of each molecular ratio. See Table 3.2 for equations.

Mass-Balance Approach

Constitutive mass-balance models have in the past been used to quantify changes in paleosol chemistry, as opposed to molecular weathering ratios, which can only be used to examine relative changes down profile (Brimhall and Dietrich, 1987; Brimhall et al., 1991; Retallack, 2001). Mass-balance is a more powerful tool because it is determined using a parent material and takes into account changes in bulk density.

Table 3.2: Molecular weathering ratios following Retallack (2001).

Hydrolysis	**Aluminum/bases**	$Al_2O_3/(CaO + MgO + K_2O + Na_2O)$
	Aluminum/silica	Al_2O_3/SiO_2
Hydration	**Silica/sesquioxides**	$SiO_2/(Fe_2O_3 + Al_2O_3)$
Salinization	**Alkali/aluminum**	$(K_2O + Na_2O)/Al_2O_3$
	Sodium/potassium	Na_2O/K_2O
	Sodium/aluminum	Na_2O/Al_2O_3
Leaching	**Barium/Strontium**	Ba/Sr

Parent Material. All geochemical data were converted from ppm to weight %. Possible parent materials were determined following Maynard (1992). Deviation from parent material is relatively small in immobile elements like Ti, Al, and Zr. The CIA-K index was then used to estimate weathering in the soil. With a CIA-K values of less than 90%, the Ti/Zr ratio should not depart from the parent material by more than 40% (Maynard, 1992). As all values of CIA-K were less than 90%, the percent deviation was calculated as follows:

$$\text{Percent Deviation} = [(Ti/Zr_{soil} - Ti/Zr_{parent})/ (Ti/Zr_{parent}) \times 100] \quad (6)$$

using the ratio of Ti/Zr of each possible parent material and the ratio of Ti to Zr of the averaged composition of each soil (Maynard, 1992). The percent deviation was calculated for all possible parent materials for each soil. Parent materials included sediment or tephra above and below each soil, an average of the tuff compositions, and an average of two samples of waxy lake clay. These lake clay samples (GA-37-99 and GA-47-99) were collected in 1999 by Gail M. Ashley and Robin W. Renaut from the center of paleo Lake Olduvai from the area referred to as Loc. 80 (Fig. 2.1B; Hay, 1976). These sediments were chosen because they were deposited between Ng'eju Tuff and Tuff IF and represent a waxy lake sample unaffected by pedogenesis. Consequently, two Loc. 80 lake samples were analyzed, one from the top and one from the bottom of the time-slice being studied. These serve as references to evaluate any changes in parent material composition due to the fluctuating chemistry, characteristic of a playa lake such as paleo Lake Olduvai. Sample GA-37-99 occurs 10 cm below Tuff IF, and GA-47-99 is 160 cm below Tuff IF. Crossplots of Zr/(Zr/Ti) and Ti/(Ti/Zr) for each soil and plots of Zr/Ti and

Ti/Zr versus depth were also used as previous research shows these plots are useful for determining parent material suitability (Ashley and Driese, 2000; Driese et al., 2000).

Mass-Balance Calculations. Calculation of constitutive mass-balance requires a bulk density value for each geochemical measurement, proper determination of parent material, and geochemical analysis of major, trace, and often rare earth elements in both the soil and parent material. Using an immobile element such as Zr or Ti, a transport function can be calculated that shows whether an element has been added or removed from the soil compared to the parent material. Where there is no volumetric or open system changes, the transport function simplifies to residual enrichment and is calculated as follows:

$$\frac{C_{i,w}}{C_{i,p}} = \frac{\rho_p}{\rho_w}. \quad (7)$$

When volumetric change is introduced to the system, strain (ε) is added to the equation:

$$\varepsilon_{i,w} = \frac{\rho_p C_{i,p}}{\rho_w C_{i,w}} - 1. \quad (8)$$

In an open system, these two equations are expanded to:

$$\tau_{j,w} = \frac{\rho_w C_{j,w}}{\rho_p C_{j,p}} (\varepsilon_{i,w} + 1) - 1. \quad (9)$$

Variables are defined in Table 3.3 and a full description of how equations were derived

Table 3.3: Modified from Brimhall and Dietrich (1987).

Glossary of Variables:

$C_{i,w}$	= concentration of immobile element (i) in weathered material
$C_{i,p}$	= concentration of immobile element (i) in parent material
ρ_p	= bulk density of parent material
ρ_w	= bulk density of weathered material
$\varepsilon_{i,w}$	= strain or volumetric change of immobile element (i) in weathered material
$\tau_{j,w}$	= translocation of element of interest (j) in weathered material
$C_{j,w}$	= concentration of element of interest (j) in weathered material
$C_{j,p}$	= concentration of element of interest (j) in parent material

can be found in Brimhall and Dietrich (1987), Brimhall et al. (1991), and Chadwick et al. (1990).

When plotted, a value of $\tau = 1$ is equivalent to a 100% increase compared to the parent material, $\tau = -1$ is a 100% decrease compared to the parent material, and a value of $\tau = 0$ indicates that none of the element has been removed from the system. For ε (strain), a positive value indicates dilation (volume gain) of the weathered material compared to the parent, a negative value indicates collapse (volume loss) of the weathered material compared to the parent, and an ε of zero indicates isovolumetric conditions (no change) during weathering. Bulk density calculations and geochemical measurements were plugged into a Microsoft Excel spreadsheet used to calculate residual enrichment, strain, and translocation for elements of interest. The results are plotted versus depth measuring down from Tuff IF.

Stable Isotope Analysis

Four bulk samples of clean unweathered tufa were prepared by powdering using a mortar and pestle. One tufa sample, EB-21, was also sampled using the drill press in 4 different areas as well as powdered using a mortar and pestle to test the homogeneity of the sample and therefore accuracy of bulk sampling. The $\delta^{13}C$ and $\delta^{18}O$ values of carbonate samples were analyzed at Rutgers University in the Stable Isotope Laboratory in the Department of Earth and Planetary Sciences. Samples were loaded into a Multi-prep device attached to a Micromass Optima mass spectrometer. The $CaCO_3$ was reacted in 100% phosphoric acid at 90°C for 800 seconds. Values are reported in standard per mil (‰) notation versus the Vienna Pee Dee Belemnite standard (V-PDB) through the analysis of an internal laboratory standard that is routinely measured with NBS-19.

Coplen et al. (1983) report values of 1.95 and -2.20‰ for $\delta^{13}C$ and $\delta^{18}O$, respectively. The long-term standard deviations on the internal lab standard are 0.05 and 0.08‰ for $\delta^{13}C$ and $\delta^{18}O$, respectively.

Petrographic Analysis

Ten paleosol samples were sampled for thin section preparation for petrographic analysis, and 5 of the 10 samples are oriented. Nineteen thin sections were commercially prepared by Spectrum Petrographics. Oriented samples were stabilized in the field using Hillquist® Thin Section Epoxy C/D formula. The remaining samples were vacuum-impregnated with epoxy by Spectrum Petrographics prior to thin section preparation. Where possible thin sections were prepared from each paleosol at both the top and bottom in order to determine whether any changes in pedogenic microstructures had occurred down profile. In some cases, fine ped size and damage during transport made thin sectioning at every level impossible. Thin sections were also prepared from other lithologies sampled within the four trenches including: tufa, tuffs, and volcaniclastic-rich sediment.

Micromorphological analysis was conducted according soil micromorphological techniques established by Brewer (1976) and Fitzpatrick (1993) using an Olympus BX-51 polarized light microscope equipped with a 12.5 MPx digital camera and UV fluorescence attachment (at Baylor University). Abundance of organic content was visually estimated by subjecting the thin section to ultraviolet light (UV) causing the organic matter to autofluoresce. Photomicrographs were taken using three different wavelength filters, Nu, Nb, and TXRED in addition to reflected light, cross-polarized light (XPL), and plane polarized light (PPL) of unique and representative features.

4. RESULTS

The results are organized geographically from northwest to southeast (Figs. 2.1 and 2.3). Results are reported first with a physical description of macroscale features and petrographic features followed by geochemical results. The geochemical analyses were used to calculate molecular weathering ratios, mass balance translocations, and MAP estimates. Finally, results of the stable isotopes analysis of tufa are described. Paleosols are all depicted using Tuff IF as a datum for continuity and ease of reference to Fig. 2.3.

Macroscale Features

Trench OLD-3

Trench OLD-3 is located in FLK North about 7 m from Trench FLK-N-3 referred to in Ashley et al. (Fig. 2.1; 2010a). The trench is ~3 meters deep, but only the top 2 meters were studied (Figs. 2.3 and 4.1A). The lower beds show evidence of mass movement and were not included, and the Ng'eju Tuff was not exposed at this location. One paleosol with four distinct horizons was identified directly beneath Tuff IF. The paleosol overlies a thin discontinuous tuff (Figs. 4.1B and 4.2). Carbonate nodules (5 to 10 cm in diameter) as well as concretions (10 cm) are numerous in the top 5 cm and aligned horizontally. The top 20 cm layer is classified as a Bw horizon and is characterized by columnar peds with secondary angular blocky peds and a dark grayish-brown color (2.5Y4/2). The pale yellow colored (2.5Y8/4) Bk horizon, which formed between 20 and 30 cm, has no ped development (Fig. 4.1B). The Bss1 horizon (30-45 cm) is characterized by angular blocky peds, pedogenic slickensides (Fig. 4.1C), and an abundance of carbonate-filled root traces about 1 cm in diameter and of various lengths 5 cm or less (Fig. 4.1D). The lowest Bss2 horizon (45 to 60 cm) has similar pedogenic

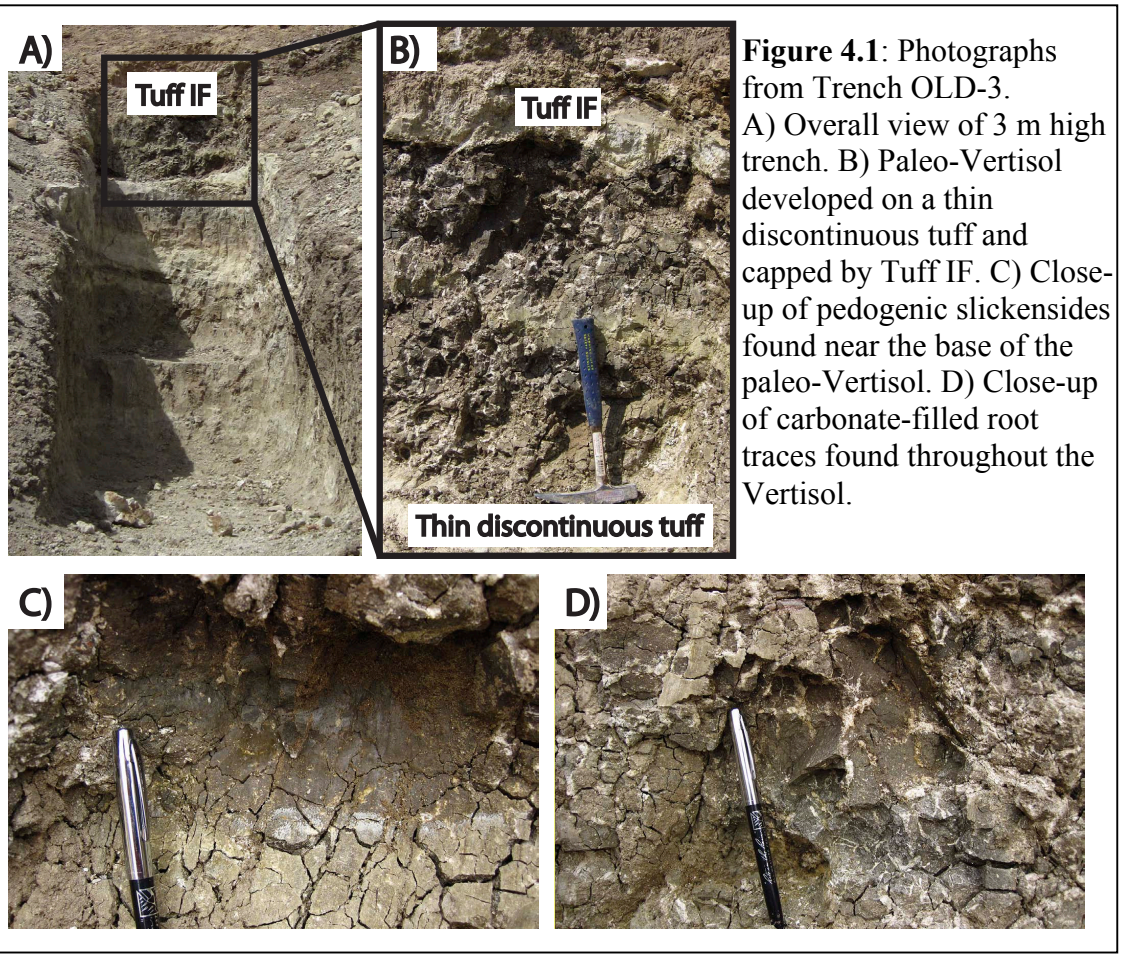

Figure 4.1: Photographs from Trench OLD-3. A) Overall view of 3 m high trench. B) Paleo-Vertisol developed on a thin discontinuous tuff and capped by Tuff IF. C) Close-up of pedogenic slickensides found near the base of the paleo-Vertisol. D) Close-up of carbonate-filled root traces found throughout the Vertisol.

features, but a slight color change to olive brown (2.5Y4/3). Beneath the tuff is a 10 cm bed of waxy clay with no evidence of pedogenic modification. Below this thin bed of waxy clay is another 70 cm thick tuff with alternating beds of ash fall and lapilli (Fig. 4.1A).

Trench FLK-1

Trench FLK-1 is located in FLK and is 80 m to the southeast of Trench OLD-3 (Figs. 2.1 and 2.3). Trench FLK-1 was sampled and described by Gail M. Ashley in 2007 and data regarding the freshwater spring tufa found at this location are presented in Ashley et al. (2010a, b). A total of 2.5 m of sediment containing two paleosols were described between Tuff IF and the Ng'eju Tuff (Figs. 2.3 and 4.3A). The uppermost

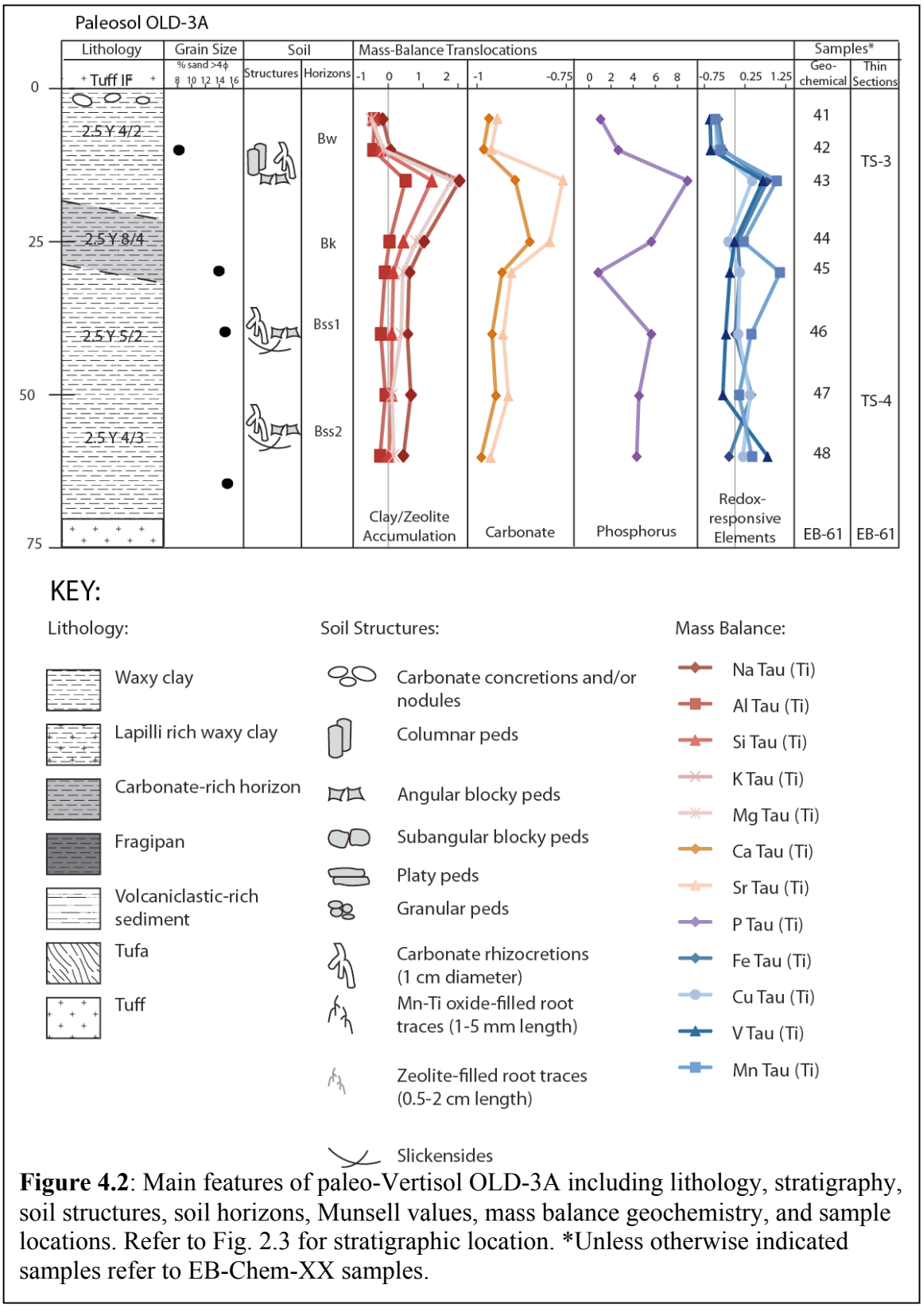

Figure 4.2: Main features of paleo-Vertisol OLD-3A including lithology, stratigraphy, soil structures, soil horizons, Munsell values, mass balance geochemistry, and sample locations. Refer to Fig. 2.3 for stratigraphic location. *Unless otherwise indicated samples refer to EB-Chem-XX samples.

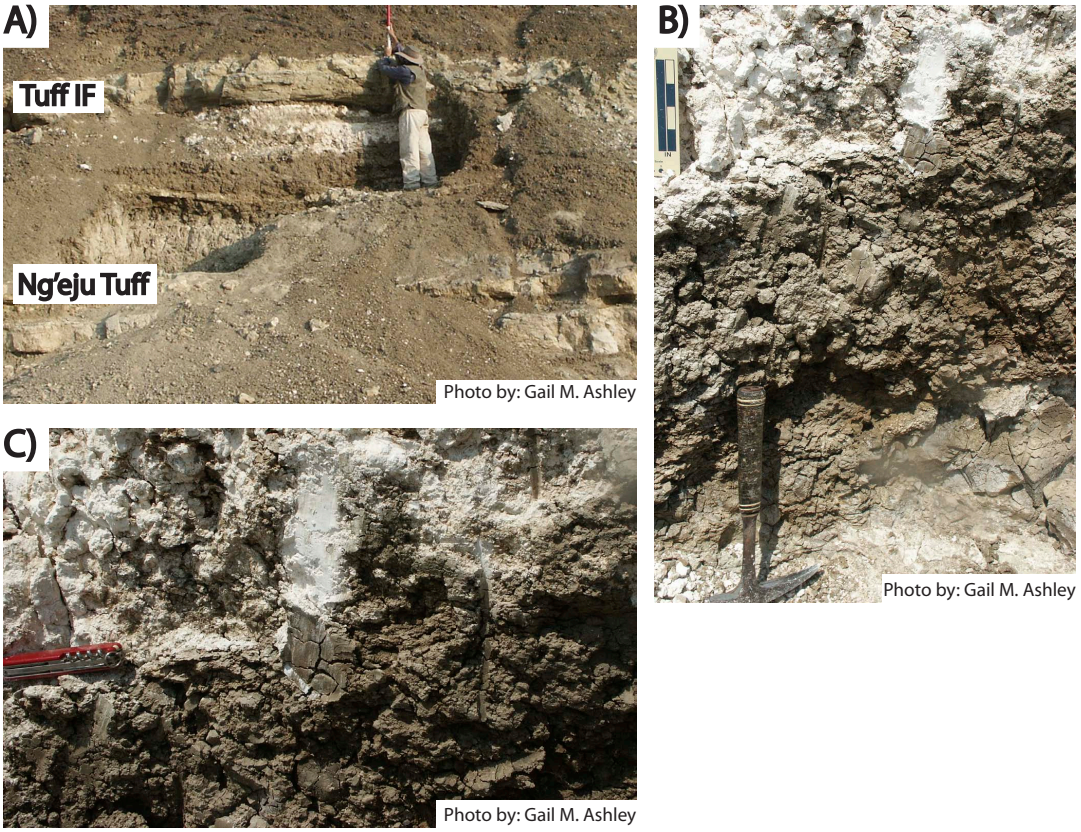

Figure 4.3: Photographs from Trench FLK-1. A) Overall view of trench with stratigraphic location of Tuff IF and Ng'eju Tuff identified. B) 70 cm thick paleo-Vertisol FLK-1A found beneath tufa deposit. C) Close-up of tufa-paleosol boundary in Fig. 4.3B; pocketknife for scale.

portion of the Trench consists of 60 cm of tufa with waxy clay intermixed. At 65 cm, a paleosol referred to as FLK-1A was identified beneath the thick bed of tufa (Figs. 4.3B and 4.4). The top 10 cm are characterized by granular peds and an olive brown color (2.5Y4/3) and are designated as an A horizon (Figs. 4.3B and C). Between 75 and 110 cm there is no color change but peds are angular blocky in shape, and the geochemistry suggests an enrichment of carbonate related elements (Ca and Sr) forming a Bk horizon (Fig. 4.4). Near the base of the paleosol pedogenic slickensides developed, along with columnar peds and angular blocky secondary peds, forming a separate a Bss horizon between 45 and 60 cm depth (Figs. 4.3C and 4.4).

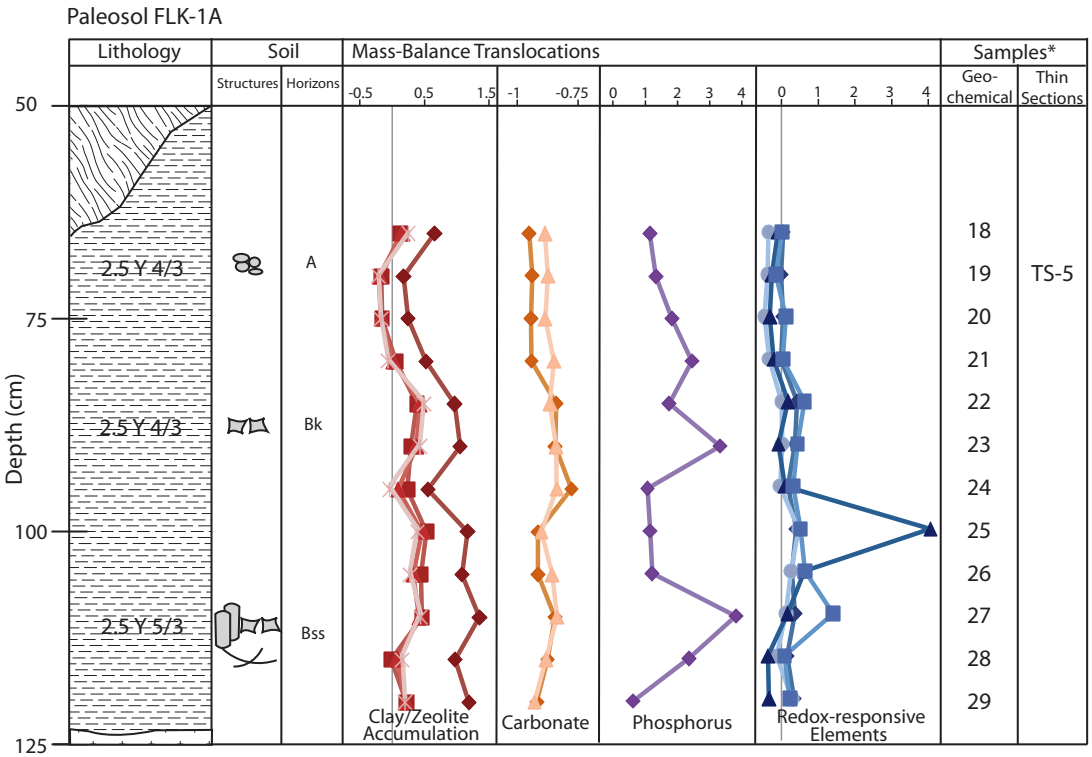

Figure 4.4: Main features of paleo-Vertisol FLK-1A including lithology, stratigraphy, soil structures, soil horizons, Munsell values, mass balance geochemistry, and sample locations. Refer to Fig. 2.3 for stratigraphic location and Fig. 4.2 for legend. *Unless otherwise indicated, samples refer to GA-OLD-XX-07.

A thin, discontinuous tuff separates FLK-1A and the 85 cm thick paleosol FLK-1B (Figs. 4.3A and 4.5). The top 20 cm are thinly laminated and grayish brown in color (2.5Y5/2), but show no physical evidence of pedogenesis. An abundance of carbonate concretions formed between 155 and 165 cm. The first clear evidence for pedogenically modified sediment occurss at 165 cm with a Bw horizon. There are abundant zeolite-filled root traces and subangular blocky peds in the grayish-brown (2.5Y5/2) clay to a depth of 205 cm. The boundary between these two horizons also has evidence of bioturbation. The Bk horizon (205 to 250 cm) is olive brown in color (2.5Y4/3), has subangular blocky peds, and both zeolite- and carbonate-filled root traces. Above the

Ng'eju Tuff are pedogenic slickensides and an accumulation of fine carbonate nodules (~3 mm diameter) possibly pedogenic in origin at the base of the paleosol classified as a Bss horizon.

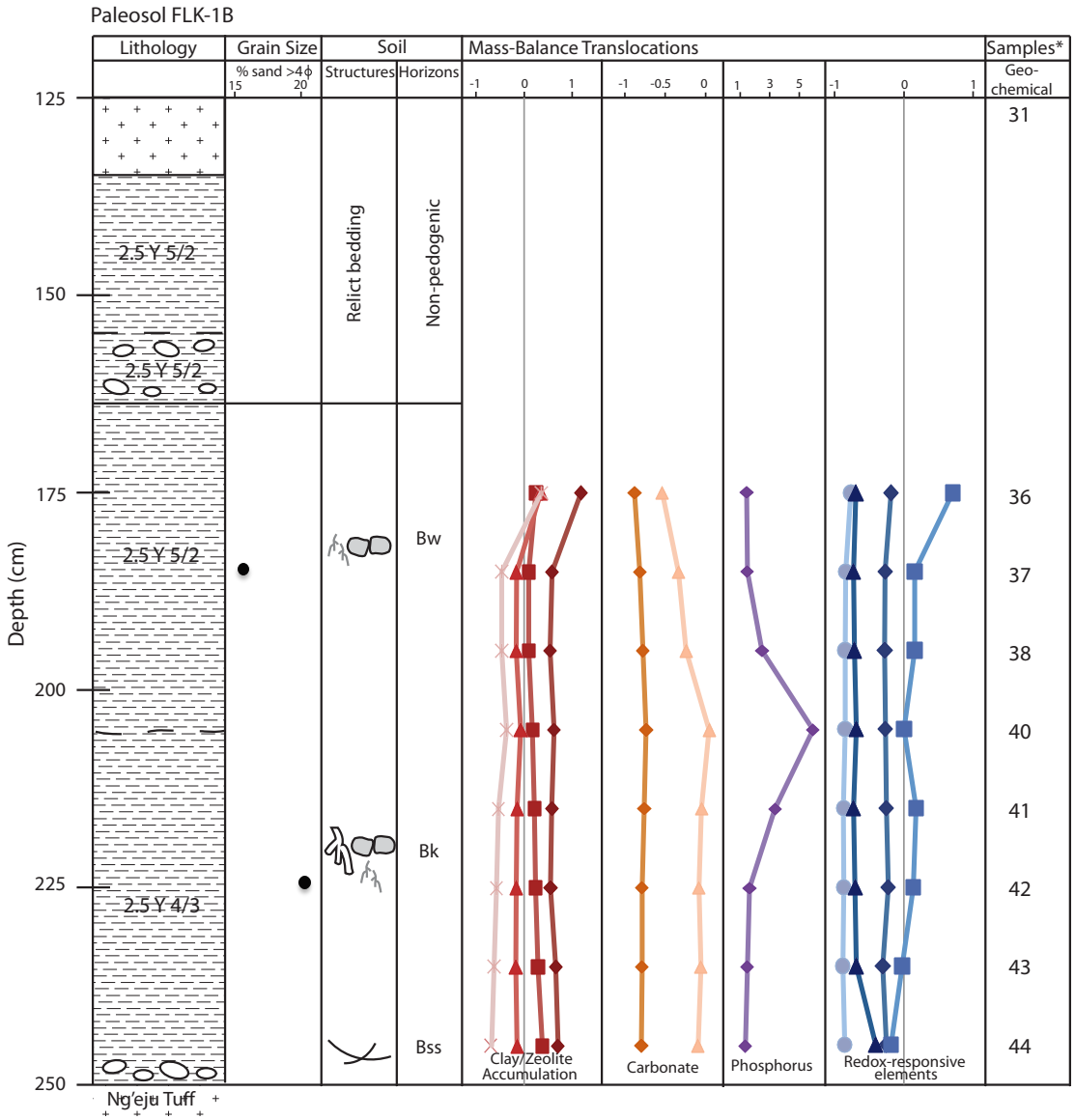

Figure 4.5: Main features of paleo-Vertisol FLK-1B including lithology, stratigraphy, soil structures, soil horizons, Munsell values, mass balance geochemistry, and sample locations. Refer to Fig. 2.3 for stratigraphic location and Fig. 4.2 for legend. *Samples refer to GA-OLD-XX-07.

Trench OLD-1

Trench OLD-1 is located in Maiko Gully in the "junction" area (Fig. 2.1; Hay, 1976). The Trench exposes a 2.2 m thick package of sediment between Ng'eju Tuff and Tuff IF contains 3 distinct paleosols (Figs. 2.3 and 4.6). These paleosols are designated OLD-1A (upper), OLD-1B (middle), and OLD-1C (lower). Paleosol OLD-1A occurs between Tuff IF, and a large wedge of clean white tufa containing small pockets of clay (Fig. 4.7A). OLD-1A ranges from 25 to 50 cm thick and is characterized by pedogenic slickensides, angular blocky peds, and a consistent light olive brown color (2.5Y5/3) (Fig. 4.7B). This thin paleo-Vertisol contains one Bss (slickensided B) horizon (Fig. 4.8).

Paleosol OLD-1B is 35 cm thick and occurs between the tufa and a thin discontinuous tuff that can be correlated to the tuff present at a similar stratigraphic position in FLK-1 and possibly OLD-3 (Figs. 2.3 and 4.9A; Baluyot, 2011). The paleo-Vertisol can be subdivided into three horizons: Bss1, Bss2, and Bx (Fig. 4.10). A light

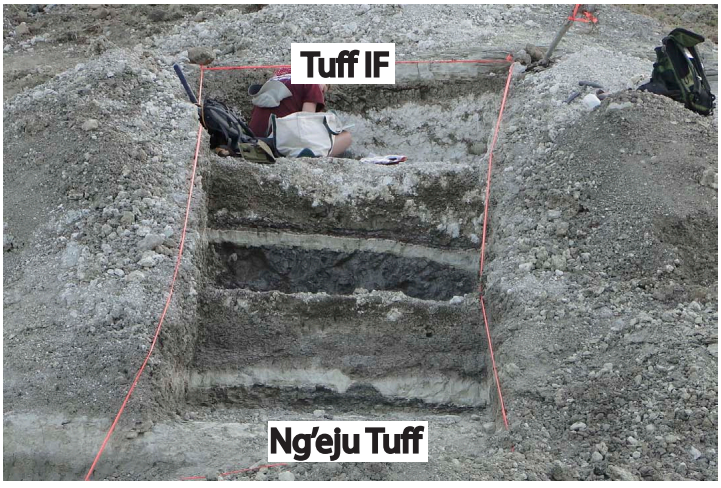

Figure 4.6: Overall view of 2.2 m Trench OLD-1. Stratigraphic positions of Tuff IF and Ng'eju Tuff are indicated for reference.

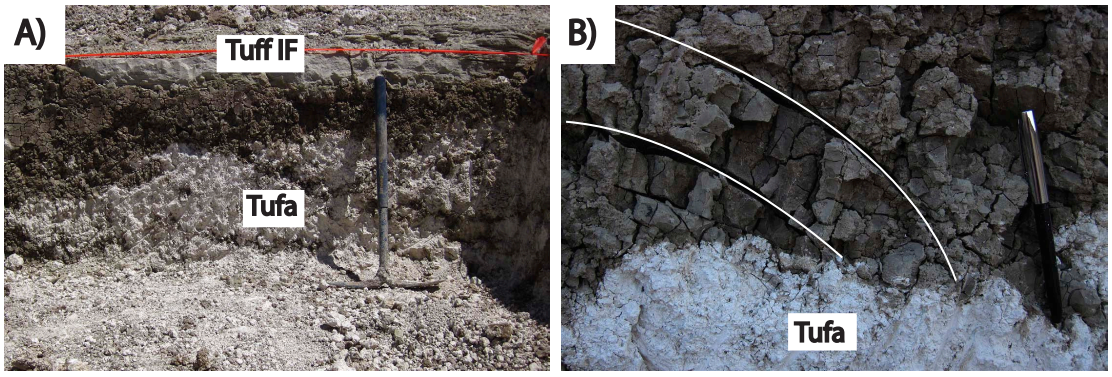

Figure 4.7: Photographs of paleo-Vertisol OLD-1A. A) Overall view; paleopick for scale (0.6 m). B) Close-up of waxy clay-tufa boundary and gilgai outlined by white line, truncating within the tufa; pen for scale.

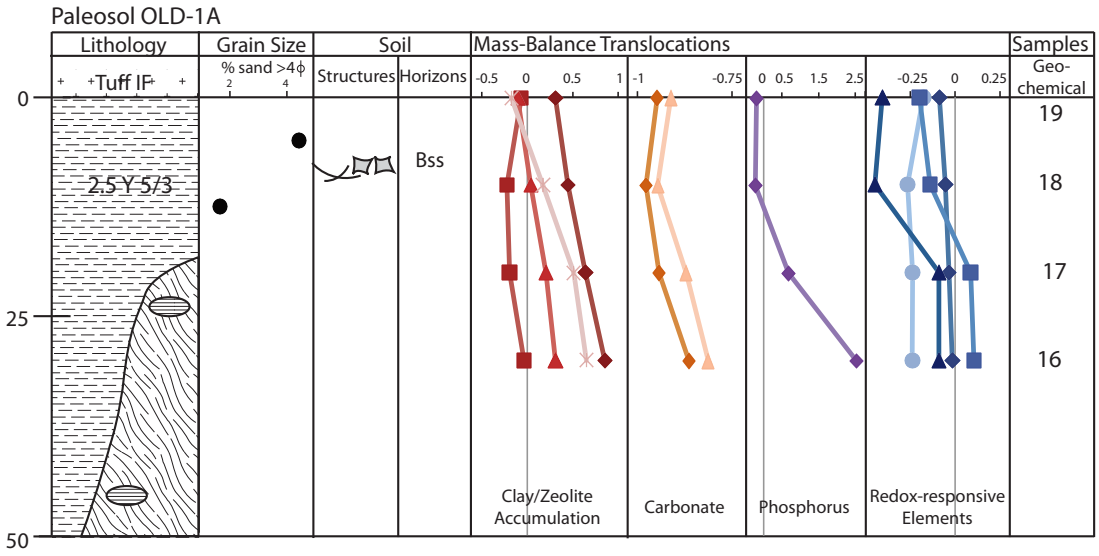

Figure 4.8: Main features of paleo-Vertisol OLD-1A including lithology, stratigraphy, soil structures, soil horizons, Munsell values, mass balance geochemistry, and sample locations. Refer to Fig. 2.3 for stratigraphic location and Fig. 4.2 for legend. Samples refer to EB-Chem-XX samples.

yellowish brown (2.5Y6/3) color, angular blocky peds, and slickensides characterize the Bss1 horizon in the top 15 cm (Fig. 4.9A). There are also an abundance of carbonate nodules ranging in size from 1 to 10 cm that are likely pedogenic in origin. Between 90 and 100 cm depth, there is a gradational change to a light olive brown color (2.5Y5/3), and the ped structure changes to dominantly columnar peds with angular blocky secondary peds in this Bss2 horizon. Small root traces, which range in size from 0.5 to

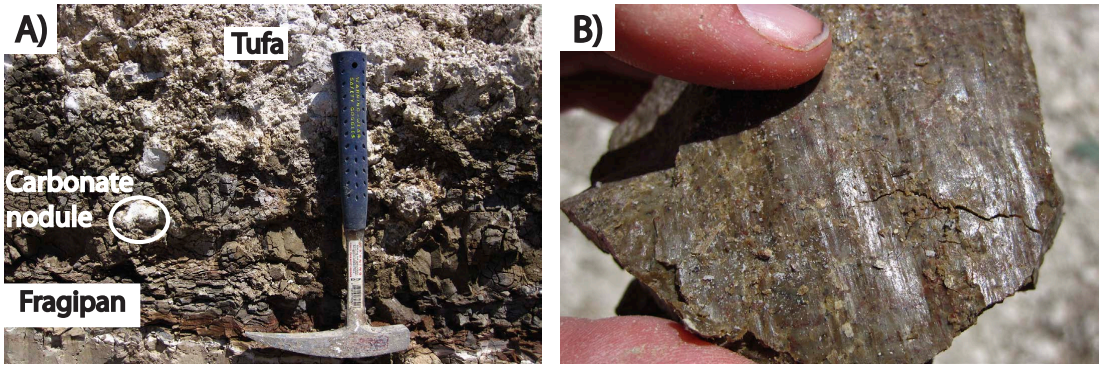

Figure 4.9: Photographs from paleo-Vertisol OLD-1B. A) Overall photograph of paleosol with tufa at the top and a fragipan at the bottom overlying a thin discontinuous tuff. B) Close-up of pedogenic slickensides and black Mn oxide filled root traces found throughout this paleo-Vertisol. C) Close-up of fragipan, which has a horizontal platy ped structure. Note pencil for scale.

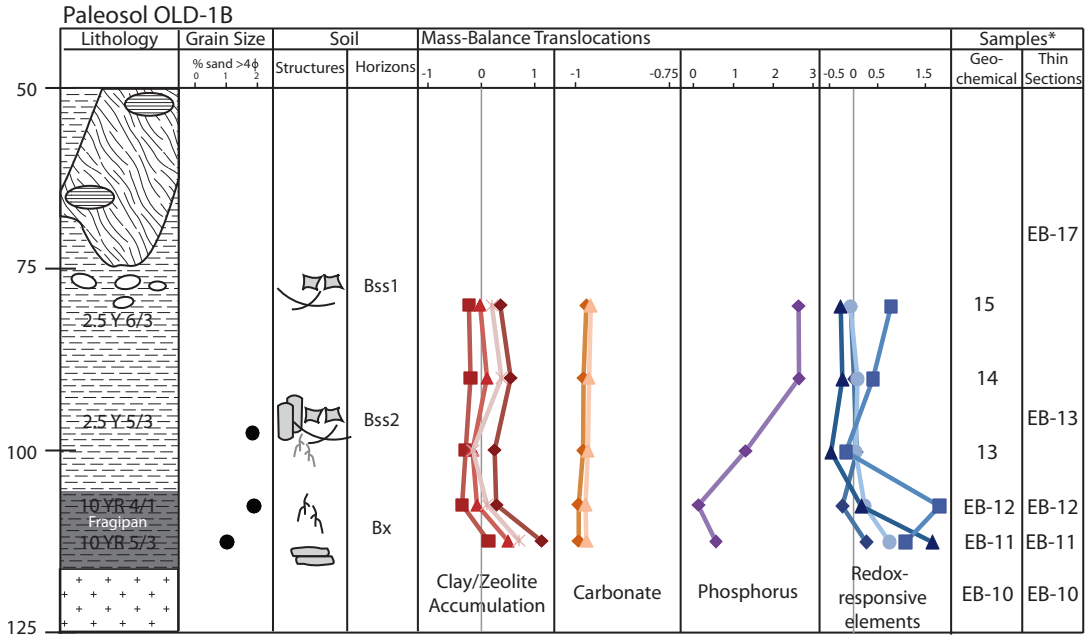

Figure 4.10: Main features of paleo-Vertisol OLD-1B including lithology, stratigraphy, soil structures, soil horizons, Munsell values, mass balance geochemistry, and sample locations. Refer to Fig. 2.3 for stratigraphic location and Fig. 4.2 for legend. *Unless otherwise indicated samples refer to EB-Chem-XX.

2 cm in length, are also present throughout this horizon filled with zeolites. At approximately 100 cm depth, a fragipan (Bx horizon) formed where the tuff likely restricted water movement (Fig. 4.9C). The fragipan is dark gray (10YR4/1) in color (105-110 cm) with platy peds and concentrations of black Mn oxide-filled root traces that do not penetrate below this level. These small root traces range in size from 1 to 5 mm in length. The paleosol at depths of 110 to 115 cm is still characterized by platy peds, but the color changes significantly to a brown (10YR5/3) alternating with layers of dark red (10R3/6) rich in a Mn oxide.

OLD-1C is a 70 cm thick paleosol that occurs between two thin discontinuous tuffs and has four distinct horizons: Bss, Bw1, Bk and Bw2 (Figs. 4.11 and 4.12). Directly beneath the thin discontinuous tuff is a concentration of both carbonate nodules and concretions. The nodules are only 1 to 2 cm in diameter, whereas the concretions are on average > 15 cm in diameter with an outer, heavily recrystallized surface. The top 25 cm is light olive brown (2.5Y5/3) clay characterized by pedogenic slickensides, columnar peds with secondary angular blocky peds, and gilgai forming a Bss horizon (Fig. 4.11A). At 150 cm depth there is another concentration of carbonate nodules, 5 to 10 cm in diameter (Fig. 4.11B). There is no change in color between 150 and 155 cm, but peds are angular blocky in shape. At ~155 cm depth, a gradual boundary exists where the peds are less developed, and the color changes to a light brownish gray (2.5Y6/2). The color change is due to an abundance of carbonate found in this Bk horizon that extends to ~160 cm (Fig. 4.12). Angular blocky peds are well defined from 160 to 195 cm, and the Bw2 horizon is light olive brown (2.5Y5/3) in color. Small zeolite-filled root traces from 0.5 to 2 cm in length are abundant in this horizon as well as zeolitized

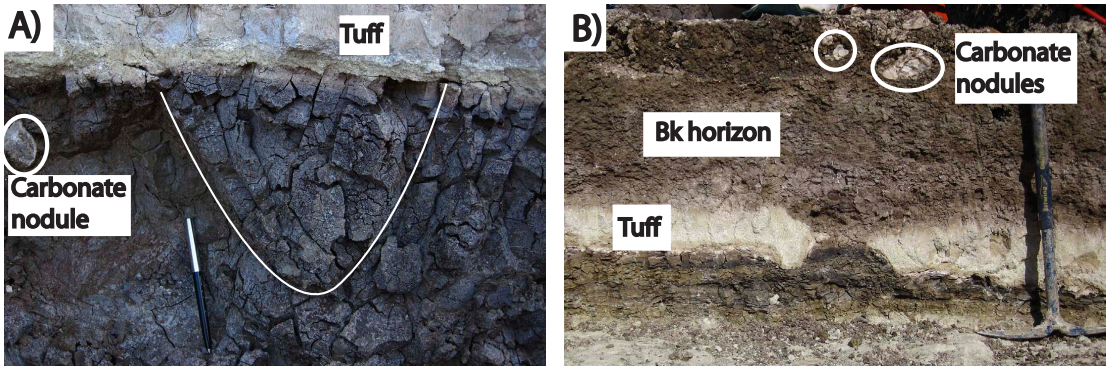

Figure 4.11: Photographs from paleo-Vertisol OLD-1C. A) Top half of paleosol with gilgai outlined by white line, which are truncated by the overlying tuff. Pen for scale. B) Bottom of Trench OLD-1 with non-pedogenic waxy clay bed, a thin discontinuous tuff, and lower half of OLD-1C. Indentation in tuff possibly a footprint. C) Close-up of small zeolite-filled root traces found throughout the bottom 50 cm.

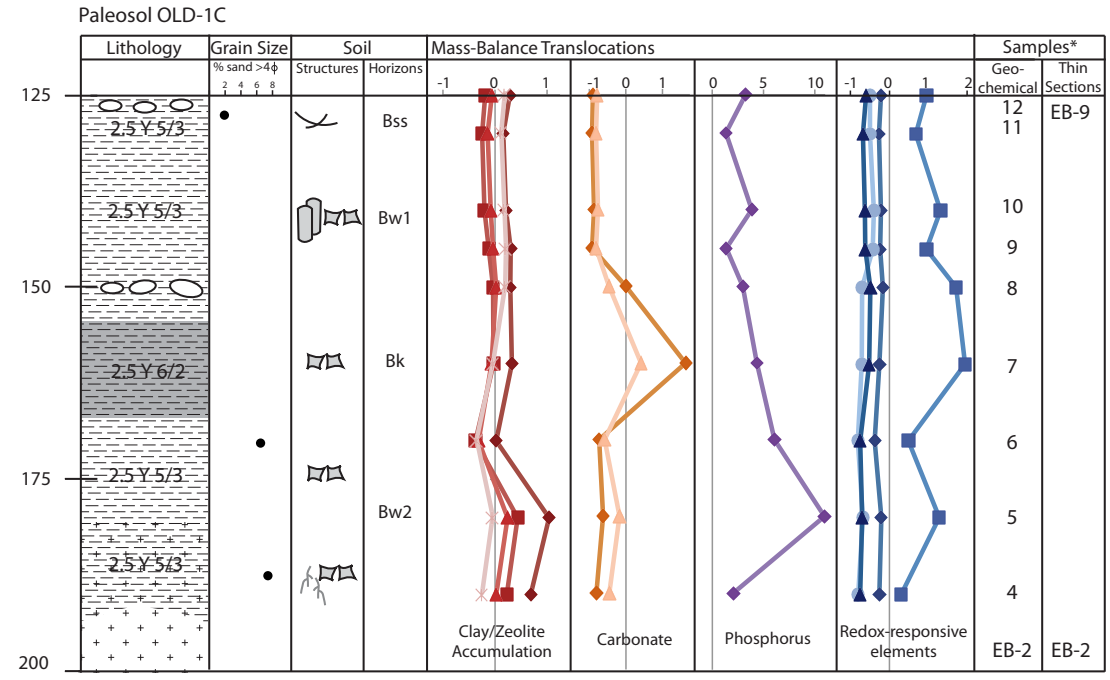

Figure 4.12: Main features of paleo-Vertisol OLD-1C including lithology, stratigraphy, soil structures, soil horizons, Munsell values, mass balance geochemistry, and sample locations. Refer to Fig. 2.3 for stratigraphic location and Fig. 4.2 for legend. *Unless otherwise indicated samples refer to EB-Chem-XX samples.

lapilli, which increase in abundance near the base of the paleosol (Fig. 4.11C). Beneath the thin discontinuous tuff is a thin 10 cm bed of olive waxy clay (5Y4/4) with no obvious pedogenic features, which was deposited on top of the Ng'eju Tuff (Fig. 4.11B). The bed contains abundant organic material that can be seen in further detail in thin-section.

Trench OLD-2

Trench OLD-2 is located in HWK-E and is 736 m southeast of Trench OLD-1 and almost 1 km from Trench OLD-3 (Figs. 2.1C and 2.3). The Trench is 2.65 m deep and contains one cumulative paleosol interval (135 cm thick) that is situated directly beneath Tuff IF (Figs. 4.13A and 4.14). It is likely that two Vertisols formed within this interval one approximately 45 cm thick and another 90 cm thick, but as no complete soil profile can be identified, these paleosols are classified as cumulative. Pedogenic slickensides are abundant throughout the paleosol. The top 5 cm contain an abundance of carbonate concretions ~10 cm in diameter. The top 25 cm is olive gray (5Y5/2) clay with angular blocky peds forming a weak Bk horizon (Figs. 4.13D and 4.14). The Bw1 horizon (25 to 35 cm depth) is characterized by both platy and angular blocky peds, an olive (5Y5/3) color, and a concentration of Mn oxide-filled root traces ranging from 1 to 5 mm in length. The concentration of these root traces and the addition of pyroclastic material in this horizon not found below both suggest that this (25-35 cm) may have been the boundary between two distinct paleosols.

Subangular blocky peds with secondary angular blocky peds characterize the light olive brown (2.5Y5/3) Bw2 horizon (35 and 55 cm). In the Bss1 horizon (55 to 75 cm depth), ped shape is more elongate and forms columnar peds with secondary angular

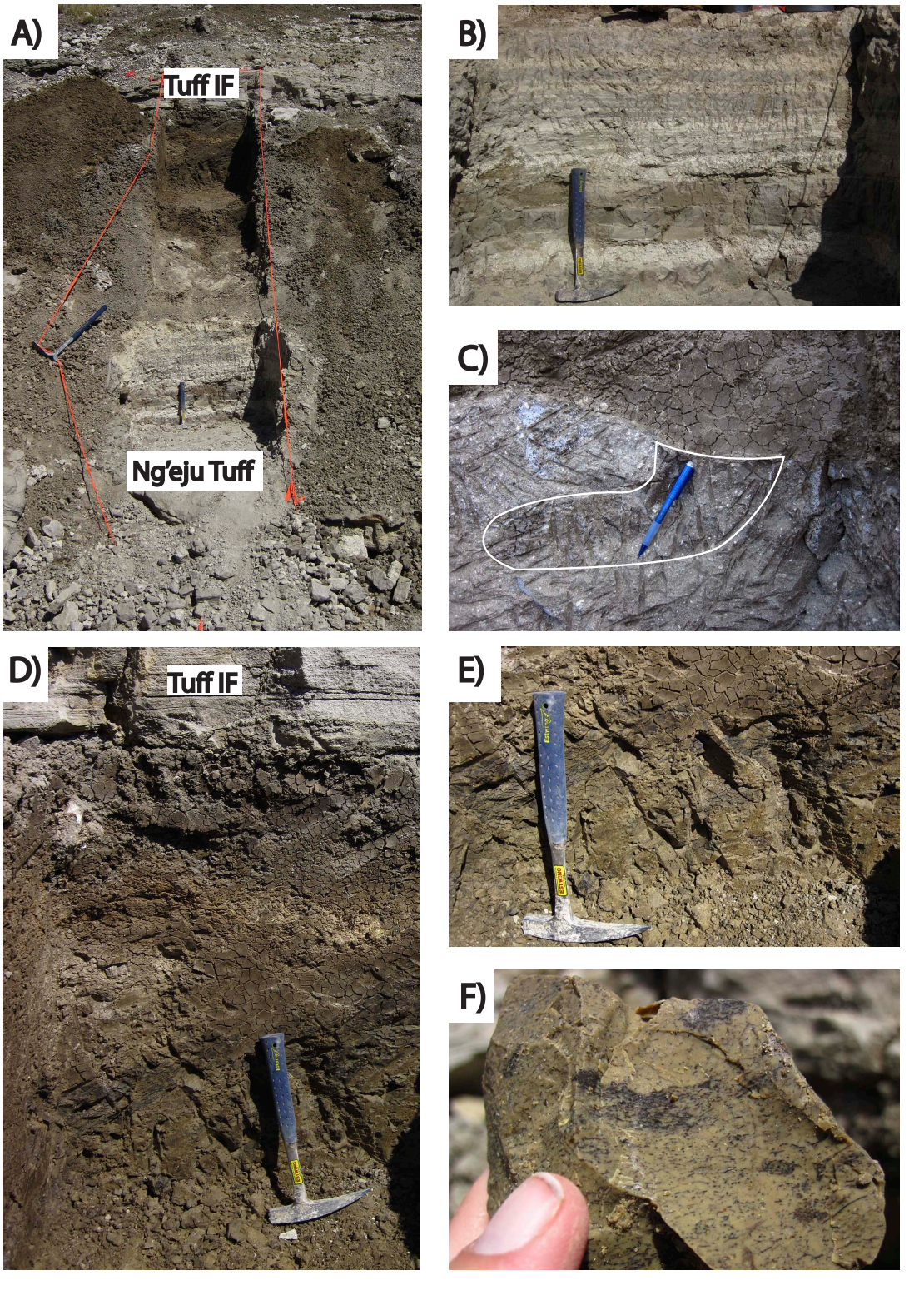
A)
Tuff IF
Ng'eju Tuff
B)
C)
D)
Tuff IF
E)
F)

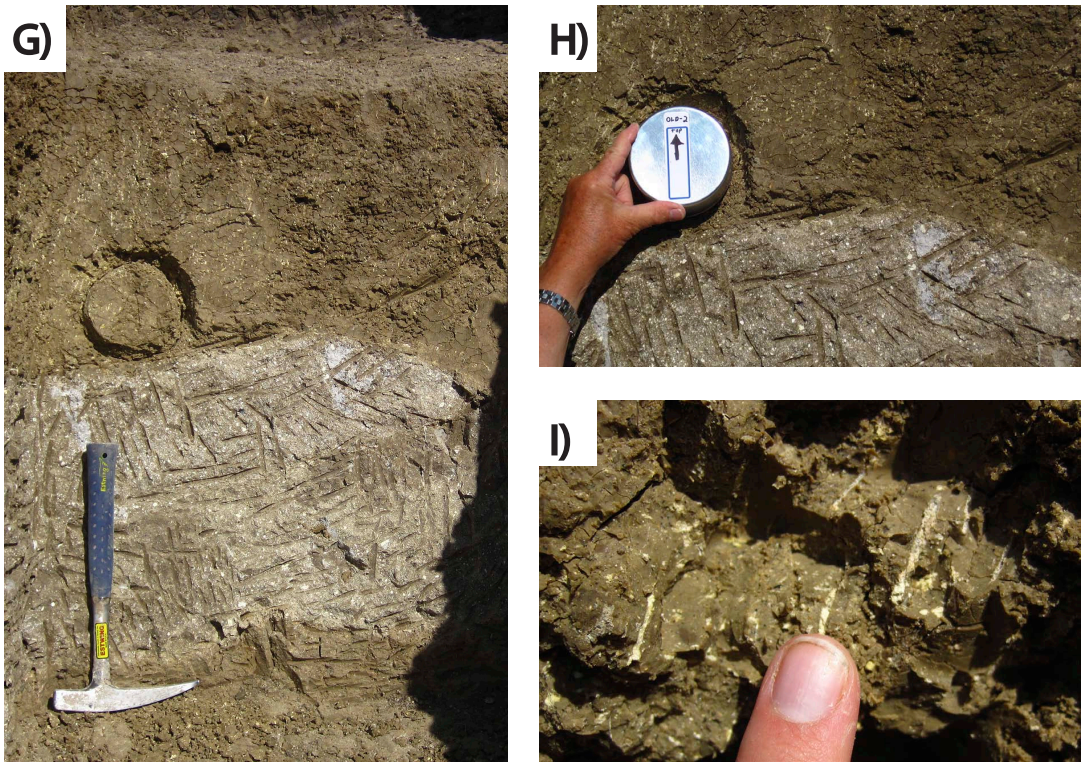

Figure 4.13: Photographs of Trench OLD-2, which contains one cumulative paleo-Vertisol. A) Overall view of trench OLD-2 with Tuff IF and Ng'eju Tuffs marked; paleopick for scale (0.6 m in length). B) 75 cm thick package of tuff above Ng'eju Tuff with alternating beds of lapilli and ash fall; hammer for scale. C) 40 cm thick reworked volcaniclastic sediment; burrow outlined in white. D) Upper section of Vertisol capped by Tuff IF; hammer for scale. E) Close-up of color changes seen at the bottom of Fig. 4.13D. F) Color changes caused by clusters of small Mn oxide filled root traces concentrating in layers as seen here. G) Boundary between Vertisol and volcaniclastic sediment. H) Close-up of boundary with sampling container for collection of oriented thin sections. I) Close-up of zeolitized lapilli and zeolite-filled root traces found throughout the lower section of the Vertisol.

blocky peds (Fig. 4.13E). There is a color change as well from light olive brown (2.5Y5/3) to a light yellowish brown (2.5Y6/3) (Fig. 4.13D and E). The Bss2 horizon features a slight color change to a light olive brown (2.5Y5/3), and the Mn-filled root traces (Fig. 4.13F) are highly concentrated between 75 and 85 cm, but ped shape is consistent. The Mn oxide-filled root traces disappear abruptly at 85 cm depth, (Bss3 horizon). Between 95 and 135 cm, there is a gradational contact where the paleosol

becomes more volcaniclastic rich that is classified as Bw3 horizon (Figs. 4.13G and H). Zeolites fill many small root traces, which range from 0.5 to 2 cm in length, and many of the lapilli are zeolitized as well (Fig. 4.13I). These features coincide with a change to angular blocky peds and a light olive brown color (2.5Y5/4). Below the paleosol is a 40 cm thick bed of volcaniclastic-rich reworked sediment containing a large burrow. The

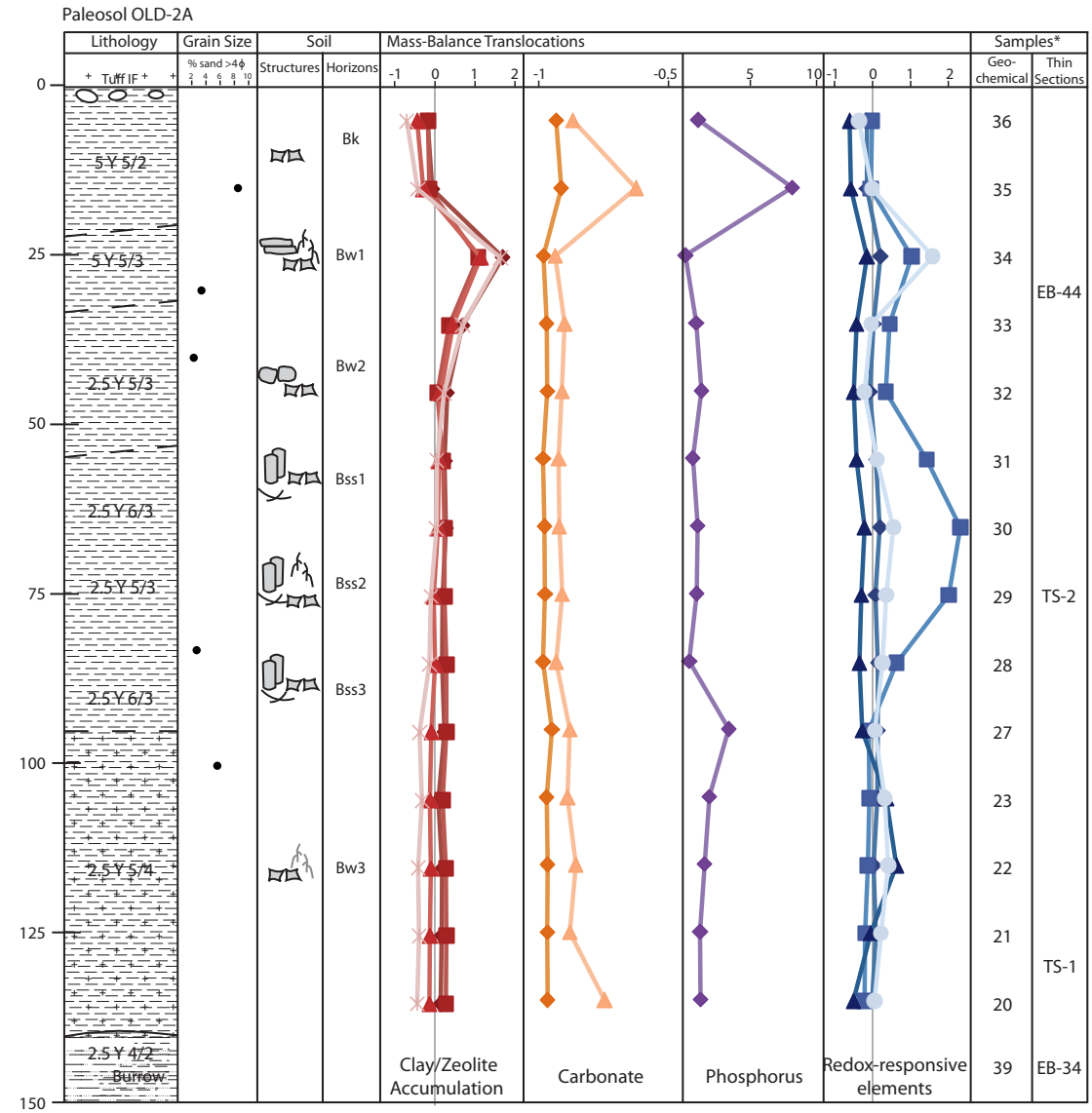

Figure 4.14: Main features of paleo-Vertisol OLD-2A including lithology, stratigraphy, soil structures, soil horizons, Munsell values, mass balance geochemistry, and sample locations. Refer to Fig. 2.3 for stratigraphic location and Fig. 4.2 for legend. *Unless otherwise indicated samples refer to EB-Chem-XX

burrow is a mixture of volcaniclastic sediment and the waxy paleosol clay from above (Fig. 4.13C). Beneath the volcaniclastic bed is a thin (12 cm) bed of waxy clay with pedogenic angular blocky peds and slickensides (Fig. 4.13G). Under the waxy clay is an 80 cm thick bed of tephra with alternating layers of lapilli and ash fall. The thick tephra directly overlies the Ng'eju Tuff (Fig. 4.13B).

Micromorphologic Features

Trench OLD-3

Three thin sections were prepared from Trench OLD-3 from both the paleosol and thin discontinuous tuff beneath it. The Bw horizon is volcaniclastic-rich, with an irregular blocky micro-ped structure (Fig. 4.15A and B) and stress cutans forming around grains (Fig. 4.15C). Most grains show little evidence of alteration and show no evidence of rounding due to transport, but some grains have pitting and alteration along the grain boundary and following cleavage planes and twin lamellae (Fig. 4.15D). The horizon contains little organic matter except for remnants of either a seed or other reproductive plant organ (Fig. 4.15E and F).

The Bss horizon is also volcaniclastic-rich, with irregular blocky micro-ped structure (Fig. 4.16A). With the exception of those zeolitized (Fig. 4.16B), most grains show almost no alteration and are very angular. Compared to the Bw horizon, the stress cutans are weakly developed and no organic matter was identified. Zeolite-filled root traces were identified similar to those found in the Bw horizon (Fig. 4.16D). Below paleosol OLD-3A is a thin, discontinuous tuff with abundant phenocrysts partially altered to clay, and reworked fragments (Fig. 4.17).

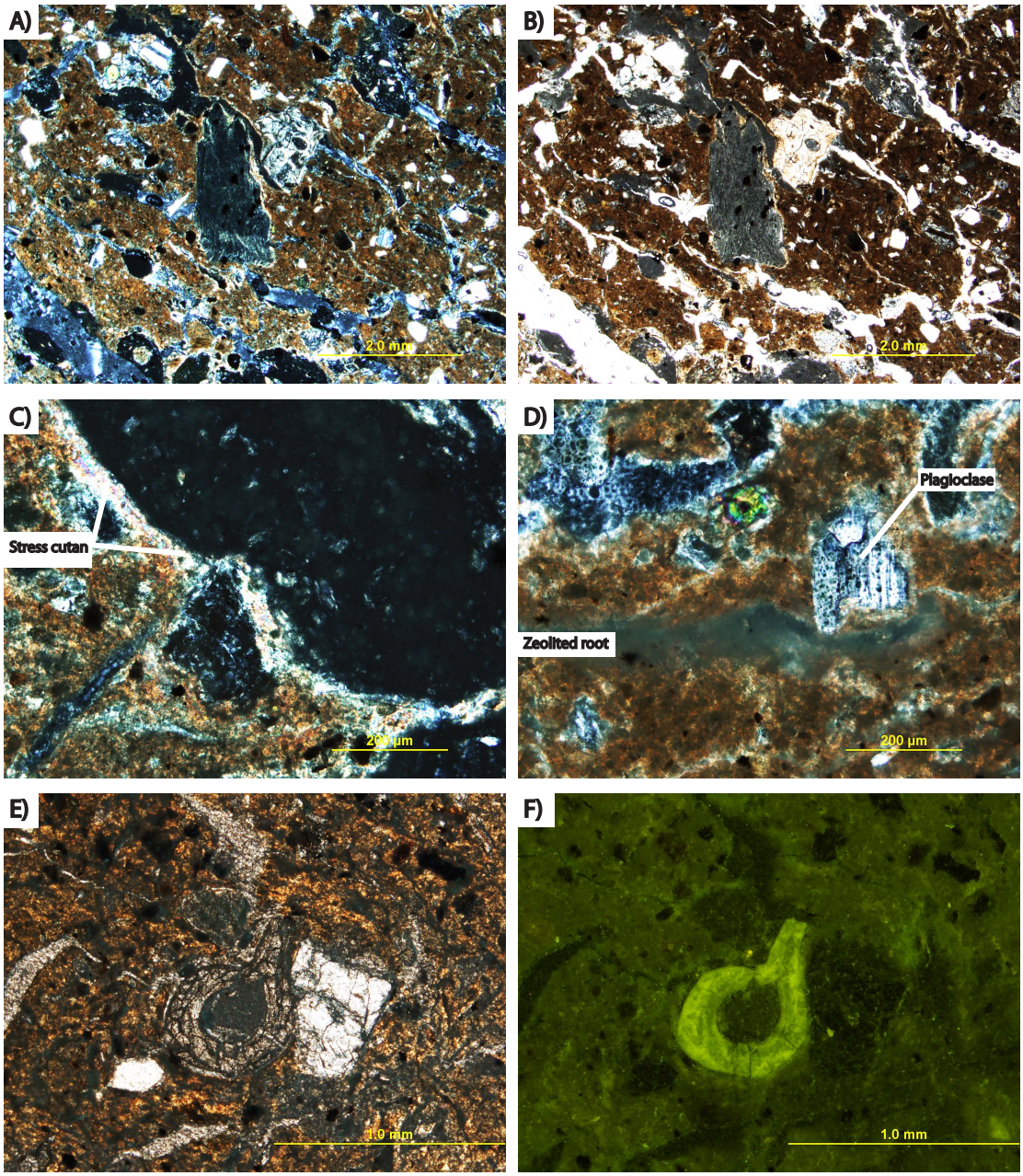

Figure 4.15: Photomicrograph of thin section TS-3 from the Bw horizon of paleosol OLD-3A. See Fig. 4.2 for stratigraphic location. A) Volcaniclastic-rich matrix; 1.25x XPL. B) Same view that better illustrates irregular blocky micro-ped structure; 1.25x PPL. C) Close-up of highly birefringent clay forming stress cutan around zeolitized grain in A and B; 10x XPL. D) Plagioclase grain showing evidence of pitting and zeolitized root trace; 10x XPL. E,F) Little to no organic matter in matrix except for either small seeds or fragments of reproductive plant organs; 4x XPL. (E) 4x NB Filter (F).

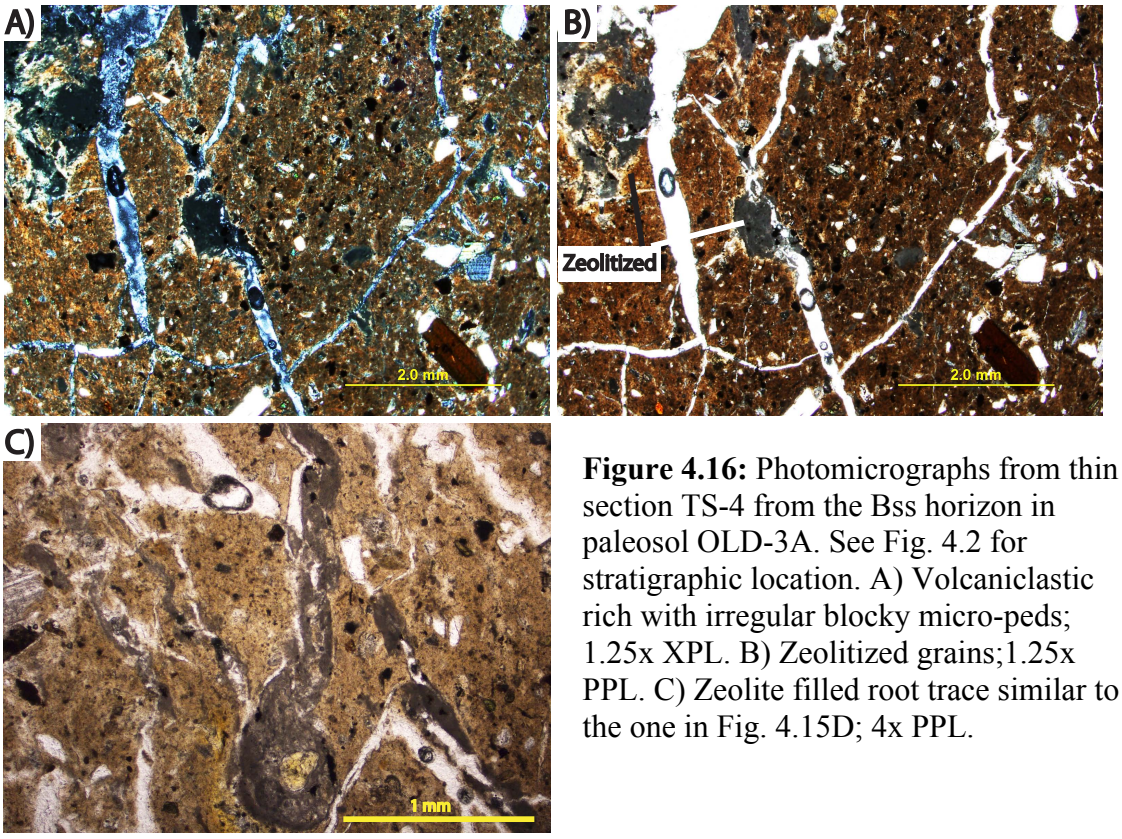

Figure 4.16: Photomicrographs from thin section TS-4 from the Bss horizon in paleosol OLD-3A. See Fig. 4.2 for stratigraphic location. A) Volcaniclastic rich with irregular blocky micro-peds; 1.25x XPL. B) Zeolitized grains;1.25x PPL. C) Zeolite filled root trace similar to the one in Fig. 4.15D; 4x PPL.

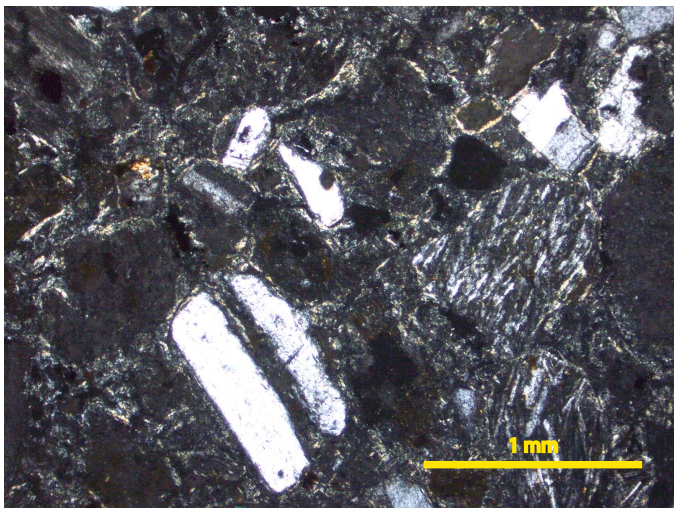

Figure 4.17: Photomicrograph of thin section EB-61 from the thin discontinuous tuff found below paleosol OLD-3A (Fig. 4.2).

Trench FLK-1

One thin section from the upper portion of paleosol FLK-1A (A horizon) was prepared (Fig. 4.4). A very weak insepic fabric and very little pyroclastic materials were identified (Fig. 4.18A). The paleosol matrix also contains an abundance of Mn oxides (Fig. 4.18B) and a weak organic signature throughout the horizon (Fig. 4.18C).

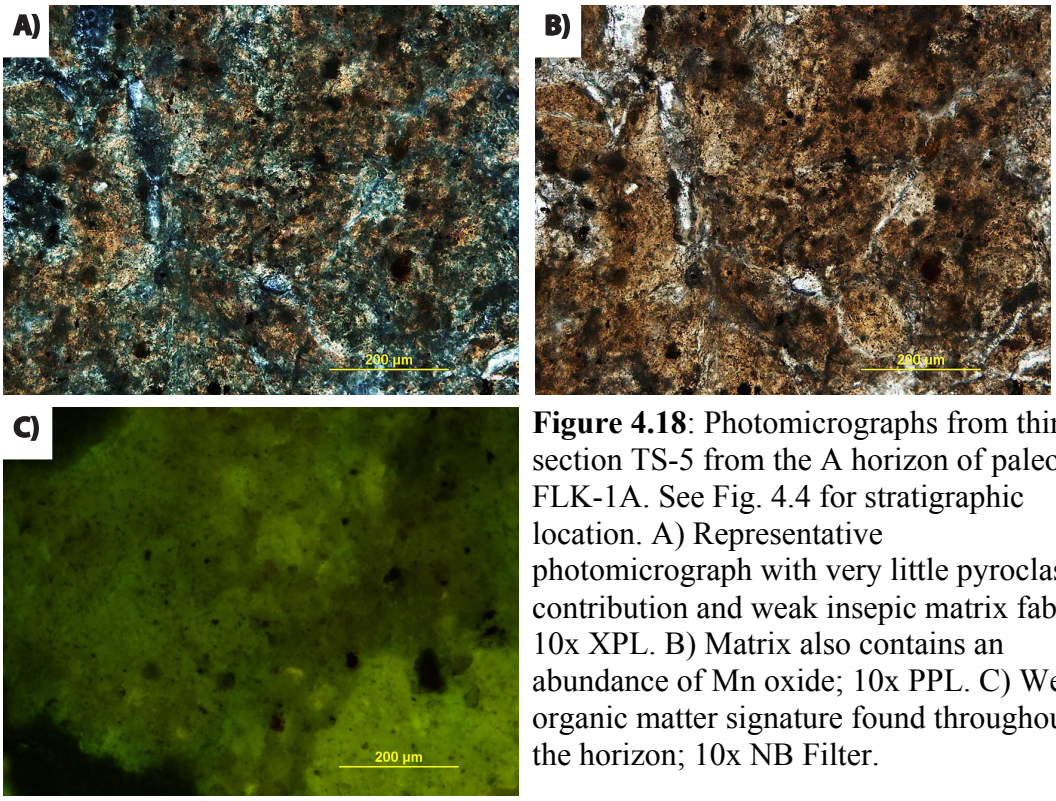

Figure 4.18: Photomicrographs from thin section TS-5 from the A horizon of paleosol FLK-1A. See Fig. 4.4 for stratigraphic location. A) Representative photomicrograph with very little pyroclastic contribution and weak insepic matrix fabric; 10x XPL. B) Matrix also contains an abundance of Mn oxide; 10x PPL. C) Weak organic matter signature found throughout the horizon; 10x NB Filter.

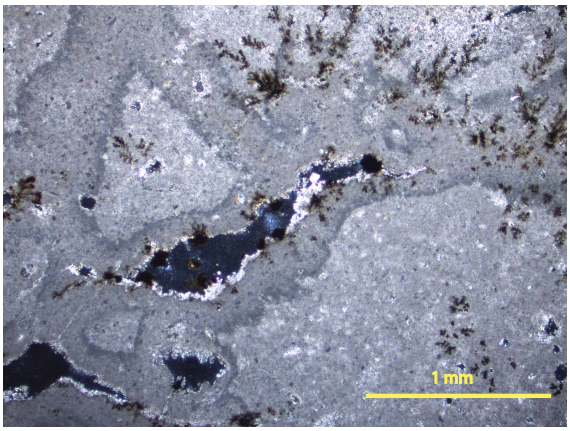

Figure 4.19: Representative photomicrograph of thin section EB-17 from tufa in Trench OLD-1; 4x XPL. See Fig. 4.10 for stratigraphic location. Note multiple phases of carbonate precipitation and dendritic Mn oxides.

Trench OLD-1

Seven thin sections were prepared from various lithologies sampled within Trench OLD-1. The tufa between OLD-1B and B contains minimal clastic contribution. Porosity is rare, but where present it typically shows evidence for another phase of precipitation of tufa (Fig. 4.19). Dendritic precipitation of Mn oxides is found throughout the tufa.

Three thin sections were prepared from paleosol OLD-1B from both the Bss and Bx horizons (See Fig. 4.10 for stratigraphic location of thin sections). The matrix of the Bss horizon has an insepic matrix fabric (Fig. 4.20A) and an irregular blocky micro-ped structure. Grains within the matrix are predominately mafic minerals and are, on average, much smaller than those observed in other paleosols (~100 μm). The grains show little evidence of weathering and are angular in shape. The horizon also has an abundance of Mn oxides in the soil matrix (Fig. 4.20B).

The top of the fragipan (Bx horizon) is characterized by very little clastic input and by an abundance of both Mn oxide-filled root traces (Fig. 4.21A and D) and organic matter (Fig. 4.21A, C, and D). The clay is highly birefringent and oriented parallel to the horizon (Fig. 4.21D). The base of the fragipan is similar to the upper section in that the

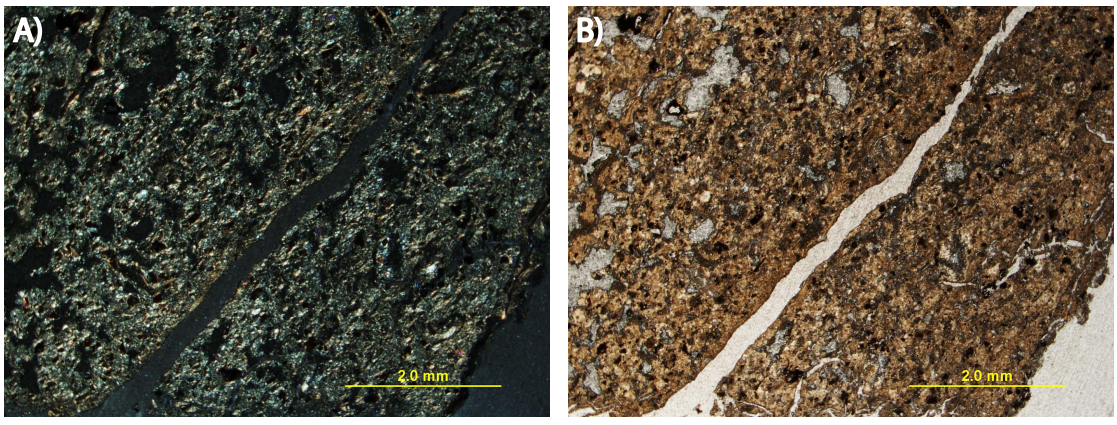

Figure 4.20: Photomicrographs from thin section EB-13 in the Bss2 horizon of Paleosol OLD-1B. A) Insepic matrix fabric; 1.25x XPL. B) Abundant Mn oxides in soil matix; 1.25x PPL.

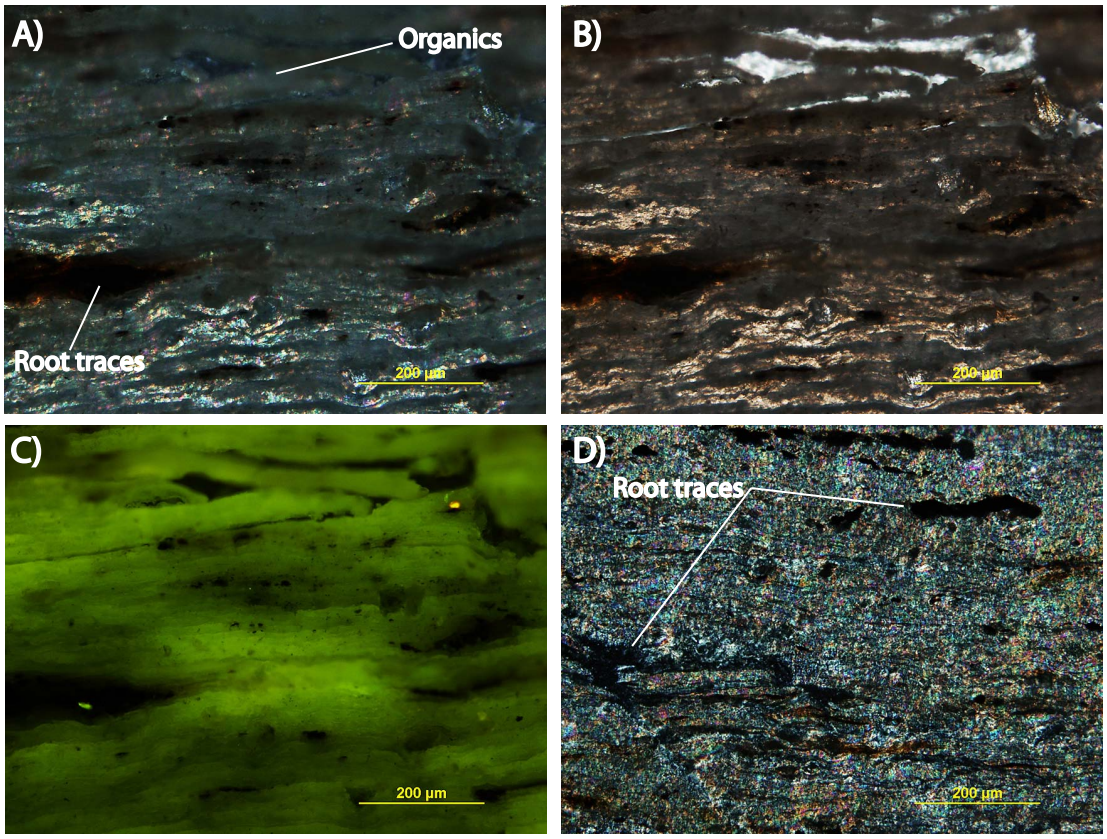

Figure 4.21: Photomicrographs of thin section EB-12 from upper portion of fragipan in paleosol OLD-1B. See Fig. 4.10 for location in profile. A) High concentrations of Mn oxides in root traces and abundant opaque organics; 10x XPL. B) High concentrations of Mn oxides in root traces; 10x PPL. C) Same view as 4.17A and B with fluorescence of abundant organic matter; 10x NB Filter. D, E) Highly birefringent clay and Mn oxide root races; 10x XPL (D), 10x PPL (E).

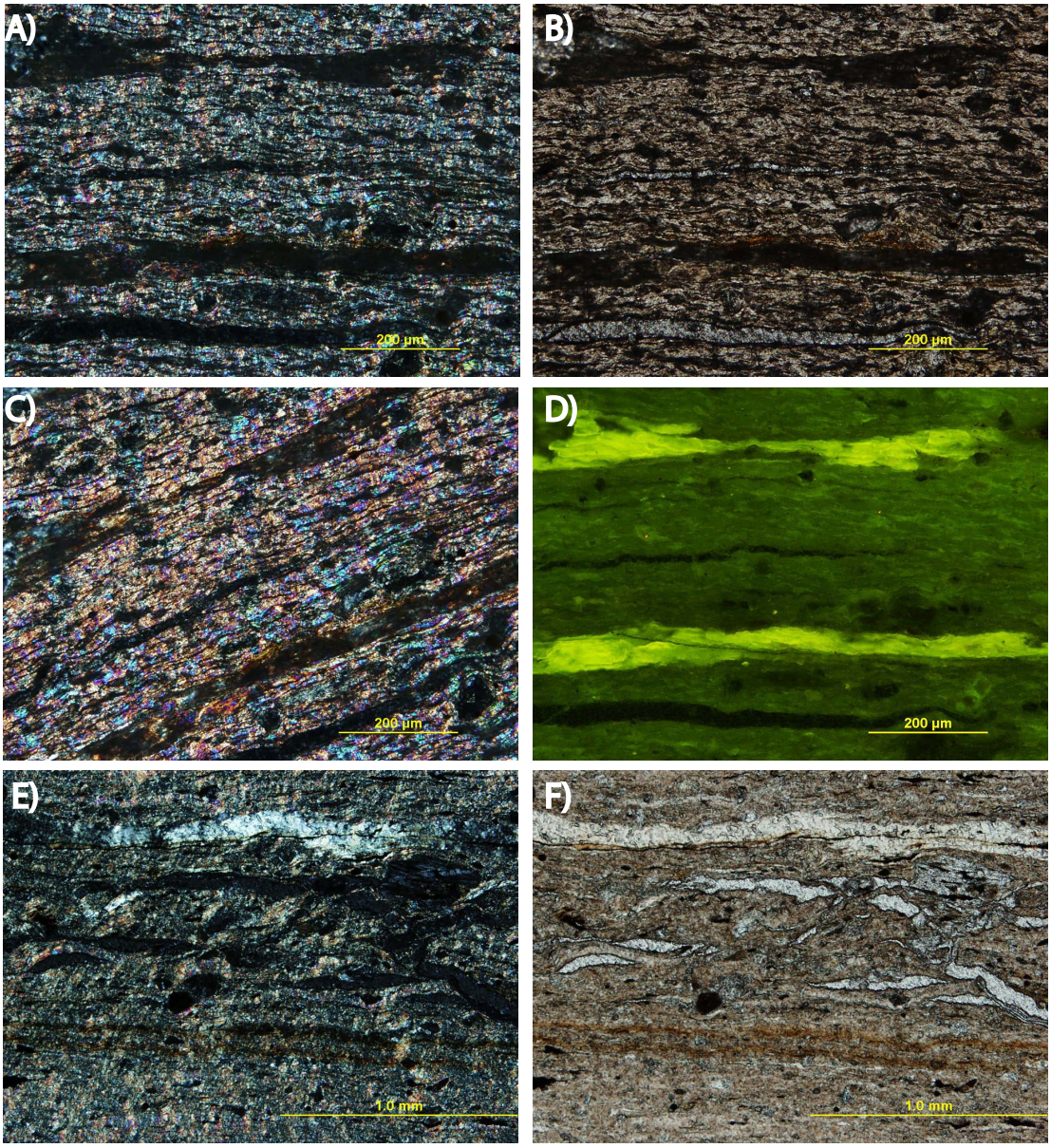

Figure 4.22: Photomicrographs of thin section EB-11 from fragipan at base of paleosol OLD-1B. See Fig. 4.10 for location in profile. A, B) Oriented and highly birefringent clays characteristic of the fragipan; 10x XPL (A), 10x PPL (B). C) Same view as 4.18A and B with stage rotated to demonstrate birefringence; 10x XPL. D) Organic matter concentrated in layers; 10x NB Filter. E, F) Photomicrograph of concentrations of red Mn oxide shown in photograph in Fig. 4.9C; 4x XPL.

clay is highly birefringent, but organic matter is more distinctly concentrated in layers (Fig. 4.22A, C, and D). The concentration of Mn oxide depicted in Fig. 4.9C can be observed in photomicrographs as well. At this scale, the fragipan shows no evidence for micro-ped or other pedogenic structures.

Between paleosols OLD-1B and C, the thin discontinuous tuff contains mostly ash with some reworked fragments and phenocrysts of quartz, feldspar, and plagioclase (Fig. 4.23). The ash is heavily weathered and stained by Fe oxides. Paleosol OLD-1C is characterized by a skelsepic matrix fabric and stress cutans surrounding both Mn oxide-filled root traces (Fig. 4.24C and D) as well as volcaniclastic grains. The volcaniclastic grains are composed of feldspar, plagioclase, and quartz, which are angular and show little evidence of weathering. Irregular blocky micro-ped structure formed in OLD-1C with sesquans along the ped boundaries (Fig. 4.24D).

Below paleosol OLD-1C is another thin, discontinuous tuff with similar characteristics and composition to the tuff in Fig. 4.19, but this tuff shows much greater alteration. Both reworked ash fragments and phenocrysts show alteration to clay along the edges of most grains (Fig. 4.25). The thin, non-pedogenic waxy clay present at the

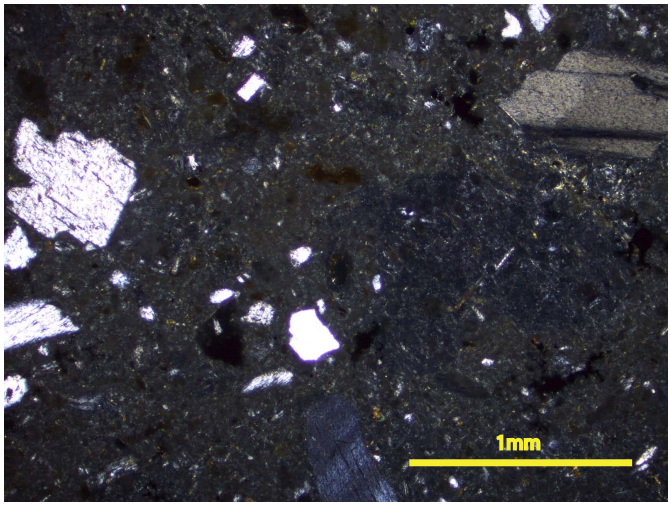

Figure 4.23: Representative photomicrograph of thin section EB-10, a thin discontinuous tuff between paleosols OLD-1B and C; 4x XPL. See Fig. 2.3 for stratigraphic location.

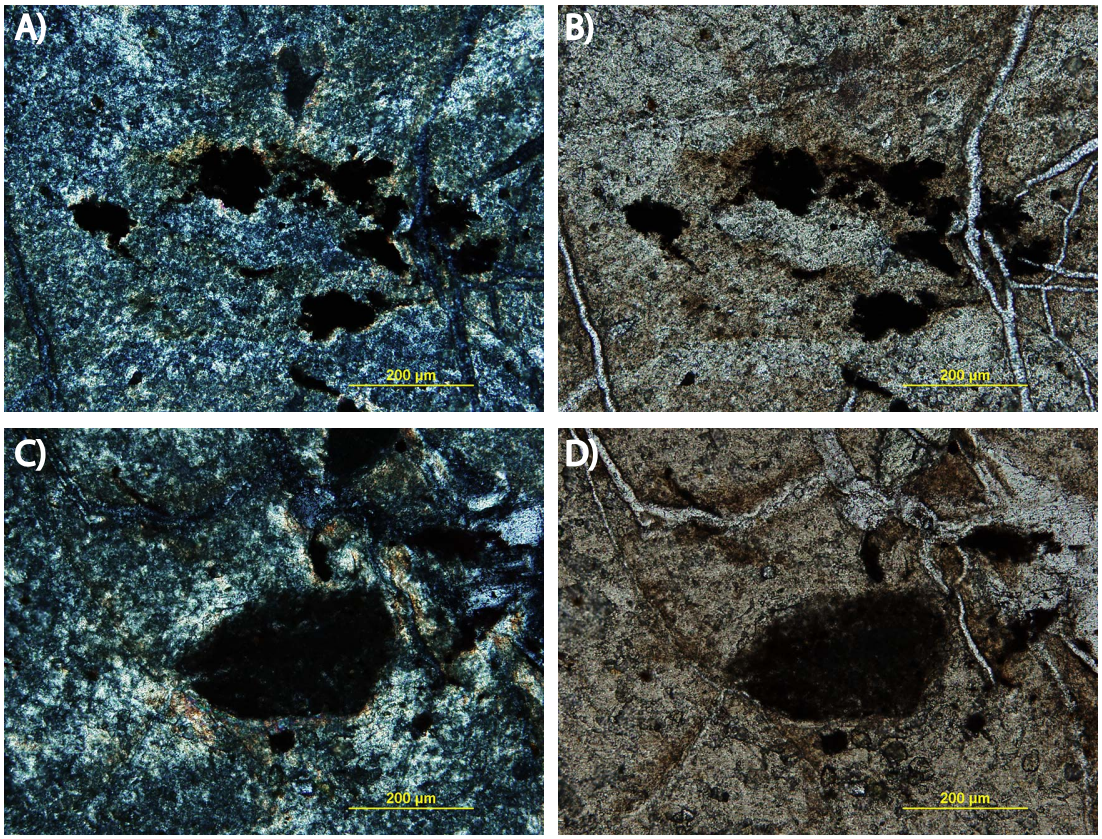

Figure 4.24: Photomicrographs of thin section EB-9 from Bss horizon of paleo-Vertisol OLD-1C. See Fig. 4.12 for location in profile. A) Birefringent clay surrounding Mn oxide precipitated in small root trace; 10x XPL. B) Irregular blocky micro-ped structure, 10x PPL. C) Cross section of Mn oxide root trace with stress cutan; 10x XPL. D) Irregular blocky micro-ped structure with sesquans along ped boundaries; 10x PPL.

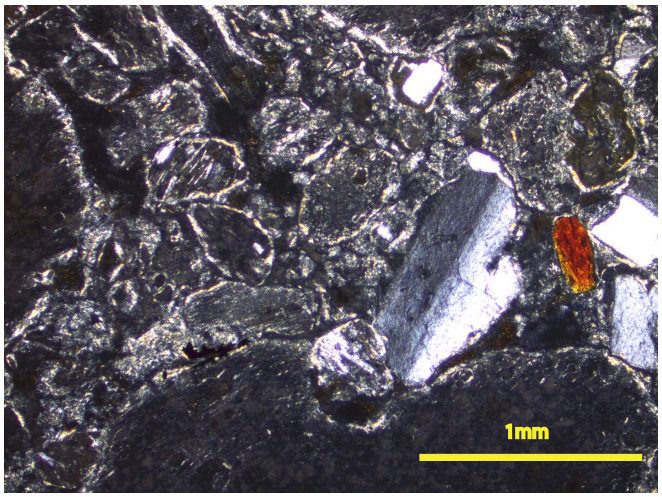

Figure 4.25: Representative photomicrograph of thin section EB-2 , a thin discontinuous tuff below paleosol OLD-1C; 4x XPL. See Fig. 4.12 for stratigraphic location. Most grains show alteration and weathering to clay along the edge.

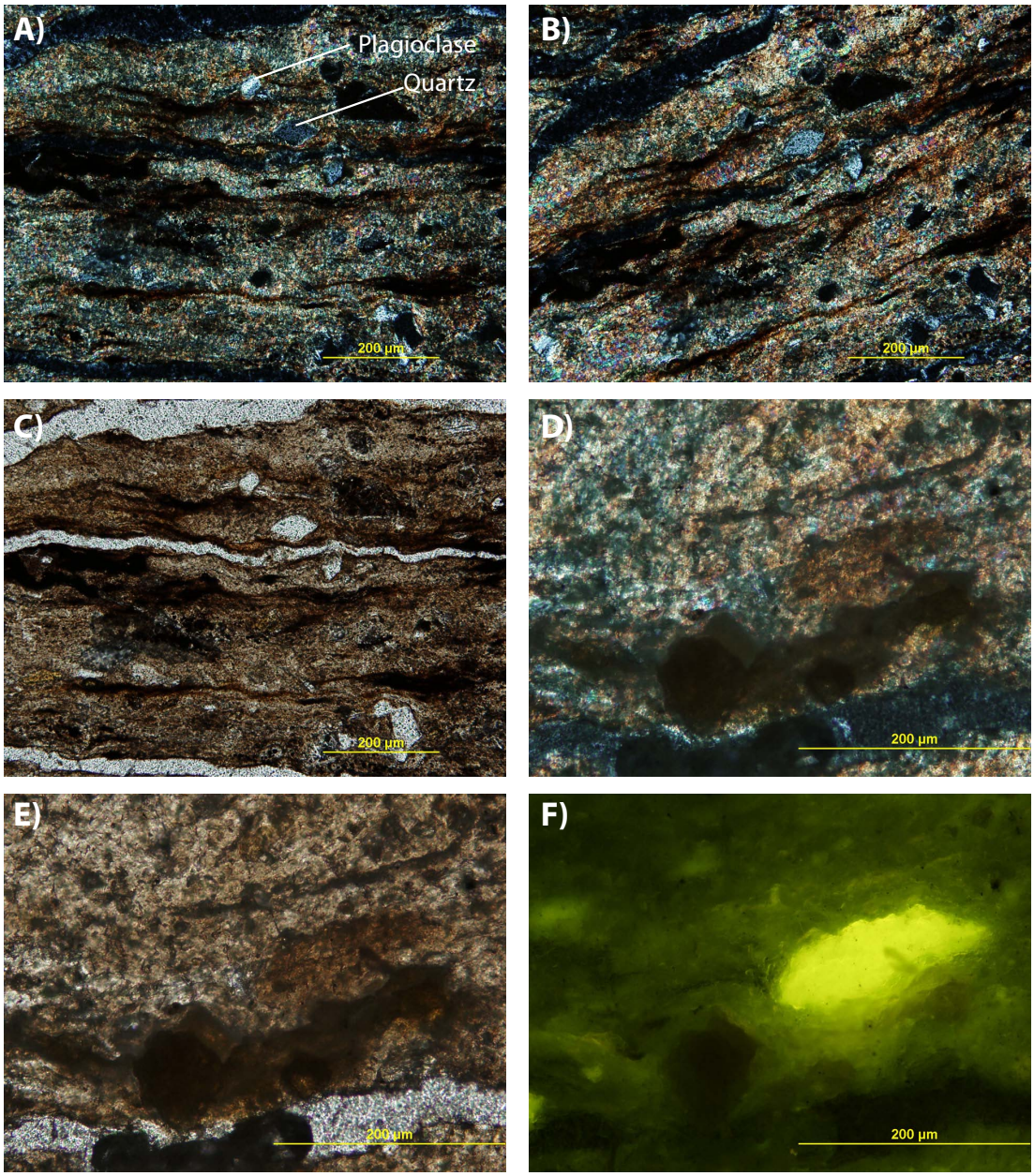

Figure 4.26: Photomicrographs from thin section EB-1 in the thin non-pedogenic bed found at the base of Trench OLD-1 (See Fig. 2.3). A) Oriented clay with high birefringence and grains of quartz and plagioclase found throughout; 10x XPL. B) Stage rotated to demonstrate how clays oriented parallel to the horizon; 10x XPL. C) Mn oxides aligned horizontally, 10x PPL. D, E) Close-up of highly birefringent clays; 20x XPL (D), 20x PPL (E). F) Same view as 4.26D and E illustrating organic matter characteristic of this bed unidentifiable without UV fluorescence; 20x NB Filter.

base of Trench OLD-1 shows minimal volcaniclastic contributions consisting mostly of angular grains of quartz and plagioclase with evidence of alteration (Fig. 4.26A). The clay is highly birefringent and oriented parallel to the horizon (Figs. 4.26A and B). Figures 4.26C, D, and E show a close-up view of this clay and the abundance of organic matter found throughout this bed (Fig. 4.26F).

Trench OLD-2

Five thin sections were prepared from various lithologies sampled within Trench OLD-2 (See Fig. 4.14 for stratigraphic locations). The matrix fabric is both weakly insepic and skelsepic with stress cutans surrounding both root traces (Fig. 4.27A) and grains. Grains show little evidence of weathering and are angular in shape. This Bw1 horizon also shows evidence for a complex history of soil moisture conditions. Root voids were first lined with Mn oxide and then zeolite crystals (Fig. 4.27B). Micro-peds have an irregular blocky shape, and little to no organic matter is present.

The Bss2 horizon also has evidence for a skelsepic fabric with stress cutans

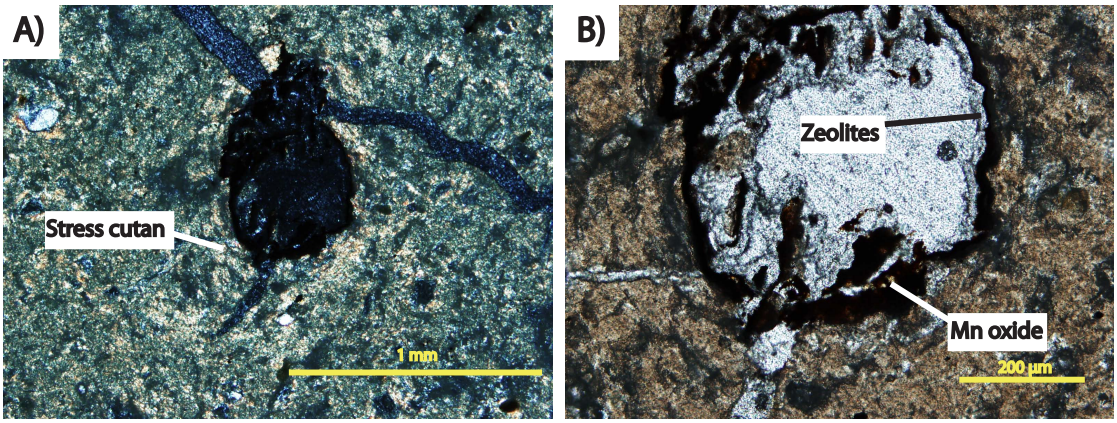

Figure 4.27: Photomicrographs of thin section EB-44 from the Bw1 horizon of paleosol OLD-2A. See Fig. 4.14 for stratigraphic location. A) Weakly birefringent matrix fabric with a stress cutan surrounding a root trace; 4x XPL. B) Close-up of root trace with complex history. First lined with Mn oxide and then zeolite crystals; 10x PPL.

surrounding both grains and root traces as well as a generally masepic fabric (Figs. 4.28A-C). This horizon also contains volcaniclastic-rich pedorelicts (Figs. 4.28A and B). Although there is no evidence for multiple phases of soil moisture conditions in this horizon, minerals were precipitated along ped faces with irregular blocky structure (Fig. 4.28D). These minerals do not have the characteristic crystal habits of zeolites and may either be carbonate or evaporite precipitates. This horizon contains little to no organic matter (Fig. 4.28E).

The lowest horizon (Bw3) is very different from the horizons above (Fig. 4.29). The horizon is rich in volcaniclastic material with an insepic matrix fabric, and although stress cutans can be identified, they are less numerous than in the horizons above. Pedorelicts are similar to the surrounding matrix, but are much darker in color (Fig. 4.29A). Volcaniclastic grains show evidence of weathering along the grain boundaries and pitting (Fig. 4.29B). In addition, sesquans have formed around grains and along ped boundaries in some cases (Figs. 4.29B and C). Irregular blocky micro-ped structure is common and in some cases, clay and silt filled in cracks between two peds (Fig. 4.29E and F). This horizon contains the highest amount of organic matter compared to that in any other horizon within paleosol OLD-2A (Fig. 4.29D), but it is still significantly less than paleosols within Trench OLD-1.

Below paleosol OLD-2A is a volcaniclastic-rich bed, which is composed of reworked tuff and clay. The grains are relatively unweathered and the clay is highly birefringent (Fig. 4.30). Trench OLD-2A also contains a thick tuff with alternating layers of ash and lapilli. The tuff is relatively unweathered with both phenocrysts and reworked fragments (Fig. 4.31).

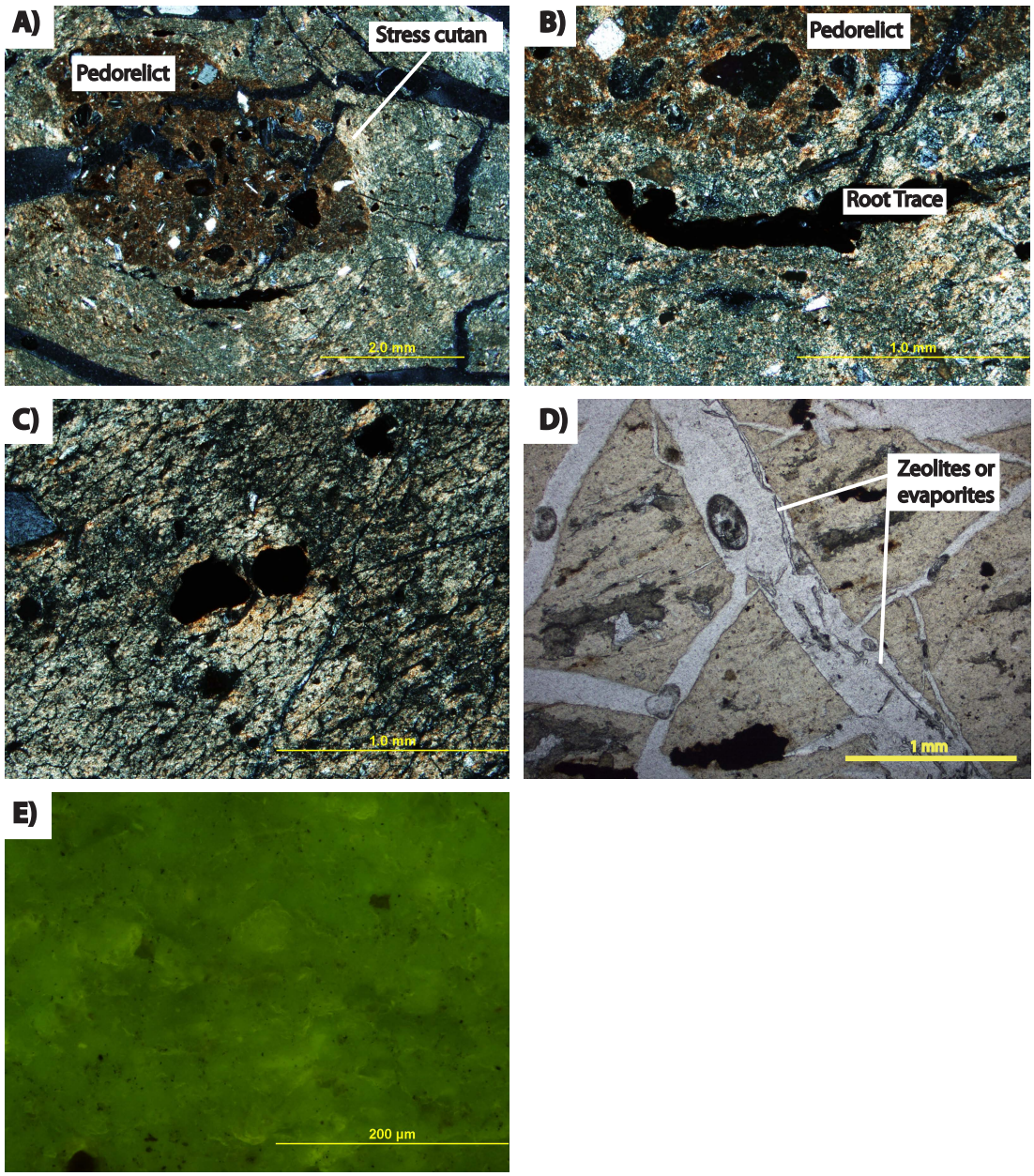

Figure 4.28: Photomicrograph of thin section TS-2 in Bss2 horizon in paleosol OLD-2A. See Fig. 4.14 for stratigraphic location. A) Overall view of anisotropic matrix with stress cutan forming around a pedorelict; 1.25x XPL. B) Close-up of volcaniclastic-rich pedorelict and matrix boundary and Mn-oxide filled root trace; 4x XPL. C) Highly birefringent clay aligned in a mosepic fabric with another stress cutan surrounding Mn oxide filled root trace. D) Zeolites or possibly evaporites precipitating along faces of irregular blocky micro-peds. E) Little to no organic matter; 20x NB Filter.

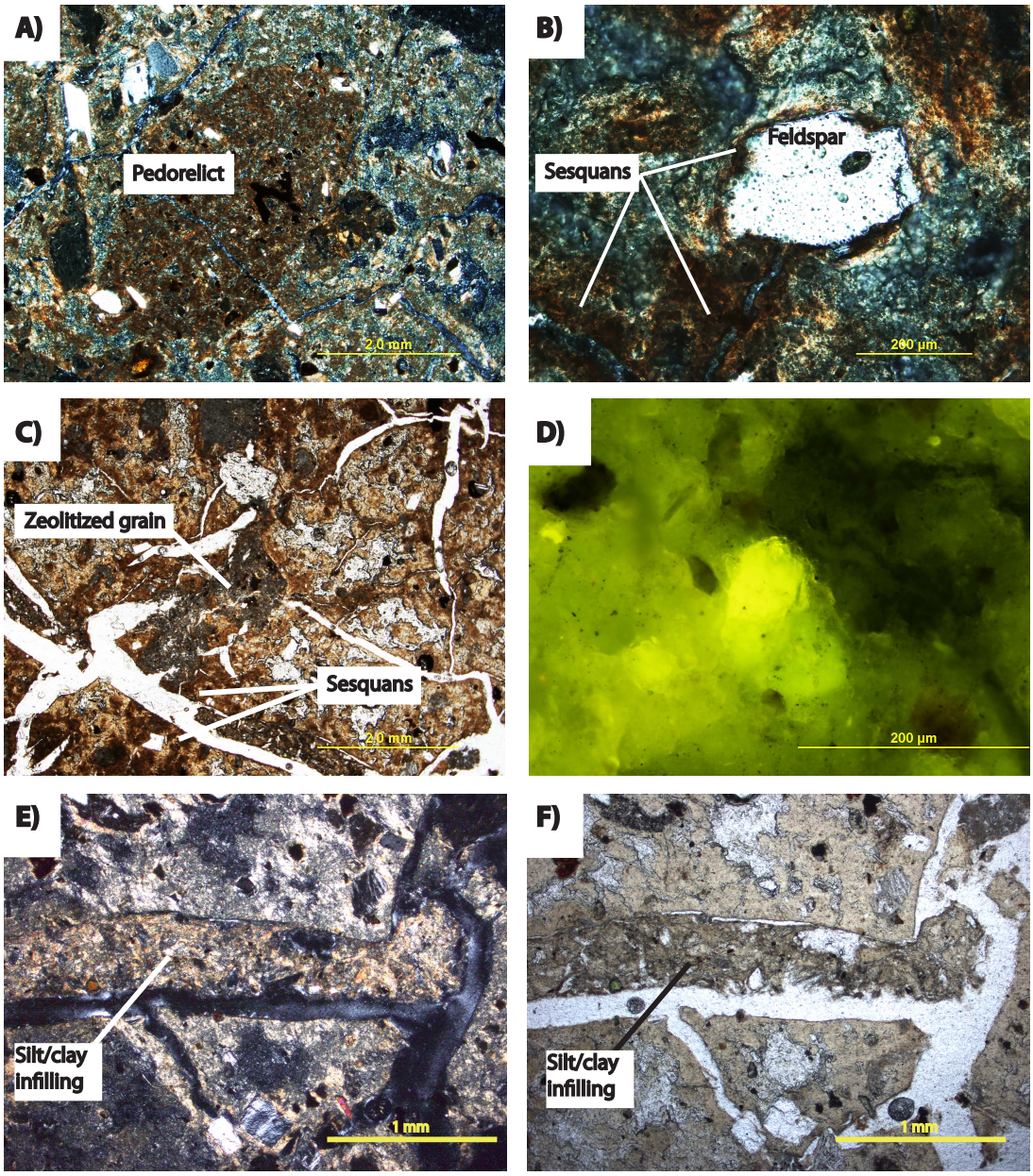

Figure 4.29: Photomicrographs of thin section TS-1 from paleosol OLD-2A. See Figure 4.14 for stratigraphic location. A) Pedorelict within a matrix full of volcaniclastic material; 1.25x XPL. B) Grain of feldspar showing evidence of pitting and sesquans around the grain and also along ped boundaries; 10 XPL. C) Volcaniclastic-rich matrix with irregular blocky micro-ped structure, sesquans along ped boundaries, and zeolitized grain in the center; 10x PPL. D) Slight amounts of organic matter, but not abundant; 20x NB Filter. E,F) Silt/clay filling in the space between two peds; 4x XPL (E), 4x PPL (F).

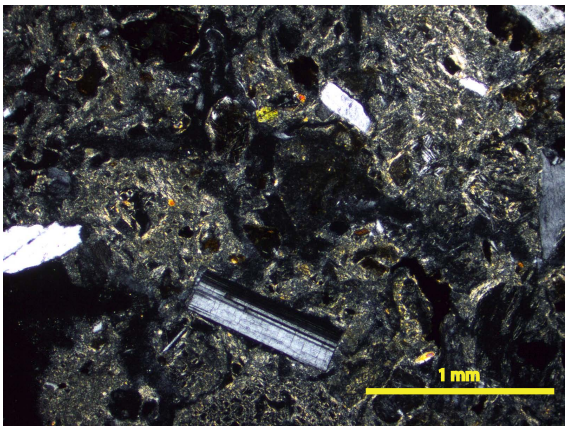

Figure 4.30: Photomicrograph of thin section EB-34 of volcaniclastic-rich sediment found at the base of paleosol OLD-2A. See Fig. 4.14 for stratigraphic location. The reworked volcaniclastic sediment contains abundant unweathered grains and highly birefringent clays.

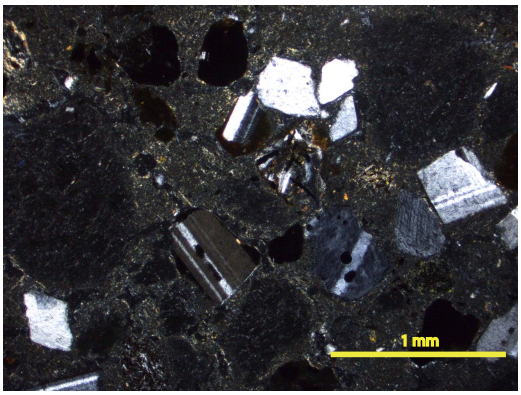

Figure 4.31: Photomicrograph of EB-29 from the 40 cm thick tuff found directly above Ng'eju Tuff in Trench OLD-2. See Fig. 4.14 for stratigraphic location.

Grain Size and Grain Composition

The amount of the sand-sized fraction increases with depth from 8.1% to 15.1% in paleosol OLD-3A (Fig. 4.2). The upper sample has a range of sizes from coarse to medium sand. The middle of the paleosol is very fine sand-sized and well sorted with an abundance of volcaniclastic material, whereas the lower samples are poorly sorted and with range of sand sizes from fine to coarse and contain less volcaniclastic material. The percentage of the sand-sized fraction increases with depth from 15.7 to 20.3% in paleosol FLK-1B (Fig. 4.5). The samples are poorly sorted with very coarse- to coarse-sized sand and the amount of volcaniclastic material decreases with depth. Paleosol OLD-1A has decreasing amounts of sand > 4ϕ with depth (Fig. 4.8) as well as grain size changes. The

upper sample is fine- to very fine sand-sized and is well sorted, but the grain size increases to medium sand that is moderately sorted with depth. Paleosol OLD-1B has fine sand-sized grains, which are well sorted, and has little to no change in the amount of sand-sized grains with depth but significant changes in mineral abundances (Fig. 4.10). The paleosol is very volcaniclastic-rich in the upper portion of the fragipan but decreases with depth. Paleosol OLD-1C is more poorly sorted and has increasing amounts of sand-sized grains with depth, from 1.9% up to 7.4% (Fig. 4.12) with the upper horizons being richer in volcaniclastic material. The highest percentages (~8%) of the sand-sized fraction are found at the top and bottom of paleosol OLD-2A (Fig. 4.14). The majority of the paleosol has sand fractions between 2.4 and 3.5%. The paleosol has medium sand-sized grains that are moderately to well sorted in the upper portion of the paleosol, and coarser and poorly sorted in the lower part of the paleosol.

Molecular Weathering Ratios

The comparison of bulk chemistry of paleosols and lithologies identified within this time-slice are presented in Table 4.1. Overall the paleosols geochemically resemble the Loc. 80 lake clay rather closely, although the volcaniclastic-rich sediment, and other waxy clays unmodified by pedogenesis have similar average chemistries. The average chemical composition of tuffs found within the time slice has a very different signature than any of the paleosols (Table 4.1). Molecular weathering ratios of each paleosol and lithology were also calculated to estimate changes in hydrolysis, hydration, salinization, and leaching. The average values for each molecular weathering ratio are shown in Table 4.1 as well as plots versus depth in Figure 4.32. The averaged ratios of hydrolysis,

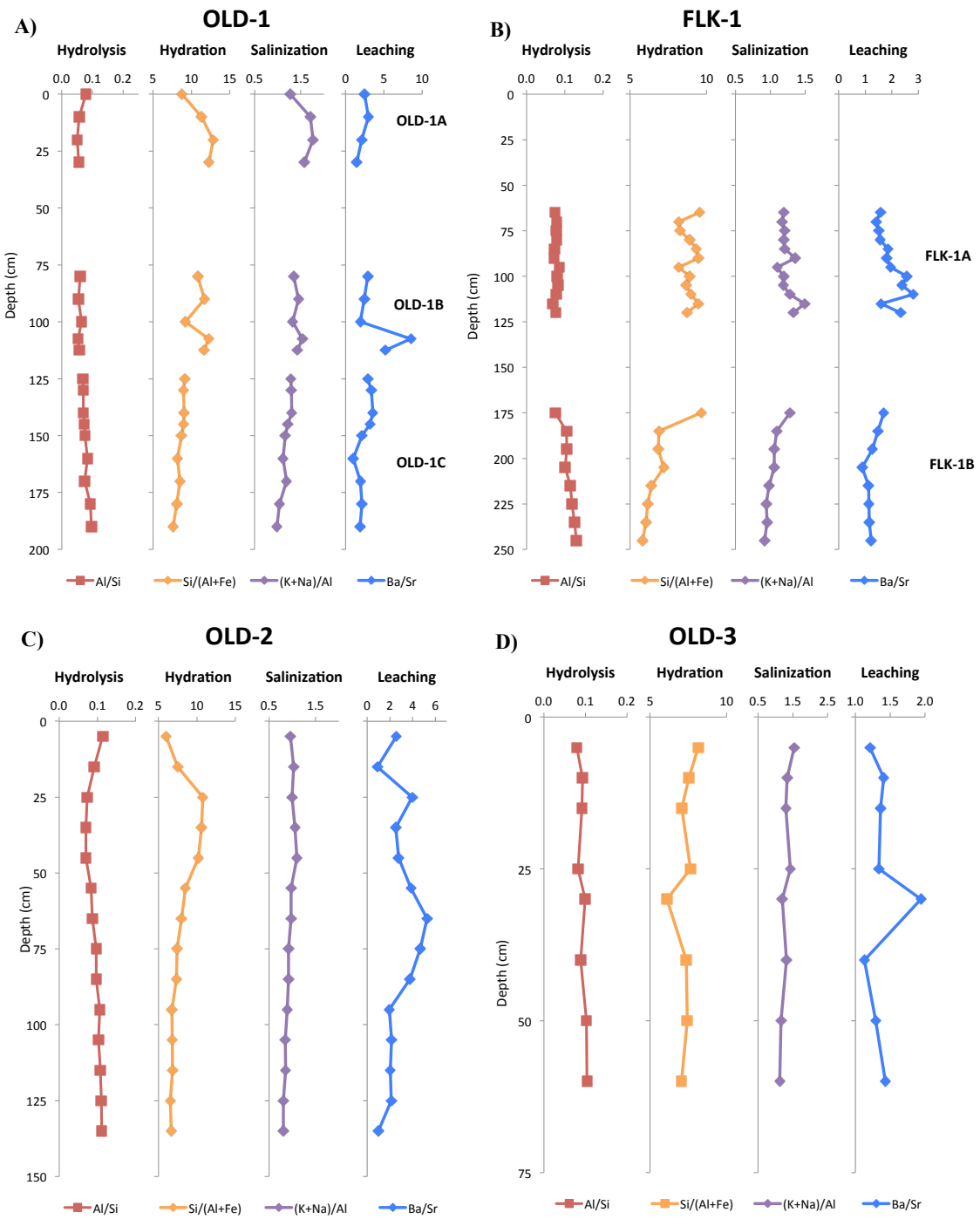

Figure 4.32: Molecular weathering ratios organized by trench and labeled with each paleosol. A) Note increasing molecular weathering ratios up section in Trench OLD-1. B) Molecular weathering ratios also increase up section in Trench FLK-1. C) The paleosol in Trench OLD-2 shows the least amount of salinization and higher ratios in the center of the paleosol. D) The paleosol in Trench OLD-3 overall has lower ratios than any other paleosol found in time-slice.

hydration, and salinization share the most similarities with the Loc. 80 waxy clay with the exception of the leaching ratio (Ba/Sr) (Table 4.1). This is reasonable as a higher leaching ratio is to be expected in a pedogenic setting.

The molecular weathering ratios plotted versus depth show a few general trends. The extent of hydrolysis increases slightly with depth in paleosols identified in both OLD-1 and FLK-1 (Figs. 4.32A and B). Hydration, salinization, and leaching ratios for paleosols in OLD-1 and FLK-1 all decrease with depth. There is no lower paleosol for comparison at OLD-3 (Fig. 4.32D), but the molecular weathering ratios are similar to those calculated for the upper paleosols at OLD-1and FLK-1. OLD-2 has similar values of hydrolysis, hydration, and leaching, but the least amount of salinization compared to other sites (Table 4.1; Fig. 4.32C).

Mass Balance Translocations

Determination of Parent Material

Grain size analyses demonstrated that all of the paleosols have 80% or greater clay/silt-sized fractions. This fine grain size is unlikely to have been produced strictly from pedogenesis and therefore the parent material must have been clay-rich. Because of proximity to the paleo lake margin (Fig. 2.4), this area would have intermittently been flooded, periodically depositing waxy lake clay sediment that then was later pedogenically modified to some degree.

Paleosols in Trenches OLD-1, OLD-3, and FLK-1 are closer to the composition of lake clay compared to any other potential parent material, and all deviate by less than 17%. Other possible parent materials can deviate by up to 900% from the lake clay (Tables 4.2 and 4.3). Suitability of the lake clay parent material can also be demonstrated

Table 4.1 Comparison of bulk chemistries of paleo-Vertisols and other lithologies (all values in given in wt %)

	FLK-1A	FLK-1B	OLD-1A	OLD-1B	OLD-1C	OLD-2	OLD-3	Paleosol Mean	Tuff Mean	Loc. 80 Waxy Clay	Waxy Clay (OLD-1)	Volcaniclastic-rich Sediment
Ba	0.3562	0.5345	0.3568	0.3143	0.4751	0.5289	0.4359	0.4288	0.9360	0.2310	0.3180	1.3540
Ce	0.0940	0.1060	0.1058	0.0651	0.1168	0.1531	0.1409	0.1117	0.1344	0.0894	0.1026	0.1679
Co	0.0105	0.0101	0.0098	0.0126	0.0112	0.0112	0.0141	0.0114	0.0046	0.0090	0.0218	0.0115
Cr	0.0425	0.0338	0.0425	0.0367	0.0310	0.0388	0.0513	0.0395	0.0233	0.0400	0.0300	0.0475
Cs	0.0024	0.0024	0.0026	0.0010	0.0020	0.0048	0.0052	0.0029	0.0026	0.0016	0.0013	0.0049
Cu	0.0333	0.0305	0.0313	0.0460	0.0687	0.0479	0.0405	0.0426	0.0138	0.0930	0.0323	0.0308
Dy	0.0043	0.0052	0.0029	0.0042	0.0051	0.0058	0.0066	0.0049	0.0054	0.0052	0.0034	0.0067
Er	0.0021	0.0027	0.0014	0.0024	0.0025	0.0028	0.0034	0.0025	0.0026	0.0027	0.0015	0.0033
Eu	0.0015	0.0022	0.0013	0.0013	0.0022	0.0021	0.0025	0.0019	0.0027	0.0017	0.0017	0.0030
Ga	0.0137	0.0170	0.0124	0.0107	0.0146	0.0193	0.0183	0.0151	0.0198	0.0117	0.0212	0.0183
Gd	0.0050	0.0064	0.0047	0.0046	0.0074	0.0064	0.0075	0.0060	0.0072	0.0066	0.0056	0.0079
Hf	0.0058	0.0060	0.0069	0.0042	0.0061	0.0081	0.0059	0.0061	0.0076	0.0048	0.0074	0.0072
Ho	0.0008	0.0010	0.0005	0.0009	0.0009	0.0011	0.0013	0.0009	0.0010	0.0010	0.0006	0.0012
La	0.0616	0.0686	0.0464	0.0318	0.0705	0.0881	0.0882	0.0650	0.0789	0.0464	0.0562	0.1013
Lu	0.0002	0.0003	0.0001	0.0002	0.0003	0.0004	0.0004	0.0003	0.0003	0.0003	0.0001	0.0004
Nb	0.1037	0.0852	0.1033	0.0809	0.1019	0.1236	0.1168	0.1022	0.0909	0.0750	0.0610	0.1130
Nd	0.0366	0.0443	0.0309	0.0243	0.0468	0.0520	0.0578	0.0418	0.0483	0.0359	0.0389	0.0633
Pr	0.0106	0.0127	0.0090	0.0066	0.0133	0.0150	0.0161	0.0119	0.0138	0.0097	0.0114	0.0176
Rb	0.0807	0.1018	0.1224	0.0364	0.1059	0.1159	0.0745	0.0911	0.0607	0.1033	0.0365	0.0929
Sm	0.0062	0.0078	0.0053	0.0046	0.0080	0.0087	0.0096	0.0072	0.0087	0.0070	0.0063	0.0103
Sn	0.0017	0.0019	0.0013	0.0013	0.0015	0.0024	0.0015	0.0016	0.0033	0.0010	0.0020	0.0020
Sr	0.1897	0.4496	0.1729	0.1300	0.2388	0.2586	0.3238	0.2519	0.5240	0.7750	0.1538	0.6248
Ta	0.0038	0.0043	0.0038	0.0023	0.0042	0.0057	0.0045	0.0041	0.0080	0.0032	0.0048	0.0058
Tb	0.0008	0.0009	0.0006	0.0007	0.0011	0.0010	0.0011	0.0009	0.0011	0.0010	0.0008	0.0012
Th	0.0077	0.0094	0.0107	0.0079	0.0106	0.0136	0.0117	0.0102	0.0098	0.0152	0.0094	0.0122
Tm	0.0003	0.0004	0.0002	0.0003	0.0003	0.0004	0.0005	0.0003	0.0003	0.0004	0.0002	0.0005
U	0.0023	0.0024	0.0031	0.0057	0.0041	0.0017	0.0015	0.0030	0.0014	0.0124	0.0021	0.0013
V	0.1503	0.0898	0.1010	0.1050	0.0829	0.1321	0.1585	0.1171	0.1050	0.1535	0.3030	0.0658
W	0.0020	0.0020	0.0020	0.0020	0.0021	0.0022	0.0024	0.0021	0.0025	0.0020	0.1077	0.0020
Y	0.0228	0.0286	0.0118	0.0209	0.0218	0.0287	0.0364	0.0244	0.0231	0.0232	0.0129	0.0355
Yb	0.0016	0.0023	0.0010	0.0017	0.0018	0.0025	0.0029	0.0020	0.0019	0.0022	0.0010	0.0028
Zn	0.0889	0.0883	0.0788	0.0710	0.0970	0.1249	0.1161	0.0950	0.0997	0.0740	0.0777	0.1240
Zr	0.2786	0.2734	0.2898	0.1807	0.2626	0.3806	0.2608	0.2752	0.2772	0.1850	0.2450	0.3163
SiO2	50.9500	52.3250	53.6500	53.0333	49.1400	52.7235	51.0750	51.8424	53.5167	39.9500	51.1000	52.1500
Al2O3	6.6383	9.6675	5.4975	5.3200	6.6750	8.9165	7.9900	7.2435	13.5250	5.3000	8.9500	11.8250
Fe2O3	4.8867	5.5488	4.3000	5.1267	4.9280	5.3882	6.1875	5.1951	5.5550	4.4750	6.6833	6.1225
CaO	1.3033	2.0850	1.5725	1.3100	3.8810	1.0547	1.8625	1.8670	1.7817	12.7750	0.7367	2.7375
MgO	12.7292	7.6638	15.3750	15.4167	12.3410	10.4671	9.1763	11.8813	2.4217	9.8350	7.0867	5.0025
Na2O	3.9758	4.7813	3.8100	3.8233	3.5460	3.4382	5.3700	4.1064	6.2100	1.9950	3.9633	4.4425
K2O	1.5425	1.8200	2.0475	0.9167	1.6950	2.0224	1.3600	1.6291	2.2750	3.9250	1.1467	2.4850
TiO2	0.8267	0.9738	0.7375	0.8267	0.8580	0.8253	1.0450	0.8704	0.8567	0.6350	0.6533	1.0625
MnO	0.1308	0.1175	0.1050	0.1633	0.1880	0.1624	0.1063	0.1390	0.1150	0.0800	0.0700	0.1450
P2O5	0.2825	0.3563	0.1725	0.3900	0.5050	0.3271	0.5250	0.3655	0.1467	0.0800	0.1533	0.4450
SrO	0.0208	0.0475	0.0200	0.0167	0.0300	0.0267	0.0300	0.0274	0.0633	0.1050	0.0200	0.0625
BaO	0.0375	0.0550	0.0425	0.0367	0.0560	0.0576	0.0475	0.0475	0.1050	0.0250	0.0400	0.1600
Total:	84.9461	87.4727	88.9029	87.5985	85.6621	87.5977	86.7932	86.9962	89.0916	81.2030	82.2816	89.8968
Al/Si	0.0768	0.1089	0.0603	0.0574	0.0784	0.0944	0.0922	0.0823	0.1489	0.0782	0.1032	0.1336
Si/(Al+Fe)	8.8593	6.7210	11.0439	10.4719	8.4898	7.2399	7.2580	8.3298	5.3192	8.3102	6.5602	5.6240
(K+Na)/Al	1.2404	1.0335	1.5777	1.4158	1.1763	0.9391	1.3016	1.0937	0.8707	1.3661	0.8029	0.7909
Ba/Sr	1.9445	1.2442	2.2391	4.1905	2.4538	2.8187	1.3883	1.7023	1.7863	0.2981	2.0672	2.1673
Ti/Zr	30.1023	35.5242	25.6007	40.0243	33.8285	21.5822	40.4657	31.0425	28.2909	34.3061	26.6012	33.5968
Zr/Ti	0.0341	0.0282	0.0393	0.0272	0.0310	0.0469	0.0262	0.0349	0.0353	0.0291	0.0379	0.0298
	n=12	**n=8**	**n=4**	**n=3**	**n=10**	**n=17**	**n=8**	**n=62**	**n=6**	**n=2**	**n=3**	**n=4**

Table 4.2: Percent deviation of all possible parent materials above and below each paleosol.

Lithology:	OLD-1 Upper	OLD-1 Middle	OLD-1 Lower	OLD-2A	OLD-3A	FLK-01 Upper	FLK-01 Lower
Average Loc. 80 Lake Clay	-0.3	13.4	-4.8	-36.8	16.8	-13.5	3.8
Unnamed Tuff 1	–	–	-3.3	–	–	–	–
Unnamed Tuff 2	–	99.3	–	–	–	–	–
Unnamed Tuff 3	–	–	–	-7.1	–	–	–
Unnamed Tuff 4	–	–	–	–	-10.4	–	–
Unnamed Tuff 5	–	–	–	–	–	43.7	–
Ng'eju Tuff	–	–	–	–	–	–	-25.7
Tuff IF	65.4	966.5	–	20.9	123.4	65.4	–
Average Tuff Composition	–	37.6	5.7	-29.8	29.7	-4.0	15.2
Volcaniclastic Sediment	–	–	–	-35.5	–	–	–

Table 4.3: Percent deviation of parent material chosen for each paleosol.

	Percent Deviation (Ti/Zr)	Parent Material
FLK-1A Upper Paleosol	-13.5	Average Loc. 80 Lake Clay
FLK-1B Lower Paleosol	3.8	Average Loc. 80 Lake Clay
OLD-1A Upper Paleosol	-0.3	Average Loc. 80 Lake Clay
OLD-1B Middle Paleosol	13.4	Average Loc. 80 Lake Clay
OLD-1C Lower Paleosol	-4.8	Average Loc. 80 Lake Clay
OLD-2A Paleosol	-36.8	Average Loc. 80 Lake Clay
OLD-3A Paleosol	16.8	Average Loc. 80 Lake Clay

in cross-plots of Ti/Zr vs. weight % of Ti and Zr/Ti vs. weight % Zr. Generally, the waxy lake clay compositions (solid circles) plot near the center of each paleosol (Figs. 4.33A-D). The waxy lake clay, in general, contains less Ti and Zr than the paleosols, and therefore plots slightly lower than the paleosol samples. Thus it is the best choice of parent material because the strata above and below are well outside the range of paleosol values. Furthermore, when Ti/Zr is plotted versus depth, the lake clay parent material is geochemically very similar to the paleosols identified in OLD-1, OLD-3, and FLK-1 (Fig. 4.34). The average ratio of Ti/Zr of the Loc. 80 waxy clay (34.3), indicated by the black line, demonstrates how closely the ratios of Ti/Zr match the paleosols. The averaged value of the Ti/Zr ratio for paleosols sampled in OLD-1, OLD-3, and FLK-1 is also 34.3.

In contrast, the paleosol in Trench OLD-2 has a more complicated parent material history and the percent deviation is much less (-7.1%) in the 40 cm thick tuff above Ng'eju Tuff as compared to the -36.8% deviation in the lake clay. The Ti/Zr vs. depth plot (Fig. 4.34) and the Ti/Zr vs. weight % Ti and Zr/Ti vs. weight % Zr crossplots (Fig. 4.33B) indicate that this unnamed, discontinuous tuff is geochemically a closer match to the paleosol. However, the high percentage of clay present within this paleosol makes it unlikely that the tuff is the only parent material source, and it is more likely that the parent material is a combination of the waxy lake clay and pyroclastic material similar in composition to this tuff. The cumulative paleosol in Trench OLD-2 is ~ 1 km from Trench OLD-3, and paleogeographically is furthest from paleo Lake Olduvai (~2 km) (Hay and Kyser, 2001) and closest to the NVC (McHenry, 2005). This is an ideal location for a parent material characterized by less lake clay contribution and more tephra.

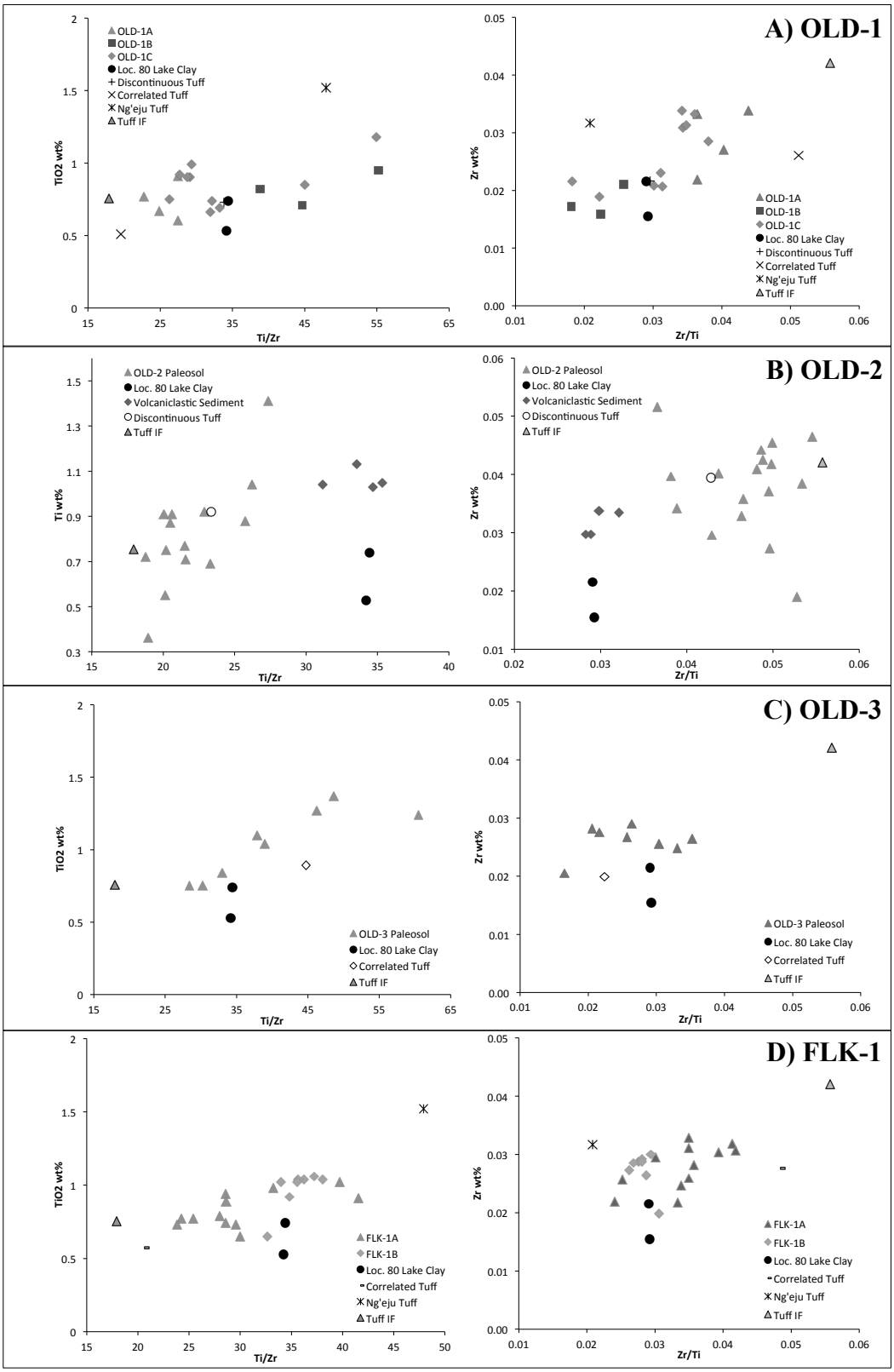

Figure 4.33: Ti/Zr vs. wt% Ti and Zr/Ti vs. wt% Zr crossplots indicate that the waxy lake clay is the appropriate parent material for mass-balance calculations.

Various combinations of Loc. 80 waxy lake clay (GA-37-99) and the unnamed discontinuous tuff were tested in order to approximate the composition of the parent material. Further analysis demonstrated that a combination ("model") parent material, which more closely approximated the parent material, was not necessary. Inclusion of such a combination parent material did not significantly change the mass balance results. In most cases, the translocation values were enriched approximately 10% compared to a solely lake clay parent material. This was true except where large translocations occurred, and a combination parent material further exaggerated the already large translocations. Thus, it is clear that using a combination parent material might actually introduce more error into the mass-balance calculations and therefore was not appropriate. As a result, the bulk density and geochemical measurements from the lower waxy lake clay sample (GA-47-99) were used for mass-balance calculations for the paleosols OLD-1C and FLK-1B, and the measurements from

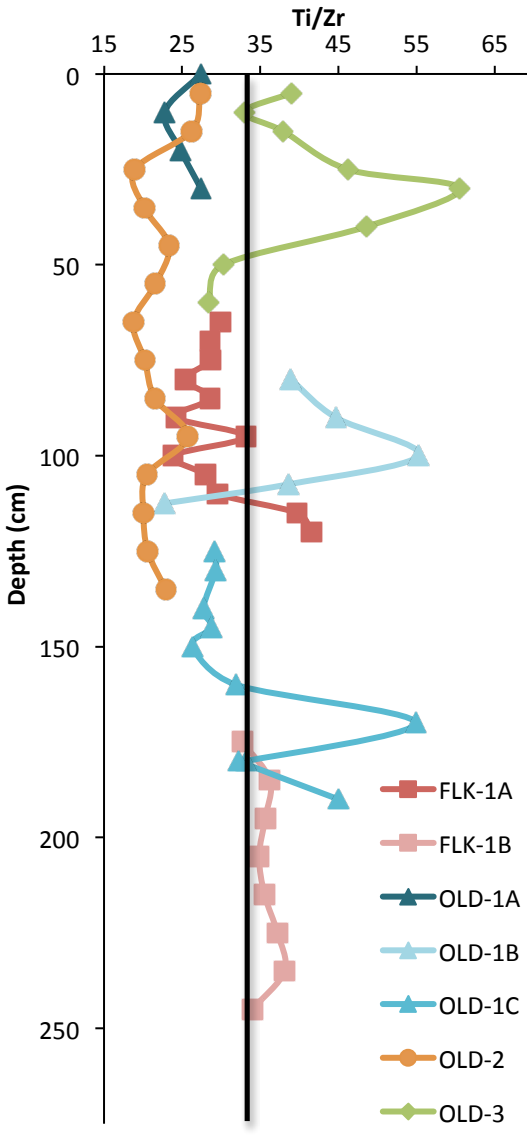

Figure 4.34: Plot of the ratio of Ti to Zr versus depth down from Tuff IF. The black line indicates Ti/Zr of Loc. 80 waxy lake clay, assumed to represent an unweathered clay parent material.

the upper sample (GA-37-99) were used for calculations for OLD-1A and B, OLD-2A, OLD-3A, and FLK-1A.

Determination of Immobile Index Element

Both Zr and Ti are commonly used as an immobile index element in constitutive mass-balance calculations, and the appropriate immobile index element can be evaluated in several ways (Chadwick et al., 1990; Sheldon and Tabor, 2009; and references therein). First, at Olduvai Gorge, two extraneous sources of Zr are possible: the semi-arid climate allows for the introduction of zircon silt grains in windblown dust, and the easterly trade winds blow volcanic ash containing zircon from the volcaniclastic alluvial fan on the eastern margin of the basin (Fig. 2.4). Secondly, as determined by Stiles et al. (2003a, b) for Texas Vertisols, the Zr content of is mainly located in the sand and coarser silt-sized fractions of the paleosol, whereas Ti is preferentially located in the <20 μm clay and fine silt-size fractions. Because these Olduvai paleo-Vertisols have 80% (or greater) clay/silt content, Ti is the better choice of immobile index element because it is less grain-size dependent. Finally, if two elements such as Ti and Zr have similar immobility, traditionally the more abundant element is chosen because there is less analytical uncertainty (Sheldon and Tabor, 2009). In these paleosols, Ti is generally about 30 times more abundant than Zr.

Translocation Calculations

The results of translocation calculations are grouped into four categories: 1) clay and/or zeolite accumulation, 2) carbonate, 3) phosphorus, and 4) redox-responsive elements. Certain elements react predictably due to biological processes in the soil or during pedogenesis forming minerals (e.g. authigenic clay or zeolites). Translocation of

Na, Al, Si, and Mg are grouped together to illustrate any change in smectite clay or Na-zeolite accumulation with depth. Typically, Mg does not react with these elements, but rather with Ca and Sr, which are often indicators for translocation of carbonate. The abundance of Mg-rich smectite in this system obscures any signal associated with carbonate. Phosphorus is an important nutrient often associated with biocycling within the soil. The redox-sensitive elements (V, Fe, Cu, and Mn) can be important in determining the paleohydrology of the system. Cu is also important in the formation of organic ligands (Brantley et al., 2007), and where Cu deviates from other redox-sensitive elements may be an indicator of biologic activity within the soil. The Mn profile is inconsistent with other redox-responsive elements throughout the paleosols. The variability may be due to concentration of these elements in minerals that are not distributed evenly. Mn is heavily concentrated in root traces, and the Mn translocations are indicative of concentrations of Mn oxide precipitating around root pores. In some horizons, these root traces are concentrated in layers representative of the entire paleosol, but are also found in laterally uneven distributions that may contribute to some of the irregularity in the Mn signal (e.g. Figs. 4.9B; 4.13E and F).

OLD-3 Paleo-Vertisol. The clay and/or zeolite accumulation category has the greatest amount of translocation in this order: Na>Mg>Si>Al (Fig. 4.2). All four elements are depleted at the surface and highly enriched between 50 and 200% at 15 cm depth and then become less enriched with depth. The redox-responsive elements show a similar depletion-enrichment profile near the top of the paleosol in V, Fe, Cu, and Mn. Depletions are approximately -50% and enrichments are between 40 and 100%. Below 15 cm, Mn does not correspond to other redox sensitive elements because of irregular

concentrations of Mn oxide-filled root traces. Fe and Cu show increasing enrichment toward down section, but depletion near the base of the paleosol. Both V and Mn are enriched near the base.

Sr and Ca are almost consistently depleted between -90 and -100% with Sr slightly less depleted that Ca overall. Between 15 and 30 cm depth, both Sr and Ca are less depleted between 10 and 20% less in Sr and 3 and 5% less in Ca, a horizon identified in the field as a Bk horizon. P is also significantly enriched in this horizon by up to 800%. The remainder of the P profile is highly enriched between 200 and 400% compared to the parent material, but does not correlate with any other feature.

FLK-1 Paleo-Vertisols. The two paleosols (FLK-1A and FLK-1B) identified in Trench FLK-1 have several comparable overall trends to those observed in the paleosols in Trench OLD-3 (Figs. 4.2, 4.4, and 4.5). Na is significantly more enriched in paleosols at both FLK-1A and FLK-1B, but unlike the paleosol at OLD-3 the greatest amount of translocation occurs in the following order: Na>Al>Si>Mg (Figs. 4.4 and 4.5). Excluding P, all translocation profiles in paleosol FLK-1A generally show more variability within in the profile and greater amounts of translocation than in paleosol FLK-1B. Paleosol FLK-1A shows general positive translocation with depth in both the clay/zeolite and redox-responsive categories. Paleosol FLK-1B shows a significant enrichment in Na, Mg, Al, and Si near the top of the paleosol, ranging from 25 to 110% (Fig. 4.5). Whereas Na enrichments are significantly higher than Al, below this depth both Na and Al show a gradual enrichment with an ~20% proportional increase with depth. Si shows little change with depth, but Mg continually decreases with depth from 30% to -60%.

In paleosol FLK-1A, the redox-responsive elements, Fe, Cu, and V, are depleted at the surface and enriched down profile (Fig. 4.4). Cu shows the greatest amount of depletion of -46% and Fe, V, and Cu are all enriched at depth to between 20-30%. On average, these elements are more depleted in paleosol FLK-1B, with very little variability down profile (Fig. 4.5). Cu is depleted to approximately -85%, V to -70%, and Fe to -25%. Similar to paleosol OLD-3, Mn does not correspond to other redox sensitive elements probably because of irregular concentrations of Mn oxide-filled root traces (Fig. 4.13F).

Paleosols from FLK-1 also have large depletions of Ca (-80 to -90%), with Sr generally less depleted than Ca. Sr is also much less depleted (~ -17%) in FLK-1B compared to paleosols in Trenches OLD-1, 2, and 3 as well as paleosol FLK-1A. The mass-balance profiles from paleosols FLK-1A and FLK-1B also show evidence for carbonate accumulation in Bk horizons. In paleosol FLK-1B, this carbonate is concentrated in root traces.

OLD-1 Paleo-Vertisols. The three paleosols within Trench OLD-1 have distinct overall trends (Figs. 4.8, 4.10, and 4.12). The clay/zeolite accumulation category has the greatest amounts of translocation in this order: Na>Mg>Si>Al. Sr is generally slightly less depleted than Ca, but both elements are generally depleted 90 to 100% compared to the parent material in all three paleo-Vertisols. In OLD-1A, both Sr and Ca are less depleted at depth, but no carbonate enrichment was detectable in the field (Fig. 4.8). OLD-1B contains no enrichments concentrated in a horizon (Fig. 4.10). In OLD-1C, the over 100% enrichment in Sr and ~40% in Ca was detectable in the field and was identified there as a Bk horizon (Figs. 4.11B and 4.12).

In both paleosols OLD-1A and OLD-1B the majority of the translocation profiles indicate that elements are being retained at the base with some elements showing varying degrees of depletion at the surface. Paleosols OLD-1A and OLD-B also have greater negative and positive translocations than those at OLD-1C, with the exception of P and Mn. Mn translocations are probably indicative of concentrations of Mn oxide precipitating around root pores rather than weathering of the element. In all the paleosols in Trench OLD-1, the P signal consistently does not correspond with any other geochemical profile and has very large enrichments ranging from 300 to 1100%.

The redox-responsive elements in paleosol OLD-1A indicate depletion from the surface and retention to slight enrichment at the base. OLD-1B has little to no depletion at the surface, but significant gains at the base, especially in V (~160%). In comparison, OLD-1C shows a much more consistent depletion of V (-60%). Cu is similarly depleted on average ~ 60%, but is ~10% less depleted at the surface possibly due to biologic concentration. Additionally, greater Fe translocations occur in paleosol OLD-1C. Paleosols OLD-1A and OLD-1B have an average Fe translocation value of -5% and 1%, respectively, whereas paleosol OLD-1C is consistently depleted about -25%.

OLD-2 Paleo-Vertisol. Similar to paleosols from Trench OLD-1, Na generally shows the highest amount of translocation, with Al>Si>Mg in paleosol OLD-2A (Fig. 4.14). These elements are depleted at the surface, ranging from -70% to as little as -16%, but at 25 cm depth Na, Al, Si, and Mg are all enriched over 100%. The remainder of the profile shows a gradual depletion in these elements with depth. The redox-responsive elements, Fe, Cu, V, and Mn also show depletion at the surface with V showing the greatest amounts of depletion (-60%), and enrichment at 25 cm depth with the greatest

translocations in Cu of 160%. Beneath 25 cm depth, Mn reflects locations of concentrations of Mn oxide-filled root traces rather than redox concentrations (Figs. 4.13F and 4.14). Sr and Ca are almost consistently depleted between -90 and -100% compared to the parent material. Near the surface Ca is slightly less depleted by ~10% and Sr by 30%. The P signal is highly irregular, does not consistently correspond with any other geochemical profile, and has very large translocations of up to 800%.

Mean Annual Precipitation (MAP) Estimates

Because Trenches OLD-1 and FLK-1 contain multiple paleosols, two weathering indices, namely CIA-K and CALMAG, were used to evaluate the Olduvai paleosols for changes in MAP through time. The CALMAG method proved not applicable to the Olduvai Gorge paleo-Vertisols because of the unusual chemistry of the volcanically influenced parent material. In their calculations, Nordt and Driese (2010) report values of <4% CaO and < 3% MgO for Vertisols used to develop the CALMAG proxy. In contrast,

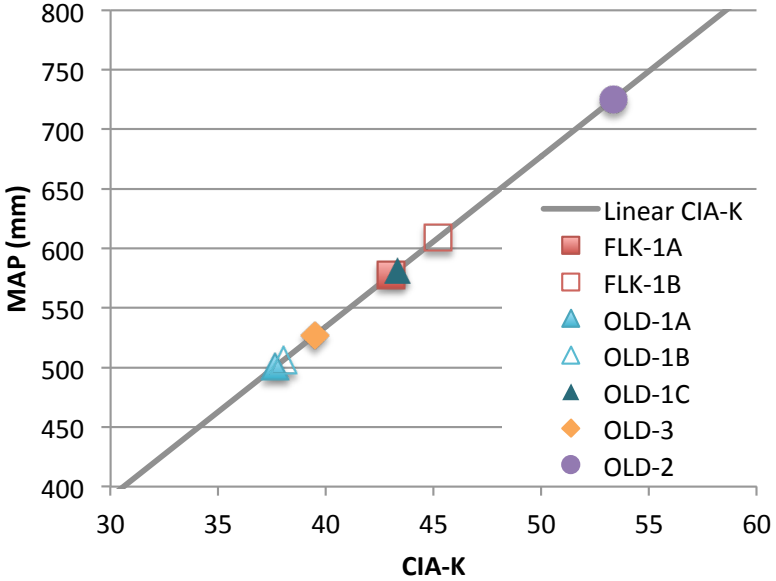

Figure 4.35: Mean annual precipitation estimates using the CIA-K index. Note the decrease in precipitation in paleosols found in trenches OLD-1 and FLK-1.

Olduvai paleosols contain less CaO (from 0.5% to 2%) and significantly greater amounts of MgO, ranging from 7% to as high as 17% MgO in some cases. The high Mg content is attributed to the characteristic Mg-rich smectites that formed in paleo Lake Olduvai weathering environments (Hay and Kyser, 2001; Hover and Ashley, 2003; Deocampo et al., 2009) in which these paleo-Vertisols formed, and the MgO-rich lavas erupting from Olmoti and Ngorongoro (Mollel, 2007; McHenry, 2009; Mollel et al., 2009). These lavas can range from 3 to 11% Mg (Mollel, 2007; Mollel et al., 2009). The CIA-K index indicates that estimated MAP decreased through time (Fig. 4.35). The older paleosols, OLD-1C and FLK-1B, have an estimated MAP of 582 and 609 mm/yr, respectively. Up-section, paleosols OLD-1A and OLD-1B have an estimated MAP of 501 and 506 mm/yr, respectively, and paleosol FLK-1A also indicates a drop in rainfall to 578 mm/yr. An estimated MAP of 527 mm/yr in the paleosol in Trench OLD-3 also falls within the range of the younger paleosols in the time slice. However, the thick, cumulative paleosol in Trench OLD-2, which is located almost 1 km away, has a much higher estimated MAP of 725 mm/yr.

Stable Isotopes

A limited number of isotopic analyses were conducted on carbonate samples collected from this time slice (Table 4.4; Fig. 4.36). The four samples collected from the tufa in Trench OLD-1 and those analyzed by Ashley et al. (2010) in Trench FLK-1 indicate an evolving stable isotope composition, with both $\delta^{18}O$ and $\delta^{13}C$ values becoming more less negative through time. The $\delta^{13}C$ values range from -4.4 to -6.27‰ V-PDB and the $\delta^{18}O$ values from -5.05 to -6.34‰ V-PDB.

Table 4.4: Stable isotopes organized by depth.

Sample #	Locality	Trench #	Depth (cm)	Type of Carbonate	$\delta^{13}C$	$\delta^{18}O$
EB-21A	FLK	OLD-1	20	Tufa	-4.40	-5.05
EB-21B	FLK	OLD-1	20	Tufa	-4.56	-5.24
EB-21C	FLK	OLD-1	20	Tufa	-4.83	-5.47
EB-21D	FLK	OLD-1	20	Tufa	-5.11	-5.24
EB-20	FLK	OLD-1	35	Tufa	-4.96	-5.38
EB-18	FLK	OLD-1	57.5	Tufa	-4.92	-5.37
EB-17	FLK	OLD-1	70	Tufa	-5.52	-5.81
EB-14A	FLK	OLD-1B	90	Nodule	-5.90	-5.95
EB-14B	FLK	OLD-1B	90	Nodule	-6.27	-6.34
EB-14C	FLK	OLD-1B	90	Nodule	-6.09	-5.93
EB-16A	FLK	OLD-1C	130	Nodule	-4.62	-5.79
EB-16B	FLK	OLD-1C	130	Nodule	-4.64	-5.63
EB-6A	FLK	OLD-1C	155	Nodule	-4.55	-5.89
EB-6B	FLK	OLD-1C	155	Nodule	-4.85	-6.04

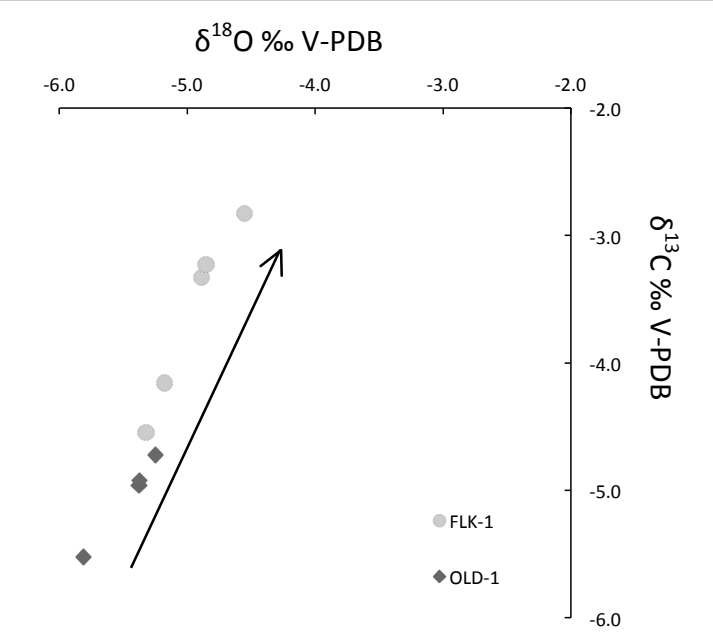

Figure 4.36: Stable isotopes of tufa from Trenches OLD-1 and FLK-1. Data from FLK-1 are reported from Ashley et al. (2010a). Both tufa deposits have an evolving signature becoming less negative through time. See Table 4.4 for stratigraphic location in trench.

5. DISCUSSION

This ~20 ka time-slice of uppermost Bed I encompasses 4 sites which expose intercalated tuffs, tufa, lake clay, and volcaniclastics on the eastern margin of paleo Lake Olduvai. Most of the sediment has been pedogenically modified with tuffs bracketing these paleo-Vertisols, which allow for correlation and interpretation as a paleocatena as well as paleoclimate. In soil science, catena is defined as a sequence of soils with similar parent materials and climate, but topography has a significant effect on the development of the soil (Klaus et al., 2005). The paleocatena extends across the lake margin in a NW-SE direction over ~1 km towards the alluvial fan at the base of the NVC (Figs. 2.1 and 2.4). The complex history of pedogenesis recorded in this time-slice also gives great insight into a previously unstudied soil-forming environment (i.e. lake margin) and the heterogeneous nature of soil development.

Soils are traditionally described using 5 soil-forming factors: climate, organisms, topography, parent material, and time (Jenny, 1941). Results suggest that paleotopography, parent material, and climate (paleohydrology) are the principal factors affecting pedogenesis on the margin of paleo Lake Olduvai. A topographic relief of ~1 m affected thickness and type of soil forming on the landscape (stacked or cumulative soil). Trenches OLD-1 and FLK-1 have stacked paleosols, whereas Trench OLD-3 has only one paleosol and Trench OLD-2 has a thicker cumulative paleosol. The location of the soil with respect to the lake and the NVC particularly affected the composition of the parent material and the development of the soil through periodic additions of pyroclastic material. Lastly, a drying climate allowed for better soil drainage and removal of elements from the system or translocation down soil profile.

Paleoenvironment and Paleocatena

Macroscale, micromorphological, and geochemical analyses reveal a complex paleocatena formed on the lake margin of paleo Lake Olduvai. Periodic expansions of the lake deposited waxy clay on the lake margin flat (Hay and Kyser, 2001; Ashley and Hay, 2002) that was then pedogenically modified during lake low stands (Beverly et al., 2010). The abundant clay content (>80%) and vertic features identify these paleosols as weakly developed Vertisols (Blokhuis et al., 1990; Soil Survey Staff, 1999; Southard et al., 2011). Specifically, abundant pedogenic slickensides identified in the field, and ubiquitous stress cutans and irregular blocky micro-peds identified throughout all thin sections are indicative of the shrink-swell behavior that dominates Vertisol formation (Blokhuis et al., 1990; Retallack, 2001). These paleo-Vertisols also have distinct horizons defined by color changes, differing ped shapes, and element translocations (determined by mass-balance calculations).

The heterogeneous nature of the paleocatena is evident in thickness changes, range of vertic feature development, amount of pyroclastic contribution, organic content, and mass-bass translocations. Closest to paleo Lake Olduvai, paleosol OLD-3A shows the least amount of pedogenesis. The area may have been submerged for longer periods of time, and therefore pedogenesis did not affect the site to the same extent as other sites. The stress cutans surrounding the pyroclastic material are very weakly developed compared to paleosols elsewhere in the time-slice (Fig. 4.15C). No matrix fabric was apparent in thin section and mass-balance calculations also show evidence for less pedogenesis. A >100% positive translocation in all mass-balance categories occurs at the base of the Bw horizon. This is probably not a true translocation of these elements, but

rather due to the addition of pyroclastic material to this horizon. This paleosol does indicate carbonate translocation with a Bk horizon that was identified and defined in the field despite being partially overprinted by the addition of pyroclastic material in the mass balance calculations (Figs. 4.1B and 4.2). The site probably has a slightly higher relief (+1 m) as it lies between the FLK and Zinj Fault on a small horst (Ashley et al., 2010a; Barboni et al., 2010). The topographic difference was likely the reason for only one paleosol developing at this site (Fig 2.3).

On the downdip block of the Zinj Fault, both Trenches FLK-1 and OLD-1 contain stacked paleosols (Fig. 2.1). These paleosols are separated by either tuff or tufa and are more developed than the paleosol identified in Trench OLD-3 (Fig. 2.3). This development is evidenced at the macroscale by more complex ped structures, gilgai, and multiple types of minerals precipitating in root traces (Figs. 4.3 – 4.12). The micromorphology indicates greater pedogenesis with sesquans developing along irregular blocky micro-ped boundaries (Fig. 4.24) and better-developed soil matrix fabrics (Figs. 4.20 and 4.24). Organic matter is also much more abundant in paleosols identified in Trenches OLD-1 and FLK-1 (Figs. 4.18C, 4.21C, 4.22D, and 4.26F), which are closer to springs and presumably associated wetlands depositing tufa during this time-slice (Ashley et al., 2010a), than in paleosols in Trenches OLD-3 and OLD-2 (Figs. 4.15F and 4.28E). Phytolith and pollen records indicate that FLK region was similar to a groundwater forest where greater amounts of organic matter would accumulate than Trench OLD-2 almost 1 km from the spring that has a strong grass signature.

Paleosol OLD-2A, which is located almost 1 km from the lake, formed a much thicker cumulative interval and in some ways resembles paleosol OLD-3A. Both

paleosols OLD-3A and OLD-2A have a Bw horizon at the surface with evidence of mass-balance translocation at the base of the horizon, but paleosol OLD-2A is approximately twice as thick (Figs. 4.2 and 4.14). Unlike paleosol OLD-3A, this translocation may not be due to a concentrated deposition of pyroclastic material, but rather a true translocation of these elements. Only the clay/zeolite accumulation and redox-responsive categories have evidence for translocations in paleosol OLD-2A, but all categories show this trend in paleosol OLD-3A.

However, paleosol OLD-2A does have evidence for a greater abundance of pyroclastic material throughout the paleosol. The parent material cross-plots best demonstrate this. Paleosol OLD-2A is significantly different from the Loc. 80 lake clay chosen to represent the composition of the parent material. The paleosol more closely matches the composition of the discontinuous tuff below the paleosol (Fig. 2.3). This site on the paleocatena is closest to the NVC and the pyroclastic alluvial fan to the southeast and is therefore most likely to have had a steady and increased contribution of pyroclastic material (Fig. 2.4). Paleosol OLD-2A is also a better-developed soil than paleosol OLD-3A at the microscale. The matrix fabric is more developed with highly birefringent clay oriented within the matrix and surrounding grains and Mn oxides, indicative of shrink-swell behavior of Vertisols. Enrichment of sesquioxides (enrichment hypocoatings) also formed along ped boundaries and pyroclastic material (Figs. 4.29B and 4.29C). Pedorelicts (reworked clasts from older soils) are a feature unique to paleosol OLD-2A but are found only in the lower horizons of the paleosol: Bss3 and Bw3 (Figs. 4.28A and 4.29A). Pedorelicts were also identified at the top of the red paleo-Andisols intervals forming on the alluvial fan in lowermost Bed II (Ashley and Driese, 2000), and were

interpreted as a period of instability that eroded soils. The pedorelicts in paleosol OLD-2A occur within the lower two horizons and support the interpretation of the paleosol as a cumulative interval with additional lake clay depositing on the soil surface and welding to the underlying soil.

In conclusion, the ~1 km cross-section of this time-slice has a small topographic relief of ~1 m that affected thickness, number, and possibly vertic development of paleosols on the landscape. Location on the landscape with respect to paleo Lake Olduvai, the NVC, and fault-controlled springs affected composition of the parent material, development of the soil, and organic matter content. Nearest to the lake on a slight topographic high, pedogenesis was weakest. On the downthrown block, multiple stacked paleosols with stronger matrix fabrics, multiple ped structures, and greater organic matter preservation developed near fault-controlled springs and the associated wetlands. Closest to the NVC and volcaniclastic alluvial fan, the paleosol is thicker and cumulative with stronger matrix fabrics, sesquioxide enrichment, and pedorelicts.

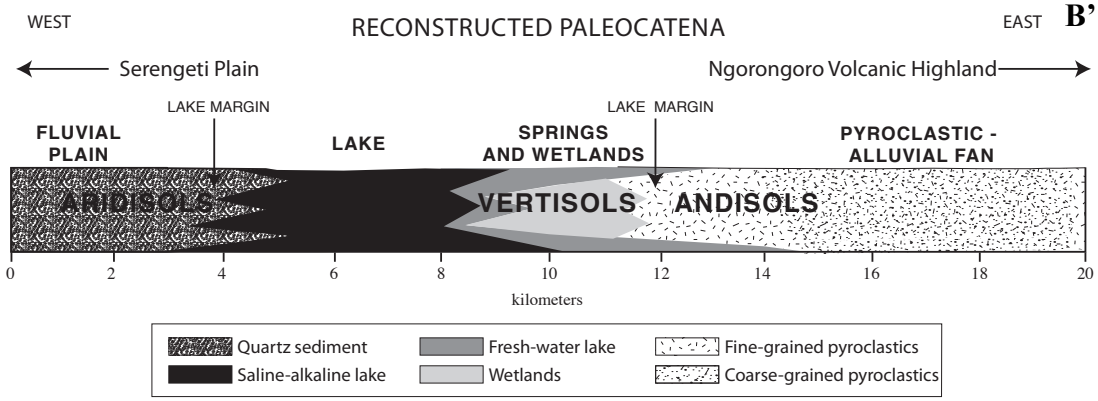

Figure 5.1: Stylized reconstruction of the paleolandscape of uppermost Bed I and lowermost Bed II at ~1.8 Ma. Facies changes, interpreted depositional environments, and types of soils forming on the landscape as well as parent materials are all indicated on this basin-wide reconstruction of the paleocatena. Modified from Ashley and Hay (2002).

These results also expand the understanding of a basin-wide paleocatena where previously two other soil-forming environments were identified (Fig. 5.1). On the fluvial plain to the west of paleo Lake Olduvai, calcium carbonate-rich Aridisols formed in the well-drained quartzofeldspathic fluvial environment (Sikes and Ashley, 2007). On the lake margin, Vertisols (this study) formed on the smectite-rich lake clay where the sediment was subjected to wetting and drying due to the fluctuating lake level and seasonal monsoons. On the volcaniclastic fan to the east, red Andisols formed as a result of episodic volcaniclastic input and redoximorphic reactions associated with fluctuation of the water table (Ashley and Driese, 2000).

Paleoclimate

Previous research has demonstrated that during the Pleistocene, east African climate was primarily influenced by orbitally induced changes in insolation rather than high latitude glaciation (Trauth et al., 2009). Sapropels from northeast Africa (Tuenter et al., 2003) and east African lakes (Trauth et al., 2007) suggest that precession is the dominant driver of climate near the equator. Previous research also demonstrates ~21 ka precession cycles heavily influenced paleo Lake Olduvai between 1.84 and 1.74 Ma (Ashley, 2007). Cycles of deposition of lake clay indicate that the last ~20 ka of uppermost Bed I end are increasingly arid (Ashley, 2007). Stable isotope, faunal, floral, and lithostratigraphic records from uppermost Bed I also indicate a drying trend (Bonnefille, 1984; Cerling and Hay, 1986; Plummer and Bishop, 1994; deMenocal, 1995; Fernandez-Jalvo et al., 1998; Andrews and Humphrey, 1999; Ashley and Hay, 2002; Ashley, 2007; Sikes and Ashley, 2007; Bamford et al., 2008).

Molecular weathering ratios and mass-balance calculations demonstrate evidence for a drying trend in uppermost Bed I. By looking at changes through time, a climosequence can also be identified using the stacked paleosols in Trenches OLD-1 and FLK-1 that cannot be explained by other soil-forming factors (i.e. parent material and topography). The molecular weathering ratios, mass-balance calculations, and MAP estimates show an important aspect of these paleo-Vertisols not clearly identifiable through physical characteristics at the macro or petrographic scale. This is likely due to the overall weak development of the paleosols. This record of increasing aridity would have been missed without the addition of high-resolution geochemical analyses to field and detailed petrographic description.

A similar pattern is found in the stacked paleosols in Trenches OLD-1 and FLK-1 (Fig. 2.3). At the base of Trench OLD-1 is a thin non-pedogenic bed with high organic content and evidence for a waterlogged, reducing environment and wetter climate. A similar bed was not preserved in Trench FLK-1, but the paleosol FLK-1B can be correlated using the unnamed tuff capping both FLK-1B and OLD-1C (Baluyot, 2010). Molecular weathering ratios for hydration, salinization, and leaching are on average less in the lower paleosols (FLK-1B and OLD-1C) than in the younger paleosols (FLK-1A, OLD-1B, and OLD-1A) indicating a lesser degree of pedogenesis (Fig. 4.32).

Mass-balance calculations show similar evidence. Paleosols FLK-1B and OLD-1C have little variability down profile in clay/zeolite accumulation or redox-responsive elements (Figs. 4.5 and 4.12). The upper paleosols generally show more variability, greater translocations (both positive and negative), and profiles more similar to a depletion-enrichment profile although most are weakly developed (Figs. 4.4, 4.8, and

4.10). However, in one upper paleosol (OLD-1B) a fragipan was identified in the field where significant translocation and accumulation occurred (Fig. 4.10). The depletion of elements in the lower paleosols (FLK-1B and OLD-1C) is almost uniformly consistent with depth (Figs. 4.5 and 4.12. This was probably due to times of saturation with a high water table. Saturation enhanced mobility rather than translocation of soluble elements as is traditional in pedogenesis. As the climate became more arid during the precession cycle that spans the last ~21 ka of uppermost Bed I, the water table dropped allowing for weathering and removal of elements in a pedogenic pattern in the younger paleosols (FLK-1A, OLD-1A, OLD-1B; Figs. 4.4, 4.8 and 4.10).

MAP estimates show a similar trend. Due to the unique geochemical environment of the Olduvai Gorge, which combines Ca-rich volcanics and a saline alkaline lake, these numbers cannot be used to give a true paleo-precipitation estimate. No paleosols with a similar geochemistry were originally analyzed in the original CIA-K study (Sheldon et al., 2002). However, these calculations do lend support to a drying climate in a relative sense. Paleosols OLD-3A, FLK-1A, FLK-1B, OLD-1C, and OLD-2A all contain a Bk horizon. Previous research has shown that a carbonate horizon cannot form in soils with a MAP >750 mm/yr (Birkeland, 1999; Royer, 1999; Retallack, 2001), and all paleosols in this climosequence indicate < 750 mm/yr (Fig. 4.35). Paleosols in Trenches OLD-1 and FLK-1 also indicate that paleoprecipitation dropped between 30 and 80 mm/yr over the time-slice consistent with other paleoclimate proxies. This suggests that while no modern proxies for this type of soil currently exist, these types of soils should be included with further research.

In addition, stable isotopes of tufa have evidence for fractionation due to evaporation (Ashley et al., 2010b; Baluyot, 2011). With no evaporation and little seasonal temperature variation (~25°C), calcite precipitated at Olduvai Gorge will have a $\delta^{18}O$ signature of approximately -6‰ (Liutkus et al., 2005). Tufa lower in the section in both FLK-1 and OLD-1 sites have calcite with $\delta^{18}O$ values between -4 and -6‰, which is evidence for precipitation of calcite with little prior evaporation (Fig. 4.36). Up section the tufa has more evolved (less negative) signature, especially in the FLK-1 samples. This suggests that the evaporation caused fractionation, and in combination with the geochemical data suggests a drying climate.

Although molecular weathering ratios, mass-balance calculations, MAP estimates, and stable isotopes all indicate a drying climate, paleo Lake Olduvai continued to flood the lake margin periodically depositing Mg-rich smectites that were then pedogenically modified despite the drying precession cycle. This is likely caused by to sub-Milankovitch climate cycles. However generally the resolution of the sedimentary record at Olduvai Gorge is not sufficient to resolve millennial or smaller climate history during the Pleistocene. Resolution of late Holocene climate record in East Africa on the order of decades (El Niño) to centuries (Medieval Warm Period and Little Ice Age) has been successful (Verschuren et al., 2000; Driese et al., 2004; Russell and Johnson, 2007). Evidence suggests that these climate events had a profound effect of precipitation of East Africa, and it is likely that similar climate oscillations were present in the past. Stable isotope analysis of lake margin rhizoliths suggest that these sub-Milankovitch cycles are likely responsible for the variation $\delta^{18}O$ signature of rhizoliths in cross-section (Liutkus et al., 2005).

Additional evidence for changing climatic conditions possibly due to sub-Milankovitch oscillations can be seen in the micromorphology of these paleo-Vertisols although timing of these features is not clear. A number of the paleosols in Trenches OLD-1 and OLD-2 have evidence for complex soil moisture conditions that led to authigenic precipitation in root voids and altering lapilli. Mn oxides precipitated in root traces in paleosols OLD-1B, OLD-1C, and OLD-2A. These root traces are found throughout these paleosols and also concentrated in layers that are interpreted as root mats (Figs. 4.9B and C; 4.13E and F). In paleosol OLD-2A there are two distinct levels of root concentrations that provide additional evidence for the cumulative nature of the paleosol. Roots and their associated microbial population often affect Fe and Mn surrounding them due to the production of organic compounds (Schwertmann and Taylor, 1989; Violante et al., 2003). Mn accumulations are often associated with a silt- or clay-rich poorly drained soil (but not extremely wet soil), which has alternating reducing and oxidizing conditions (Birnie and Paterson, 1991; Kampf et al., 2000; Stiles et al., 2001; Kraus and Hasiotis, 2006). Mn likely became mobile when the water table was higher and the soil was poorly drained, and then roots promoted precipitation of Mn oxides in these paleo-Vertisols.

Zeolites are also found throughout the Olduvai basin in a variety of paleoenvironments (Hay, 1963; Ashley and Driese, 2000; Mees et al., 2005). This is primarily related to the interaction between volcanic material and the saline-alkaline lake or soil water (Mees et al., 2005). Zeolites were observed altering lapilli and precipitating in root voids in all sites within the time-slice. Paleosol OLD-3A is closest to the lake and contains the largest number of zeolitized lapilli, and thus presumably more influenced by

saline alkaline lake water. In Trenches OLD-1 and FLK-1 where the paleosols are stacked, zeolites are only found in the lower paleosols (FLK-1B, OLD-1B, and OLD-1C). In the case of paleosols FLK-1B and OLD-1C, zeolitized root traces also coincide with the appearance of lapilli. In Trench OLD-2 where the paleosols are cumulative, the zeolites are also found at the base of the profile where there are also lapilli. The occurrence of these zeolites seems connected to the amount of pyroclastic material available and depth in the soil profile.

This geochemical system shows similarities with Lake Bogoria where zeolites precipitated during prolonged dry periods (Renaut, 1993; Owen et al., 2009). Zeolitic rhizoliths are very rare and probably only precipitate in dry, saline-alkaline soils where saline-alkaline fluids are available. These types of rhizoliths are usually a result of a significant period of aridity where capillary rise and evaporative pumping drew up saline-alkaline water (Owen et al., 2009). A similar system likely formed on the margin of paleo Lake Olduvai where abundant volcaniclastic material interacted with saline-alkaline water drawn upwards during the drying trend in uppermost Bed I.

In paleosol OLD-2A, there is also evidence for the relative timing of the precipitation of the Mn oxides and zeolites. Root voids were first lined with Mn oxides and then zeolite crystals (Fig. 4.27). Ashley and Driese (2000) note a similar but better developed record with a relative sequence of formation of pedogenic features in lowermost Bed II. The paleohydrology of this red paleosol interval was recorded in 1) redoximorphic features, 2) illuviated clay coatings, 3) a second generation of redoximorphic features, 4) vadose silt, and 5) zeolite pore-fillings and alteration of volcanic glass. The redoximorphic features are interpreted to be associated with

fluctuating higher water table and wetter climate that impeded soil drainage. The illuviated clay coatings indicated a slightly drier climate and the vadose silt was evidence of a much drier climate. The zeolites were interpreted to be associated with the interaction between the soil and the saline-alkaline lake.

Future Research

The mass-balance calculations revealed P translocations all >100% and up to 1000% in some cases. The mean bulk geochemical values for P_2O_5 for the paleosols is 0.37 wt. % but can reach concentrations of up to 1.44 wt. % (Table 4.1; Appendix 2). These values considerably higher than found in other paleoenvironments and compositions of tuff found throughout the basin. The uppermost Bed I sediments from Loc. 80 sediments are ~ 0.12 wt. % P (P. Berry, pers. comm.) and all tuffs analyzed in this study and those reported by McHenry (2009) are less then 0.15 wt. % P. The only sediment that contains significantly different amounts of P is the volcaniclastic sediment found at the base of paleosol OLD-2A, which contains ~0.45 wt. % P.

Several explanations are possible for this anomalous P signature. Olduvai Gorge is a site rich in fossils that could be skewing the results. A few bones were found in paleosol OLD-2A and were removed from the samples, but no other paleosol had bones preserved in the section. In addition, no microfossils were identified in thin section. In wetland soils P usually exists in three forms: organic P, fixed mineral P, and orthophosphate (Vepraskas and Faulkner, 2001). Organic P and fixed mineral P make up 80 to 90% of P found in wetland soils, but the concentrations found in the paleosols are much higher than expected for a biological signature (Vepraskas and Faulkner, 2001). The fixed mineral P is often associated with pedogenic carbonate (Vepraskas and

Faulkner, 2001). In some of the paleosol profiles, P translocation correlated with Ca and Sr, where Bk horizons were identified (Fig. 4.5 and 4.8). Although additional large P translocations are noted where Bk horizons are not found (Fig. 4.4 and 4.10), this likely indicates that at least some of the P exists in a fixed mineral form. Further research is need to determine the source of the large amounts of P that do not exist in the lake clay parent material and are too large to be caused by nutrient biocycling of plants.

6. CONCLUSIONS

1) Paleosols in the upper Bed I time-slice formed from a lake clay parent material deposited during expansions of Lake Olduvai over a ~20 ka time-slice at ~1.8 Ma and recorded a paleocatena.
2) Field relationships, macroscale and petrographic features, and mass-balance calculations all identify these paleosols as weakly developed Vertisols.
3) The paleohydrology, paleotopography, and periodic additions of pyroclastic material resulted in a heterogeneous paleocatena along the eastern margin of paleo Lake Olduvai. In this NW-SE trending transect, the soil was poorly developed near the lake margin while stacked soils developed in the accommodation space created by faulting, and cumulative soils developed closer to the volcaniclastic alluvial fan.
4) These results also identify a soil-forming environment (not yet described) that contributes to the understanding of the paleolandscape within the Olduvai Basin. Differences in topography, depositional environment, parent material, and depth to the water table are reflected in the development of different soil types across the landscape.

5) The stacked paleo-Vertisols form a climosequence that suggests increasing aridity at the top of uppermost Bed I. The molecular weathering ratios, mass-balance calculations, MAP estimates, and stable isotopes all indicate a drying climate. This trend is likely due to the effects of a Milankovitch precession cycle and correlates well with existing faunal, floral, and lithostratigraphic records at Olduvai Gorge, as well as dust and oxygen isotope records from marine cores.
6) Multiple authigenic minerals precipitated in rhizoliths likely due to changing hydrology from a drying climate. Redox-sensitive manganese was mobilized during saturated soil conditions and precipitated during drier conditions. Zeolites altering lapilli and precipitating in root traces are a result of drying climate causing capillary rise and evaporative pumping of saline-alkaline water upward.
7) Phosphorus concentrations are significantly higher in the lake margin paleo-Vertisols compared to equivalent sediments found in this time-slice. These concentrations are likely too high for concentration due to biocycling, and P was likely fixed in a mineral. Further research is needed to fully understand the interaction between P, the complex geochemical system containing Mg-rich smectites and saline-alkaline water, and the redox reactions occurring in these wetland paleosols.

References

Andrews, P., and Humphrey, L., 1999, African Miocene environments and transition to early Hominines, *in* Bromage, T. G., and Schrenk, F., eds., African Biogeography, Climate Change, and Human Evolution: New York, Oxford University Press, p. 282-303.

Ashley, G., Tactikos, J., and Owen, R., 2009, Hominin use of springs and wetlands: Paleoclimate and archaeological records from Olduvai Gorge (~1.79–1.74 Ma): Palaeogeography, Palaeoclimatology, Palaeoecology, v. 272, no. 1-2, p. 1-16.

Ashley, G. M., 2007, Orbital rhythms, monsoons, and playa lake response, Olduvai Basin, equatorial East Africa (ca. 1.85–1.74 Ma): Geology, v. 35, no. 12, p. 1091-1094.

Ashley, G. M., Barboni, D., Dominguez-Rodrigo, M., Bunn, H. T., Mabulla, A. Z. P., Diez-Martin, F., Barba, R., and Baquedano, E., 2010a, Paleoenvironmental and paleoecological reconstruction of a freshwater oasis in savannah grassland at FLK North, Olduvai Gorge, Tanzania: Quaternary Research, v. 74, no. 3, p. 333-343.

Ashley, G. M., Barboni, D., Dominguez-Rodrigo, M., Bunn, H. T., Mabulla, A. Z. P., Diez-Martin, F., Barba, R., and Baquedano, E., 2010b, A spring and wooded habitat at FLK Zinj and their relevance to origins of human behavior: Quaternary Research, v. 74, no. 3, p. 304-314.

Ashley, G. M., Dominguez-Rodrigo, M., Bunn, H. T., Mabulla, A. Z. P., and Baquedano, E., 2010c, Sedimentary geology and human origins: A fresh look at Olduvai Gorge, Tanzania: Journal of Sedimentary Research, v. 80, no. 8, p. 703-709.

Ashley, G. M., and Driese, S., 2000, Paleopedology and paleohydrology of a volcaniclastic paleosol interval: Implications for early Pleistocene stratigraphy and paleoclimate record: Olduvai Gorge, Tanzania: Journal of Sedimentary Research, v. 70, no. 5, p. 1065-1080.

Ashley, G. M., and Hay, R. L., 2002, Sedimentation patterns in a Plio-Pleistocene volcaniclastic rift-platform basin, Olduvai Gorge, Tanzania, *in* Renaut, R. W., and Ashley, G. M., eds., Sedimentation in Continental Rifts, Volume 73, SEPM Special Publications, p. 107-122.

Baluyot, R., 2011, Paleoenvironmental reconstruction of a Pleistocene landscape, Olduvai Gorge, Tanzania [Undergraduate Honors Thesis]: Rutgers University, 46 p.

Bamford, M. K., Stanistreet, I. G., Stollhofen, H., and Albert, R. M., 2008, Late Pliocene grassland from Olduvai Gorge, Tanzania: Palaeogeography, Palaeoclimatology, Palaeoecology, v. 257, no. 3, p. 280-293.

Barboni, D., Ashley, G. M., Dominguez-Rodrigo, M., Bunn, H. T., Mabulla, A., and Baquedano, E., 2010, Phytoliths infer dense and heterogeneous paleovegetation at FLK North and surrounding localities during upper Bed I time, Olduvai Gorge, Tanzania: Quaternary Research, v. 74, p. 344-354.

Berggren, W. A., Kent, D. V., Swisher, C. C., and Aubry, M.-P., 1995, A revised Cenozoic geochronology and chronostratigraphy, Geochronology, Time Scales and Global Stratigraphic Correlation, Society of Economic Paleontologists and Mineralogists Special Publication 54, p. 129-212.

Beverly, E. J., Ashley, G. M., Driese, S. G., and Sikes, N. E., 2010, New insights into spatial variability of rift basin paleosols using sedimentology, paleopedology, and soil geomorphology, Olduvai Gorge, Tanzania: Geological Society of America Abstracts with Programs, v. 42, no. 5, p. 469.

Birkeland, P. W., 1999, Soils and Geomorphology, New York, Oxford University Press, 448 p.

Birnie, A. C., and Paterson, E., 1991, The mineralogy and morphology of iron and manganese oxides in an imperfectly drained Scottish soil: Geoderma, v. 50, p. 219-237.

Blake, G. R., and Hartge, K. H., 1986, Bulk Density *in* Klute, A., ed., Methods of soil analysis: Part I physical and mineralogical methods: Madison, Soil Science Society of America, Inc., p. 363-375.

Blokhuis, W. A., Kooistra, M. J., and Wilding, L. P., 1990, Micromorphology of cracking clayey soils (Vertisols), *in* Douglas, L. A., ed., Soil Micromorphology: A Basic and Applied Science: New York, Elsevier.

Bonnefille, R., 1984, Palynological research at Olduvai Gorge, National Geographic Society Research Reports, National Geographic Society, p. 227-243.

Brantley, S. L., Goldhaber, M. B., and Ragnarsdottir, K. V., 2007, Crossing disciplines and scales to understand the Critical Zone: Elements, v. 3, p. 307-314.

Brewer, R., 1976, Fabric and mineral analysis of soils, New York, John Wiley & Sons, Inc., 470 p.

Brimhall, G. H., and Dietrich, W. E., 1987, Constitutive mass balance relations between chemical composition, volume, density, porosity, and strain in metasomatic hydrochemical systems: Results on weathering and pedogenesis: Geochimica et Cosmochimica Acta, v. 51, p. 567-587.

Brimhall, G. H., Lewis, C. J., Ford, C., Bratt, J., Taylor, G., and Warin, O., 1991, Quatitative geochemical approach to pedogenesis: importance of parent material reduction, volumetric expansion, and eolian influx in lateritization: Geoderma, v. 51, p. 51-91.

Bunn, H. T., Mabulla, A., Dominguez-Rodrigo, M., Ashley, G., Barba, R., Diez-Martin, F., Remer, K., Yravedra, J., and Baquedano, E., 2010, Was FLK North levels 1-2 a classic "living floor" of Oldowan hominis or a taphonomically complex palimsest dominated by large carnivore feeding behavior?: Quaternary Research, v. 74, p. 355-362.

Cerling, T. E., and Hay, R. L., 1986, An isotopic study of paleosol carbonates from Olduvai Gorge: Quaternary Research, v. 25, p. 63-78.

Chadwick, O. A., Brimhall, G. H., and Hendricks, D. M., 1990, From a black to a gray box - a mass balance interpretation of pedogenesis: Geomorphology, v. 3, p. 369-390.

Coplen, T. B., Kendall, C., and Hopple, J., 1983, Comparison of stable isotope reference samples: Nature, v. 302, p. 236-238.

deMenocal, P. B., 1995, Plio-Pleistocene African Climate: Science, v. 270, p. 53-59.

Deocampo, D. M., Blumenschine, R. J., and Ashley, G. M., 2002, Wetland diagenesis and traces of early hominids, Olduvai Gorge, Tanzania: Quaternary Research, v. 57, no. 2, p. 271-281.

Deocampo, D. M., Cuadros, J., Wing-Dudek, T., Olives, J., and Amouric, M., 2009, Saline lake diagenesis as revealed by a coupled mineralogy and geochemistry of multiple ultrafine clay phases: Pliocene Olduvai Gorge, Tanzania: American Journal of Science, v. 309, p. 834-868.

Dominguez-Rodrigo, M., Barba, R., and Egelund, C. P., 2007, Deconstructing Olduvai: A taphonomic study of Bed I sites, Vertebrate Paleobiology and Paleoanthropology Series: Dordrecht, Springer, p. 127-164.

Dominguez-Rodrigo, M., Mabulla, A., Bunn, H. T., Diez-Martin, F., Baquedano, E., Barboni, D., Barba, R., Dominguez-Solera, S., Sanchez, P., Ashley, G. M., and Yravedra, J., 2010, Disentangling hominin and carnivore activities near a spring at FLK North (Olduvai Gorge, Tanzania): Quaternary Research, v. 74, p. 363-375.

Driese, S. G., Mora, C. I., Stiles, C. A., Joeckel, R. M., and Nordt, L. C., 2000, Mass-balance reconstruction of a modern Vertisol: implications for interpreting the geochemistry and burial alteration of paleo-Vertisols: Geoderma, v. 95, p. 179-204.

Driese, S. G., Ashley, G. M., Li, Z.-H., Hover, V. C., and Owen, R. B., 2004, Possible Late Holocene equatorial palaeoclimate record based upon soils spanning the Medieval Warm Period and Little Ice Age, Loboi Plain, Kenya: Palaeogeography, Palaeoclimatology, Palaeoecology, v. 213, no. 3-4, p. 231-250.

Feakins, S. J., and deMenocal, P. B., 2010, Global and African regional climate change during the Cenozoic, *in* Werdelin, L., and Sanders, W. J., eds., Cenozoic Mammals of Africa, University of California Press, p. 45-55.

Fernandez-Jalvo, Y., Denys, C., Andrews, P., Williams, T., Dauphin, Y., and Humphrey, L., 1998, Taphonomy and palaeoecology of Olduvai Bed-I (Pleistocene, Tanzania): Journal of Human Evolution, v. 34, p. 137-172.

Fitzpatrick, E. A., 1993, Soil microscopy and micromorphology, New York, John Wiley & Sons, 304 p.

Folk, R. L., 1980, Petrology of Sedimentary Rocks, Austin, Hemphill Publishing Company, 182 p.

Gabunia, L., Vekua, A., Lordkipanidze, D., Swisher III, C. C., Ferring, R., Justus, A., Nioradze, M., Tvalchrelidze, M., Anton, S. C., Bosiniski, G., Joris, O., de Lumley, M. A., Majsuradze, G., and Mouskhelishvili, A., 2000, Earliest Pleistocene hominid cranial remains from Dmanisi, Republic of Georgia: Taxonomy, geologic setting, and age: Science, v. 288, no. 1019-1025.

Gromme, C. S., and Hay, R. L., 1971, Geomagnetic polarity epochs: Age and duration of the Olduvai normal polarity event: Earth and Planetary Science Letters, v. 10, p. 179-185.

Hay, R. L., 1963, Zeolitic weathering in Olduvai Gorge, Tanganyika: Geological Society of America Bulletin, v. 74, p. 1281-1286.

Hay, R. L., 1976, Geology of the Olduvai Gorge: A study of sedimentation in a semiarid basin, Berkely, University of California Press, 203 p.

Hay, R. L., 1990, Olduvai Gorge: A case history in the interpretation of hominid paleoenvironments in East Africa, *in* Laporte, L. F., ed., Establishment of a Geologic Framework for Paleoanthropology: Boulder, GSA Special Paper 242, p. 23-38.

Hay, R. L., and Kyser, T. K., 2001, Chemical sedimentology and paleoenvironmental history of Lake Olduvai, a Pliocene lake in northern Tanzania: GSA Bulletin, v. 113, no. 12, p. 1505-1521.

Hover, V. C., and Ashley, G. M., 2003, Geochemical signatures of paleodepositional and diagenetic environments: a STEM/AEM study of authigenic clay minerals from an arid rift basin, Olduvai Gorge, Tanzania: Clays and Clay Minerals, v. 51, no. 3, p. 231-251.

Jenny, H., 1941, Factors of Soil Formation: A System of Quantitative Pedology, New York, McGraw-Hill, 288 p.

Kampf, N., Scheinost, A. C., and Schulze, D. G., 2000, Oxide minerals, *in* Sumner, M. E., ed., Handbook of Soil Sciences: Boca Raton, Florida, CRC Press, p. F125-168ßß.

Kappelman, J., 1986, Plio-Pleistocene marine-continental correlation using habitat indicators from Olduvai Gorge, Tanzania: Quaternary Research, v. 25, p. 141-149.

Klaus, K. E., Neuendorf Jr., J. P., and Jackson, J. A., 2005, Glossary of Geology: Alexandria, VA, American Geological Institute, p. 800.

Kraus, M. J., and Hasiotis, S. T., 2006, Significance of different modes of rhizolith preservation to interpreting paleoenvironmental and paleohydrologic settings: examples from Paleogene paleosols, Bighorn Basin, Wyoming, U.S.A: Journal of Sedimentary Research, v. 76, no. 4, p. 633-646.

Leakey, M. D., 1971, Olduvai Gorge: Excavations in Beds I and II, 1960-1963, Cambridge, Cambridge University Press, 309 p.

Liutkus, C. M., Wright, J. D., Ashley, G. M., and Sikes, N. E., 2005, Paleoenvironmental interpretation of lake-margin deposits using δ13C and δ18O results from early Pleistocene carbonate rhizoliths, Olduvai Gorge, Tanzania: Geology, v. 33, no. 5, p. 377.

Lordkipanidze, D., Jashashvili, T., Vekua, A., Ponce de Leon, M. S., Zollikofer, C. P., Rightmire, G. P., Pontzer, H., Ferring, R., Oms, O., Tappen, M., Bukhsianidze, M., Agusti, J., Kahlke, R., Kiladze, G., Martinez-Navarro, B., Mouskhelishvili, A., Nioradze, M., and Rook, L., 2007, Postcranial evidence from early Homo from Dmanisi, Georgia: Nature, v. 449, no. 7160, p. 305-310.

Maynard, J. B., 1992, Chemistry of modern soils as a guide to interpreting Precambrian paleosols: Journal of Geology, v. 100, p. 279-289.

McHenry, L., 2004, Characterization and correlation of altered Plio-Pleistocene tephra using a "multiple techique" approach: Case study at Olduvai Gorge, Tanzania [Ph.D. Thesis]: Rutgers University, 382 p.

McHenry, L., 2005, Phenocryst composition as a toll for correlating fresh and altered tephra, Bed I, Olduvai Gorge, Tanzania: Stratigraphy, v. 2, no. 2, p. 101-115.

McHenry, L., Mollel, G., and Swisher III, C., 2008, Compositional and textural correlations between Olduvai Gorge Bed I tephra and volcanic sources in the Ngorongoro Volcanic Highlands, Tanzania: Quaternary International, v. 178, no. 1, p. 306-319.

McHenry, L. J., 2009, Element mobility during zeolitic and argillic alteration of volcanic ash in a closed-basin lacustrine environment: Case study Olduvai Gorge, Tanzania: Chemical Geology, v. 265, no. 3-4, p. 540-552.

McHenry, L. J., 2010, Element distribution between coexisting authigenic mineral phases in argillic and zeolitic altered tephra, Olduvai Gorge, Tanzania: Clays and Clay Minerals, v. 58, no. 5, p. 627-643.

Mees, F., Stoops, G., Van Ranst, E., Paepe, R., and Van Overloop, E., 2005, The nature of zeolite occurrences in deposits of the Olduvai Basin, Northern Tanzania: Clays and Clay Minerals, v. 53, no. 6, p. 659-673.

Mollel, G. F., 2007, Petrochemistry and geochronology of Ngorongoro volcanic highland complex (NVHC) and its relationship to Laetoli and Olduvai Gorge, Tanzania. [Ph.D. Dissertation]: Rutgers University.

Mollel, G. F., Swisher III, C. C., McHenry, L. J., Feigenson, M. D., and Carr, M. J., 2009, Petrogenesis of basalt–trachyte lavas from Olmoti Crater, Tanzania: Journal of African Earth Sciences, v. 54, no. 5, p. 127-143.

Nordt, L. C., and Driese, S. D., 2010, New weathering index improves paleorainfall estimates from Vertisols: Geology, v. 38, no. 5, p. 407-410.

NRC, 2001, Basic Research Opportunities in the Earth Sciences, Washington, D.C., National Academy Press, 168 p.

NSF Advisory Committee for the Geosciences, 2009, Unraveling Earth's Complexities Through the Geosciences, Geovision Report.

Owen, R. B., Renaut, R. W., Scott, J. J., Potts, R., and Behrensmeyer, A. K., 2009, Wetland sedimentation and associated diatoms in the Pleistocene Olorgesailie Basin, southern Kenya Rift Valley: Sedimentary Geology, v. 222, no. 1-2, p. 124-137.

Plummer, T. W., and Bishop, L. C., 1994, Hominid paleoecology of Olduvai Gorge, Tanzania as indicated by antelope remains: Journal of Human Evolution, v. 27, p. 47-75.

Renaut, R. W., 1993, Zeolitic diagenesis of late Quaternary fluviolacustrine sediments and associated calcrete formation in the Lake Borgoria Basin, Kenyar Rift Valley: Sedimentology, v. 40, p. 271-301.

Retallack, G. J., 2001, Soils of the past: An introduction to paleopedology, Oxford, Blackwell Science Ltd, 512 p.

Royer, D. L., 1999, Depth to pedogenic carbonate horizon as a paleoprecipitation indicator?: Geology, v. 27, no. 12, p. 1123.

Ruddiman, W. F., 2008, Earth's Climate: Past and Future, New York, W. H. Freeman and Company, 388 p.

Russell, J. M., and Johnson, T. C., 2007, Little Ice Age drought in equatorial Africa: Intertropical Convergence Zone migrations and El Niño–Southern Oscillation variability: Geology, v. 35, no. 1, p. 21.

Schwertmann, U., and Taylor, R. M., 1989, Iron oxides, *in* Dixon, J. B., and Weed, S. B., eds., Minerals in Soil Environments: Madison, Wisconsin, Soil Science Society of America, p. 379-438.

SEPM-NSF Research Conference and Workshop, 2010, Paleosols and Soil Surface System Analogs: Petrified Forest National Park, Arizona.

Sheldon, N. D., Retallack, G. J., and Tanaka, S., 2002, Geochemical climofunctions from North America soils and applications to paleosols across the Eocene-Oligocene Boundary in Oregon: The Journal of Geology, v. 110, no. 6, p. 687-696.

Sheldon, N. D., and Tabor, N. J., 2009, Quantitative paleoenvironmental and paleoclimatic reconstruction using paleosols: Earth-Science Reviews, v. 95, no. 1-2, p. 1-52.

Sikes, N. E., and Ashley, G. M., 2007, Stable isotopes of pedogenic carbonates as indicators of paleoecology in the Plio-Pleistocene (upper Bed I), western margin of the Olduvai Basin, Tanzania: Journal of Human Evolution, v. 53, no. 5, p. 574-594.

Southard, R. J., Driese, S., and Nordt, L., 2011, Vertisols, *in* Huang, P., ed., Handbook of Soil Science: Boca Raton, Florida, CRC Press (in press).

Staff, S. S., 1999, Vertisols, Soil Taxonomy: A Basic System of Soil Classification for Making and Interpreting Soil Surveys: Washington D.C., United States Department of Agriculture, Agriculture Handbook No. 436, p. 783-817.

Stiles, C. A., Mora, C. I., and Driese, S. G., 2001, Pedogenic iron-manganese nodules in Vertisols: A new proxy for paleoprecipitation?: Geology, v. 29, no. 10, p. 943-946.

Stiles, C. A., Mora, C. I., and Driese, S. G., 2003a, Pedogenic processes and domain boundaries in a Vertisol climosequence: evidence from titanium and zirconium distribution and morphology: Geoderma, v. 116, no. 3-4, p. 279-299.

Stiles, C. A., Mora, C. I., Driese, S. G., and Robinson, A. C., 2003b, Distinguishing climate and time in the soil record: Mass-balance trends in Vertisols from the Texas coastal prairie: Geology, v. 31, no. 4, p. 331-334.

Tamrat, E., Thouveny, N., Taieb, M., and Opdyke, N. D., 1995, Revised magnetostratigraphy of the Plio–Pleistocene sedimentary sequence of the Olduvai Formation (Tanzania): Palaeogeography, Palaeoclimatology, Palaeoecology, v. 114, p. 273-283.

Trauth, M. H., Larrasoaña, J. C., and Mudelsee, M., 2009, Trends, rhythms and events in Plio-Pleistocene African climate: Quaternary Science Reviews, v. 28, no. 5-6, p. 399-411.

Trauth, M. H., Maslin, M. A., Deino, A. L., Strecker, M. R., Bergner, A. G., and Duhnforth, M., 2007, High- and low-latitude forcing of Plio-Pleistocene East African climate and human evolution: Journal of Human Evolution, v. 53, no. 5, p. 475-486.

Tuenter, E., Weber, S. L., Hilgen, F. J., and Lourens, L. J., 2003, The response of the African summer monsoon to remote and local forcing due to precession and obliquity: Global and Planetary Change, v. 36, no. 4, p. 219-235.

Vepraskas, M. J., and Faulkner, S. P., 2001, Redox chemistry of hydric soils, *in* Richardson, J. L., and Vepraskas, M. J., eds., Wetland Solis; Genesis, Hydrology, Landscapes, and Classification: New York, Lewis Publishers, p. 85-105.

Verschuren, D., Laird, K. R., and Cumming, B. F., 2000, Rainfall and drought in equatorial east Africa during the past 1,100 years: Nature, v. 403, p. 410-414.

Violante, A., Barberis, E., Pigna, M., and Boero, V., 2003, Factors affecting the formation, nature, and properties of iron precipitation products at the soil-root interface: Journal of Plant Nutrition, v. 26, p. 1889-1908.

Wentworth, C. K., 1922, A scale of grade and class terms for clastic sediments: Journal of Geology, v. 27, p. 377-392.

Appendix 1: Sample location, depth in profile, bulk density, and general description

Sample #	Location	Trench	Depth (cm)	Mean Bulk Density	Description
EB-Chem-41	FLK-N	OLD-3	5.0	1.62	paleosol
EB-Chem-42	FLK-N	OLD-3	10.0	1.42	paleosol
EB-Chem-43	FLK-N	OLD-3	15.0	1.67	paleosol
EB-Chem-44	FLK-N	OLD-3	25.0	1.58	paleosol
EB-Chem-45	FLK-N	OLD-3	30.0	1.07	paleosol
EB-Chem-46	FLK-N	OLD-3	40.0	1.58	paleosol
EB-Chem-47	FLK-N	OLD-3	50.0	1.51	paleosol
EB-Chem-48	FLK-N	OLD-3	60.0	1.65	paleosol
EB-61	FLK-N	OLD-3	75.0	0.95	unnamed tuff
GA-OLD-18-07	FLK	FLK-01	65.0	1.21	paleosol
GA-OLD-19-07	FLK	FLK-01	70.0	1.36	paleosol
GA-OLD-20-07	FLK	FLK-01	75.0	1.91	paleosol
GA-OLD-21-07	FLK	FLK-01	80.0	1.54	paleosol
GA-OLD-22-07	FLK	FLK-01	85.0	1.15	paleosol
GA-OLD-23-07	FLK	FLK-01	90.0	1.47	paleosol
GA-OLD-24-07	FLK	FLK-01	95.0	1.43	paleosol
GA-OLD-25-07	FLK	FLK-01	100.0	1.41	paleosol
GA-OLD-26-07	FLK	FLK-01	105.0	1.57	paleosol
GA-OLD-27-07	FLK	FLK-01	110.0	1.63	paleosol
GA-OLD-28-07	FLK	FLK-01	115.0	1.64	paleosol
GA-OLD-29-07	FLK	FLK-01	120.0	1.53	paleosol
GA-OLD-31-07	FLK	FLK-01	130.0	0.95	unnamed tuff
GA-OLD-36-07	FLK	FLK-01	175.0	1.38	paleosol
GA-OLD-37-07	FLK	FLK-01	185.0	1.41	paleosol
GA-OLD-38-07	FLK	FLK-01	195.0	1.38	paleosol
GA-OLD-40-07	FLK	FLK-01	205.0	1.32	paleosol
GA-OLD-41-07	FLK	FLK-01	215.0	1.50	paleosol
GA-OLD-42-07	FLK	FLK-01	225.0	1.21	paleosol
GA-OLD-43-07	FLK	FLK-01	235.0	1.20	paleosol
GA-OLD-44-07	FLK	FLK-01	245.0	1.13	paleosol
EB-Chem-19	FLK	OLD-1	0.0	1.48	paleosol
EB-Chem-18	FLK	OLD-1	10.0	1.49	paleosol
EB-Chem-17	FLK	OLD-1	20.0	1.50	paleosol
EB-Chem-16	FLK	OLD-1	30.0	1.62	paleosol
EB-Chem-15	FLK	OLD-1	80.0	1.31	paleosol
EB-Chem-14	FLK	OLD-1	90.0	1.36	paleosol
EB-Chem-13	FLK	OLD-1	100.0	1.58	paleosol
EB-12	FLK	OLD-1	107.5	1.36	fragipan
EB-11	FLK	OLD-1	112.5	0.98	fragipan

Appendix 1: continued

Sample #	Location	Trench	Depth (cm)	Mean Bulk Density	Description
EB-Chem-12	FLK	OLD-1	125.0	1.63	paleosol
EB-Chem-11	FLK	OLD-1	130.0	1.66	paleosol
EB-Chem-10	FLK	OLD-1	140.0	1.67	paleosol
EB-Chem-9	FLK	OLD-1	145.0	1.60	paleosol
EB-Chem-8	FLK	OLD-1	150.0	1.60	paleosol
EB-Chem-7	FLK	OLD-1	160.0	1.39	paleosol
EB-Chem-6	FLK	OLD-1	170.0	1.26	paleosol
EB-Chem-5	FLK	OLD-1	180.0	1.41	paleosol
EB-Chem-4	FLK	OLD-1	190.0	1.39	paleosol
EB-2	FLK	OLD-1	200.0	0.94	unnamed tuff
EB-50	FLK	OLD-1	230.0	1.09	Ng'eju tuff
EB-Chem-36	HWK-E	OLD-2	5.0	1.65	paleosol
EB-Chem-35	HWK-E	OLD-2	15.0	1.30	paleosol
EB-Chem-34	HWK-E	OLD-2	25.0	1.68	paleosol
EB-Chem-33	HWK-E	OLD-2	35.0	1.63	paleosol
EB-Chem-32	HWK-E	OLD-2	45.0	1.51	paleosol
EB-Chem-31	HWK-E	OLD-2	55.0	1.57	paleosol
EB-Chem-30	HWK-E	OLD-2	65.0	1.44	paleosol
EB-Chem-29	HWK-E	OLD-2	75.0	1.66	paleosol
EB-Chem-28	HWK-E	OLD-2	85.0	1.53	paleosol
EB-Chem-27	HWK-E	OLD-2	95.0	1.50	paleosol
EB-Chem-23	HWK-E	OLD-2	105.0	1.29	paleosol
EB-Chem-22	HWK-E	OLD-2	115.0	1.30	paleosol
EB-Chem-21	HWK-E	OLD-2	125.0	1.46	paleosol
EB-Chem-20	HWK-E	OLD-2	135.0	1.32	paleosol
EB-Chem-39	HWK-E	OLD-2	140.0	1.19	volcaniclastic
EB-Chem-40	HWK-E	OLD-2	150.0	1.34	volcaniclastic burrow
EB-Chem-38	HWK-E	OLD-2	155.0	1.37	volcaniclastic
EB-Chem-37	HWK-E	OLD-2	170.0	1.17	volcaniclastic
EB-29	HWK-E	OLD-2	190.0	1.00	unnamed tuff
GA-37-99	Loc. 80			1.43	waxy lake clay
GA-47-99	Loc. 80			1.61	waxy lake clay
46-A12	Loc. 38	46			Tuff 1F

Appendix 2: Bulk geochemical values converted to wt. %

Sample #	Ba	Ce	Co	Cr	Cs	Cu	Dy	Er	Eu	Ga	Gd
EB-Chem-41	0.0330	0.0117	0.0011	0.0050	0.0004	0.0094	0.0006	0.0002	0.0003	0.0023	0.0009
EB-Chem-42	0.0400	0.0129	0.0011	0.0030	0.0006	0.0033	0.0005	0.0003	0.0002	0.0018	0.0006
EB-Chem-43	0.0476	0.0137	0.0015	0.0050	0.0007	0.0035	0.0006	0.0003	0.0003	0.0018	0.0007
EB-Chem-44	0.0344	0.0117	0.0018	0.0060	0.0007	0.0040	0.0005	0.0003	0.0002	0.0016	0.0007
EB-Chem-45	0.0296	0.0054	0.0023	0.0060	0.0003	0.0039	0.0003	0.0001	0.0001	0.0013	0.0004
EB-Chem-46	0.0434	0.0186	0.0016	0.0060	0.0006	0.0037	0.0008	0.0004	0.0003	0.0019	0.0009
EB-Chem-47	0.0602	0.0210	0.0009	0.0040	0.0005	0.0023	0.0010	0.0006	0.0003	0.0018	0.0010
EB-Chem-48	0.0605	0.0178	0.0010	0.0060	0.0004	0.0023	0.0008	0.0004	0.0003	0.0022	0.0009
EB-61	0.0694	0.0076	0.0004	0.0020	0.0004	0.0012	0.0002	0.0001	0.0002	0.0018	0.0003
GA-OLD-18-07	0.0256	0.0060	0.0008	0.0030	0.0002	0.0023	0.0002	0.0001	0.0001	0.0012	0.0003
GA-OLD-19-07	0.0368	0.0098	0.0013	0.0050	0.0003	0.0032	0.0004	0.0002	0.0002	0.0015	0.0005
GA-OLD-20-07	0.0338	0.0084	0.0012	0.0030	0.0004	0.0026	0.0004	0.0002	0.0002	0.0014	0.0005
GA-OLD-21-07	0.0398	0.0134	0.0011	0.0040	0.0003	0.0028	0.0006	0.0003	0.0002	0.0014	0.0006
GA-OLD-22-07	0.0288	0.0082	0.0010	0.0030	0.0003	0.0029	0.0003	0.0001	0.0001	0.0013	0.0003
GA-OLD-23-07	0.0348	0.0110	0.0010	0.0030	0.0003	0.0031	0.0005	0.0003	0.0002	0.0012	0.0006
GA-OLD-24-07	0.0486	0.0103	0.0013	0.0060	0.0003	0.0037	0.0004	0.0002	0.0002	0.0015	0.0005
GA-OLD-25-07	0.0295	0.0078	0.0008	0.0060	0.0002	0.0042	0.0003	0.0001	0.0001	0.0015	0.0004
GA-OLD-26-07	0.0429	0.0107	0.0009	0.0040	0.0002	0.0039	0.0004	0.0002	0.0001	0.0014	0.0005
GA-OLD-27-07	0.0528	0.0120	0.0009	0.0030	0.0002	0.0032	0.0008	0.0004	0.0002	0.0014	0.0008
GA-OLD-28-07	0.0302	0.0093	0.0011	0.0040	0.0002	0.0035	0.0005	0.0002	0.0002	0.0013	0.0006
GA-OLD-29-07	0.0238	0.0060	0.0014	0.0070	0.0001	0.0046	0.0003	0.0001	0.0001	0.0013	0.0004
GA-OLD-31-07	0.1185	0.0250	0.0002	0.0020	0.0003	0.0019	0.0010	0.0005	0.0003	0.0021	0.0011
GA-OLD-36-07	0.0278	0.0069	0.0008	0.0020	0.0002	0.0032	0.0003	0.0001	0.0001	0.0015	0.0004
GA-OLD-37-07	0.0556	0.0094	0.0011	0.0030	0.0003	0.0035	0.0004	0.0002	0.0002	0.0015	0.0006
GA-OLD-38-07	0.0546	0.0104	0.0012	0.0040	0.0003	0.0033	0.0006	0.0003	0.0002	0.0015	0.0007

Appendix 2: continued

Sample #	Ba	Ce	Co	Cr	Cs	Cu	Dy	Er	Eu	Ga	Gd
GA-OLD-40-07	0.0465	0.0189	0.0009	0.0030	0.0003	0.0030	0.0007	0.0005	0.0002	0.0017	0.0007
GA-OLD-41-07	0.0596	0.0133	0.0010	0.0040	0.0002	0.0027	0.0007	0.0004	0.0003	0.0018	0.0008
GA-OLD-42-07	0.0606	0.0088	0.0011	0.0040	0.0002	0.0030	0.0005	0.0002	0.0002	0.0018	0.0006
GA-OLD-43-07	0.0612	0.0084	0.0010	0.0030	0.0002	0.0026	0.0005	0.0002	0.0002	0.0018	0.0007
GA-OLD-44-07	0.0617	0.0088	0.0010	0.0040	0.0002	0.0031	0.0005	0.0002	0.0002	0.0020	0.0007
EB-Chem-19	0.0426	0.0117	0.0011	0.0050	0.0003	0.0041	0.0003	0.0002	0.0001	0.0017	0.0006
EB-Chem-18	0.0262	0.0065	0.0011	0.0050	0.0003	0.0031	0.0002	0.0001	0.0001	0.0012	0.0003
EB-Chem-17	0.0389	0.0128	0.0010	0.0040	0.0002	0.0028	0.0003	0.0002	0.0001	0.0011	0.0005
EB-Chem-16	0.0350	0.0114	0.0008	0.0030	0.0002	0.0025	0.0003	0.0002	0.0001	0.0011	0.0005
EB-Chem-15	0.0413	0.0073	0.0011	0.0030	0.0002	0.0042	0.0003	0.0002	0.0001	0.0012	0.0004
EB-Chem-14	0.0272	0.0063	0.0012	0.0050	0.0001	0.0042	0.0004	0.0002	0.0001	0.0010	0.0004
EB-Chem-13	0.0258	0.0059	0.0015	0.0030	0.0001	0.0054	0.0006	0.0003	0.0002	0.0011	0.0006
EB-12	0.0797	0.0055	0.0016	0.0030	0.0001	0.0056	0.0003	0.0001	0.0001	0.0014	0.0004
EB-11	0.0326	0.0081	0.0008	0.0020	0.0001	0.0049	0.0003	0.0001	0.0001	0.0013	0.0006
EB-Chem-12	0.0305	0.0129	0.0014	0.0040	0.0002	0.0096	0.0008	0.0003	0.0003	0.0016	0.0013
EB-Chem-11	0.0338	0.0085	0.0015	0.0050	0.0003	0.0105	0.0004	0.0002	0.0002	0.0016	0.0007
EB-Chem-10	0.0429	0.0097	0.0014	0.0030	0.0003	0.0117	0.0005	0.0002	0.0002	0.0016	0.0008
EB-Chem-9	0.0286	0.0094	0.0012	0.0030	0.0003	0.0108	0.0002	0.0001	0.0001	0.0017	0.0004
EB-Chem-8	0.0466	0.0096	0.0010	0.0020	0.0003	0.0047	0.0002	0.0001	0.0001	0.0014	0.0004
EB-Chem-7	0.0511	0.0090	0.0008	0.0020	0.0002	0.0040	0.0003	0.0002	0.0001	0.0011	0.0004
EB-Chem-6	0.0510	0.0166	0.0015	0.0040	0.0002	0.0047	0.0006	0.0003	0.0003	0.0013	0.0009
EB-Chem-5	0.0663	0.0164	0.0009	0.0020	0.0001	0.0046	0.0009	0.0005	0.0003	0.0014	0.0010
EB-Chem-4	0.0483	0.0073	0.0008	0.0040	0.0001	0.0035	0.0004	0.0002	0.0002	0.0015	0.0007
EB-2	0.0734	0.0088	0.0004	0.0010	0.0001	0.0013	0.0005	0.0002	0.0003	0.0015	0.0007
EB-50	0.0921	0.0123	0.0007	0.0050	0.0001	0.0010	0.0006	0.0003	0.0004	0.0023	0.0009

Appendix 2: continued

Sample #	Ba	Ce	Co	Cr	Cs	Cu	Dy	Er	Eu	Ga	Gd
EB-Chem-36	0.1030	0.0132	0.0017	0.0140	0.0006	0.0049	0.0008	0.0004	0.0003	0.0019	0.0009
EB-Chem-35	0.0745	0.0268	0.0017	0.0060	0.0005	0.0056	0.0005	0.0004	0.0002	0.0020	0.0006
EB-Chem-34	0.0196	0.0122	0.0004	0.0010	0.0002	0.0051	0.0002	0.0001	0.0001	0.0012	0.0003
EB-Chem-33	0.0297	0.0119	0.0007	0.0010	0.0003	0.0029	0.0004	0.0002	0.0002	0.0015	0.0005
EB-Chem-32	0.0368	0.0106	0.0008	0.0020	0.0004	0.0030	0.0004	0.0002	0.0002	0.0013	0.0005
EB-Chem-31	0.0449	0.0140	0.0011	0.0010	0.0004	0.0043	0.0005	0.0002	0.0002	0.0015	0.0005
EB-Chem-30	0.0648	0.0141	0.0013	0.0020	0.0005	0.0061	0.0006	0.0003	0.0002	0.0018	0.0007
EB-Chem-29	0.0686	0.0129	0.0011	0.0020	0.0005	0.0056	0.0005	0.0002	0.0002	0.0018	0.0006
EB-Chem-28	0.0421	0.0125	0.0011	0.0020	0.0005	0.0053	0.0004	0.0002	0.0002	0.0018	0.0005
EB-Chem-27	0.0439	0.0154	0.0011	0.0030	0.0005	0.0051	0.0009	0.0004	0.0003	0.0017	0.0009
EB-Chem-23	0.0445	0.0184	0.0015	0.0030	0.0007	0.0063	0.0008	0.0004	0.0002	0.0021	0.0008
EB-Chem-22	0.0569	0.0189	0.0016	0.0040	0.0007	0.0070	0.0008	0.0004	0.0003	0.0023	0.0008
EB-Chem-21	0.0499	0.0163	0.0011	0.0050	0.0006	0.0061	0.0007	0.0003	0.0002	0.0022	0.0007
EB-Chem-20	0.0490	0.0167	0.0010	0.0050	0.0006	0.0053	0.0006	0.0003	0.0002	0.0020	0.0007
EB-Chem-39	0.2210	0.0208	0.0010	0.0040	0.0005	0.0031	0.0007	0.0004	0.0003	0.0017	0.0008
EB-Chem-40	0.0981	0.0173	0.0011	0.0040	0.0006	0.0035	0.0006	0.0003	0.0003	0.0018	0.0007
EB-Chem-38	0.1135	0.0150	0.0012	0.0060	0.0004	0.0027	0.0006	0.0003	0.0003	0.0019	0.0007
EB-Chem-37	0.1090	0.0141	0.0013	0.0050	0.0005	0.0030	0.0007	0.0004	0.0003	0.0019	0.0009
EB-29	0.0922	0.0129	0.0008	0.0030	0.0005	0.0015	0.0004	0.0002	0.0002	0.0021	0.0006
GA-37-99	0.0259	0.0110	0.0007	0.0030	0.0001	0.0029	0.0006	0.0003	0.0002	0.0010	0.0008
GA-47-99	0.0203	0.0069	0.0011	0.0050	0.0002	0.0157	0.0004	0.0002	0.0001	0.0014	0.0005
46-A12	0.0486		0.0018	0.0142		0.0043					

Appendix 2: continued

Sample #	Hf	Ho	La	Lu	Nb	Nd	Pr	Rb	Sm	Sn	Sr
EB-Chem-41	0.0006	0.0001	0.0112	0.0000	0.0123	0.0074	0.0021	0.0075	0.0012	0.0001	0.0273
EB-Chem-42	0.0006	0.0001	0.0072	0.0000	0.0138	0.0045	0.0013	0.0083	0.0007	0.0001	0.0284
EB-Chem-43	0.0007	0.0001	0.0083	0.0000	0.0115	0.0055	0.0015	0.0095	0.0009	0.0002	0.0350
EB-Chem-44	0.0006	0.0001	0.0077	0.0000	0.0129	0.0053	0.0014	0.0072	0.0009	0.0001	0.0257
EB-Chem-45	0.0004	0.0001	0.0034	0.0000	0.0044	0.0026	0.0007	0.0053	0.0005	0.0001	0.0153
EB-Chem-46	0.0006	0.0002	0.0103	0.0001	0.0180	0.0066	0.0018	0.0083	0.0011	0.0002	0.0384
EB-Chem-47	0.0006	0.0002	0.0122	0.0001	0.0105	0.0074	0.0021	0.0078	0.0012	0.0002	0.0467
EB-Chem-48	0.0007	0.0002	0.0106	0.0001	0.0102	0.0068	0.0019	0.0057	0.0011	0.0002	0.0423
EB-61	0.0006	0.0000	0.0040	0.0000	0.0085	0.0028	0.0008	0.0049	0.0005	0.0003	0.0538
GA-OLD-18-07	0.0004	0.0000	0.0037	0.0000	0.0071	0.0023	0.0006	0.0065	0.0004	0.0001	0.0163
GA-OLD-19-07	0.0007	0.0001	0.0070	0.0000	0.0117	0.0040	0.0012	0.0096	0.0007	0.0002	0.0262
GA-OLD-20-07	0.0006	0.0001	0.0068	0.0000	0.0117	0.0037	0.0011	0.0085	0.0006	0.0001	0.0224
GA-OLD-21-07	0.0006	0.0001	0.0078	0.0000	0.0111	0.0045	0.0013	0.0094	0.0007	0.0002	0.0255
GA-OLD-22-07	0.0005	0.0001	0.0049	0.0000	0.0098	0.0028	0.0008	0.0095	0.0005	0.0001	0.0155
GA-OLD-23-07	0.0006	0.0001	0.0076	0.0000	0.0127	0.0042	0.0013	0.0117	0.0007	0.0002	0.0193
GA-OLD-24-07	0.0006	0.0001	0.0067	0.0000	0.0105	0.0039	0.0012	0.0102	0.0007	0.0002	0.0250
GA-OLD-25-07	0.0007	0.0001	0.0051	0.0000	0.0111	0.0030	0.0009	0.0092	0.0005	0.0002	0.0115
GA-OLD-26-07	0.0006	0.0001	0.0054	0.0000	0.0105	0.0033	0.0010	0.0079	0.0006	0.0002	0.0180
GA-OLD-27-07	0.0006	0.0001	0.0088	0.0000	0.0105	0.0052	0.0015	0.0063	0.0009	0.0002	0.0188
GA-OLD-28-07	0.0006	0.0001	0.0064	0.0000	0.0109	0.0041	0.0012	0.0043	0.0007	0.0002	0.0189
GA-OLD-29-07	0.0005	0.0001	0.0039	0.0000	0.0070	0.0028	0.0008	0.0039	0.0005	0.0001	0.0103
GA-OLD-31-07	0.0008	0.0002	0.0122	0.0001	0.0091	0.0065	0.0019	0.0078	0.0013	0.0004	0.0527
GA-OLD-36-07	0.0004	0.0001	0.0041	0.0000	0.0071	0.0027	0.0008	0.0092	0.0005	0.0001	0.0165
GA-OLD-37-07	0.0006	0.0001	0.0065	0.0000	0.0088	0.0042	0.0012	0.0112	0.0007	0.0002	0.0377
GA-OLD-38-07	0.0006	0.0001	0.0080	0.0000	0.0095	0.0050	0.0014	0.0108	0.0008	0.0002	0.0430

Appendix 2: continued

Sample #	Hf	Ho	La	Lu	Nb	Nd	Pr	Rb	Sm	Sn	Sr
GA-OLD-40-07	0.0006	0.0002	0.0072	0.0001	0.0086	0.0043	0.0012	0.0119	0.0008	0.0002	0.0525
GA-OLD-41-07	0.0006	0.0001	0.0090	0.0000	0.0085	0.0054	0.0015	0.0106	0.0009	0.0002	0.0528
GA-OLD-42-07	0.0006	0.0001	0.0063	0.0000	0.0086	0.0044	0.0012	0.0098	0.0008	0.0002	0.0531
GA-OLD-43-07	0.0007	0.0001	0.0067	0.0000	0.0081	0.0047	0.0013	0.0091	0.0008	0.0002	0.0535
GA-OLD-44-07	0.0007	0.0001	0.0070	0.0000	0.0090	0.0049	0.0014	0.0089	0.0008	0.0002	0.0506
EB-Chem-19	0.0009	0.0001	0.0064	0.0000	0.0130	0.0040	0.0012	0.0120	0.0006	0.0002	0.0174
EB-Chem-18	0.0008	0.0000	0.0039	0.0000	0.0117	0.0024	0.0007	0.0155	0.0004	0.0001	0.0088
EB-Chem-17	0.0006	0.0001	0.0043	0.0000	0.0087	0.0030	0.0009	0.0123	0.0006	0.0001	0.0187
EB-Chem-16	0.0005	0.0001	0.0040	0.0000	0.0079	0.0030	0.0009	0.0092	0.0005	0.0001	0.0243
EB-Chem-15	0.0005	0.0001	0.0038	0.0000	0.0085	0.0026	0.0007	0.0042	0.0004	0.0002	0.0143
EB-Chem-14	0.0004	0.0001	0.0027	0.0000	0.0060	0.0019	0.0005	0.0034	0.0004	0.0001	0.0112
EB-Chem-13	0.0004	0.0001	0.0030	0.0000	0.0097	0.0028	0.0007	0.0033	0.0005	0.0001	0.0136
EB-12	0.0004	0.0000	0.0036	0.0000	0.0130	0.0026	0.0008	0.0043	0.0005	0.0001	0.0094
EB-11	0.0005	0.0001	0.0054	0.0000	0.0075	0.0037	0.0011	0.0039	0.0006	0.0001	0.0063
EB-Chem-12	0.0007	0.0001	0.0126	0.0000	0.0104	0.0081	0.0024	0.0144	0.0014	0.0001	0.0105
EB-Chem-11	0.0008	0.0001	0.0064	0.0000	0.0129	0.0043	0.0012	0.0169	0.0007	0.0002	0.0101
EB-Chem-10	0.0006	0.0001	0.0074	0.0000	0.0118	0.0050	0.0014	0.0170	0.0009	0.0001	0.0120
EB-Chem-9	0.0006	0.0000	0.0034	0.0000	0.0120	0.0024	0.0007	0.0164	0.0004	0.0002	0.0090
EB-Chem-8	0.0006	0.0000	0.0035	0.0000	0.0097	0.0025	0.0007	0.0141	0.0004	0.0001	0.0218
EB-Chem-7	0.0005	0.0001	0.0042	0.0000	0.0094	0.0027	0.0008	0.0087	0.0004	0.0001	0.0511
EB-Chem-6	0.0005	0.0001	0.0083	0.0000	0.0112	0.0054	0.0015	0.0046	0.0009	0.0001	0.0266
EB-Chem-5	0.0006	0.0002	0.0088	0.0001	0.0085	0.0058	0.0016	0.0045	0.0010	0.0002	0.0313
EB-Chem-4	0.0006	0.0001	0.0062	0.0000	0.0066	0.0048	0.0014	0.0042	0.0008	0.0002	0.0256
EB-2	0.0007	0.0001	0.0070	0.0000	0.0067	0.0042	0.0012	0.0057	0.0008	0.0003	0.0453
EB-50	0.0008	0.0001	0.0078	0.0000	0.0101	0.0055	0.0016	0.0035	0.0010	0.0002	0.0961

Appendix 2: continued

Sample #	Hf	Ho	La	Lu	Nb	Nd	Pr	Rb	Sm	Sn	Sr
EB-Chem-36	0.0011	0.0001	0.0094	0.0000	0.0156	0.0061	0.0017	0.0143	0.0010	0.0002	0.0402
EB-Chem-35	0.0007	0.0001	0.0088	0.0001	0.0191	0.0046	0.0013	0.0139	0.0008	0.0002	0.0841
EB-Chem-34	0.0003	0.0000	0.0049	0.0000	0.0057	0.0025	0.0008	0.0055	0.0005	0.0002	0.0050
EB-Chem-33	0.0005	0.0001	0.0069	0.0000	0.0097	0.0040	0.0012	0.0104	0.0007	0.0001	0.0118
EB-Chem-32	0.0005	0.0001	0.0068	0.0000	0.0113	0.0039	0.0011	0.0113	0.0006	0.0002	0.0133
EB-Chem-31	0.0006	0.0001	0.0071	0.0000	0.0108	0.0039	0.0012	0.0120	0.0007	0.0002	0.0117
EB-Chem-30	0.0008	0.0001	0.0089	0.0000	0.0127	0.0052	0.0015	0.0148	0.0008	0.0002	0.0123
EB-Chem-29	0.0008	0.0001	0.0088	0.0000	0.0120	0.0052	0.0015	0.0142	0.0008	0.0002	0.0147
EB-Chem-28	0.0008	0.0001	0.0078	0.0000	0.0115	0.0045	0.0013	0.0143	0.0008	0.0002	0.0112
EB-Chem-27	0.0008	0.0002	0.0126	0.0001	0.0115	0.0071	0.0020	0.0111	0.0012	0.0002	0.0225
EB-Chem-23	0.0009	0.0002	0.0111	0.0001	0.0130	0.0065	0.0019	0.0139	0.0011	0.0003	0.0207
EB-Chem-22	0.0010	0.0001	0.0115	0.0000	0.0148	0.0069	0.0020	0.0131	0.0011	0.0003	0.0281
EB-Chem-21	0.0010	0.0001	0.0103	0.0000	0.0137	0.0063	0.0018	0.0125	0.0010	0.0003	0.0236
EB-Chem-20	0.0010	0.0001	0.0093	0.0000	0.0138	0.0052	0.0016	0.0110	0.0010	0.0003	0.0504
EB-Chem-39	0.0007	0.0001	0.0104	0.0000	0.0120	0.0066	0.0019	0.0091	0.0011	0.0002	0.0826
EB-Chem-40	0.0008	0.0001	0.0101	0.0000	0.0116	0.0061	0.0017	0.0107	0.0010	0.0002	0.0546
EB-Chem-38	0.0007	0.0001	0.0092	0.0000	0.0106	0.0057	0.0016	0.0085	0.0009	0.0002	0.0586
EB-Chem-37	0.0008	0.0001	0.0108	0.0000	0.0112	0.0068	0.0019	0.0089	0.0011	0.0002	0.0541
EB-29	0.0011	0.0001	0.0090	0.0000	0.0126	0.0051	0.0015	0.0073	0.0008	0.0004	0.0399
GA-37-99	0.0004	0.0001	0.0055	0.0000	0.0067	0.0045	0.0012	0.0084	0.0008	0.0001	0.1145
GA-47-99	0.0005	0.0001	0.0037	0.0000	0.0083	0.0027	0.0007	0.0123	0.0006	0.0001	0.0405
46-A12								0.0087			0.0146

Appendix 2: continued

Sample #	Ta	Tb	Th	Tm	U	V	Y	Yb	Zn	Zr	SiO2
EB-Chem-41	0.0004	0.0001	0.0011	0.0000	0.0002	0.0193	0.0027	0.0002	0.0156	0.0267	50.50
EB-Chem-42	0.0004	0.0001	0.0011	0.0000	0.0002	0.0182	0.0032	0.0003	0.0098	0.0255	52.00
EB-Chem-43	0.0005	0.0001	0.0011	0.0000	0.0002	0.0147	0.0033	0.0003	0.0117	0.0290	51.40
EB-Chem-44	0.0004	0.0001	0.0009	0.0000	0.0002	0.0165	0.0028	0.0002	0.0115	0.0275	51.60
EB-Chem-45	0.0002	0.0001	0.0004	0.0000	0.0001	0.0135	0.0014	0.0001	0.0091	0.0205	47.80
EB-Chem-46	0.0005	0.0001	0.0013	0.0001	0.0002	0.0163	0.0048	0.0004	0.0120	0.0282	51.60
EB-Chem-47	0.0005	0.0002	0.0016	0.0001	0.0002	0.0148	0.0061	0.0005	0.0113	0.0248	50.80
EB-Chem-48	0.0006	0.0001	0.0018	0.0001	0.0001	0.0135	0.0047	0.0004	0.0119	0.0264	52.90
EB-61	0.0006	0.0000	0.0006	0.0000	0.0001	0.0096	0.0011	0.0001	0.0076	0.0199	51.20
GA-OLD-18-07	0.0004	0.0000	0.0005	0.0000	0.0001	0.0112	0.0009	0.0001	0.0080	0.0217	50.30
GA-OLD-19-07	0.0004	0.0001	0.0006	0.0000	0.0001	0.0133	0.0019	0.0001	0.0119	0.0329	50.00
GA-OLD-20-07	0.0004	0.0001	0.0006	0.0000	0.0001	0.0116	0.0018	0.0001	0.0111	0.0311	49.10
GA-OLD-21-07	0.0004	0.0001	0.0012	0.0000	0.0001	0.0116	0.0032	0.0002	0.0100	0.0303	52.40
GA-OLD-22-07	0.0004	0.0001	0.0005	0.0000	0.0001	0.0119	0.0014	0.0001	0.0087	0.0259	50.80
GA-OLD-23-07	0.0004	0.0001	0.0010	0.0000	0.0001	0.0097	0.0032	0.0002	0.0091	0.0318	50.70
GA-OLD-24-07	0.0005	0.0001	0.0007	0.0000	0.0003	0.0146	0.0019	0.0001	0.0084	0.0295	51.40
GA-OLD-25-07	0.0004	0.0001	0.0006	0.0000	0.0003	0.0503	0.0016	0.0001	0.0079	0.0306	51.10
GA-OLD-26-07	0.0004	0.0001	0.0008	0.0000	0.0007	0.0176	0.0022	0.0002	0.0080	0.0282	50.30
GA-OLD-27-07	0.0004	0.0001	0.0012	0.0001	0.0004	0.0116	0.0048	0.0003	0.0078	0.0247	49.60
GA-OLD-28-07	0.0004	0.0001	0.0008	0.0000	0.0002	0.0088	0.0027	0.0002	0.0086	0.0257	53.10
GA-OLD-29-07	0.0002	0.0001	0.0006	0.0000	0.0001	0.0082	0.0017	0.0001	0.0072	0.0219	52.60
GA-OLD-31-07	0.0010	0.0002	0.0013	0.0001	0.0002	0.0079	0.0047	0.0004	0.0093	0.0276	56.40
GA-OLD-36-07	0.0003	0.0001	0.0006	0.0000	0.0001	0.0055	0.0015	0.0001	0.0071	0.0199	52.50
GA-OLD-37-07	0.0004	0.0001	0.0008	0.0000	0.0002	0.0078	0.0023	0.0002	0.0090	0.0287	52.80
GA-OLD-38-07	0.0005	0.0001	0.0010	0.0000	0.0002	0.0082	0.0033	0.0002	0.0091	0.0292	52.30

Appendix 2: continued

Sample #	Ta	Tb	Th	Tm	U	V	Y	Yb	Zn	Zr	SiO2
GA-OLD-40-07	0.0004	0.0001	0.0012	0.0001	0.0004	0.0080	0.0048	0.0006	0.0086	0.0264	51.40
GA-OLD-41-07	0.0004	0.0001	0.0012	0.0001	0.0002	0.0078	0.0040	0.0003	0.0089	0.0287	52.40
GA-OLD-42-07	0.0005	0.0001	0.0009	0.0000	0.0003	0.0087	0.0026	0.0002	0.0095	0.0285	53.30
GA-OLD-43-07	0.0005	0.0001	0.0008	0.0000	0.0002	0.0090	0.0022	0.0002	0.0094	0.0273	51.70
GA-OLD-44-07	0.0005	0.0001	0.0009	0.0000	0.0003	0.0168	0.0023	0.0002	0.0090	0.0300	52.20
EB-Chem-19	0.0005	0.0001	0.0011	0.0000	0.0002	0.0103	0.0013	0.0001	0.0104	0.0332	54.40
EB-Chem-18	0.0004	0.0000	0.0007	0.0000	0.0003	0.0081	0.0008	0.0001	0.0078	0.0338	53.40
EB-Chem-17	0.0003	0.0001	0.0012	0.0000	0.0003	0.0116	0.0013	0.0001	0.0068	0.0270	54.20
EB-Chem-16	0.0003	0.0001	0.0013	0.0000	0.0004	0.0104	0.0014	0.0001	0.0065	0.0219	52.60
EB-Chem-15	0.0004	0.0001	0.0008	0.0000	0.0008	0.0115	0.0015	0.0001	0.0080	0.0211	53.50
EB-Chem-14	0.0002	0.0001	0.0008	0.0000	0.0006	0.0104	0.0021	0.0002	0.0061	0.0159	52.70
EB-Chem-13	0.0002	0.0001	0.0008	0.0000	0.0003	0.0096	0.0026	0.0002	0.0072	0.0172	52.90
EB-12	0.0003	0.0001	0.0005	0.0000	0.0003	0.0183	0.0012	0.0001	0.0071	0.0215	51.00
EB-11	0.0003	0.0001	0.0007	0.0000	0.0002	0.0258	0.0011	0.0001	0.0088	0.0224	51.20
EB-Chem-12	0.0004	0.0002	0.0009	0.0000	0.0004	0.0100	0.0027	0.0002	0.0124	0.0309	50.60
EB-Chem-11	0.0004	0.0001	0.0006	0.0000	0.0003	0.0088	0.0013	0.0001	0.0110	0.0338	50.90
EB-Chem-10	0.0004	0.0001	0.0007	0.0000	0.0002	0.0095	0.0021	0.0001	0.0104	0.0332	50.50
EB-Chem-9	0.0004	0.0001	0.0004	0.0000	0.0002	0.0094	0.0008	0.0001	0.0102	0.0313	52.10
EB-Chem-8	0.0004	0.0001	0.0008	0.0000	0.0002	0.0106	0.0010	0.0001	0.0091	0.0285	46.10
EB-Chem-7	0.0003	0.0001	0.0007	0.0000	0.0002	0.0089	0.0013	0.0001	0.0069	0.0207	36.80
EB-Chem-6	0.0005	0.0001	0.0011	0.0000	0.0003	0.0082	0.0023	0.0002	0.0090	0.0215	48.20
EB-Chem-5	0.0005	0.0002	0.0022	0.0001	0.0009	0.0057	0.0041	0.0004	0.0091	0.0208	51.40
EB-Chem-4	0.0005	0.0001	0.0011	0.0000	0.0006	0.0059	0.0015	0.0001	0.0101	0.0189	52.00
EB-2	0.0007	0.0001	0.0007	0.0000	0.0002	0.0058	0.0018	0.0001	0.0097	0.0216	51.50
EB-50	0.0006	0.0001	0.0009	0.0000	0.0002	0.0125	0.0025	0.0002	0.0118	0.0317	53.30

Appendix 2: continued

Sample #	Ta	Tb	Th	Tm	U	V	Y	Yb	Zn	Zr	SiO2
EB-Chem-36	0.0006	0.0001	0.0019	0.0001	0.0001	0.0106	0.0041	0.0003	0.0128	0.0516	52.40
EB-Chem-35	0.0005	0.0001	0.0011	0.0001	0.0002	0.0085	0.0034	0.0006	0.0109	0.0397	49.30
EB-Chem-34	0.0005	0.0000	0.0011	0.0000	0.0001	0.0058	0.0012	0.0001	0.0088	0.0190	51.70
EB-Chem-33	0.0004	0.0001	0.0010	0.0000	0.0001	0.0061	0.0021	0.0002	0.0080	0.0273	53.70
EB-Chem-32	0.0004	0.0001	0.0009	0.0000	0.0001	0.0067	0.0019	0.0001	0.0090	0.0296	53.10
EB-Chem-31	0.0004	0.0001	0.0010	0.0000	0.0002	0.0078	0.0022	0.0002	0.0102	0.0329	52.20
EB-Chem-30	0.0005	0.0001	0.0012	0.0000	0.0002	0.0109	0.0027	0.0002	0.0125	0.0384	51.70
EB-Chem-29	0.0005	0.0001	0.0012	0.0000	0.0003	0.0100	0.0023	0.0002	0.0131	0.0371	48.80
EB-Chem-28	0.0005	0.0001	0.0011	0.0000	0.0002	0.0095	0.0019	0.0001	0.0136	0.0358	51.80
EB-Chem-27	0.0006	0.0001	0.0018	0.0001	0.0002	0.0122	0.0047	0.0004	0.0130	0.0342	54.00
EB-Chem-23	0.0006	0.0001	0.0017	0.0001	0.0002	0.0226	0.0043	0.0004	0.0160	0.0425	51.00
EB-Chem-22	0.0007	0.0001	0.0016	0.0001	0.0002	0.0282	0.0038	0.0003	0.0165	0.0454	54.70
EB-Chem-21	0.0007	0.0001	0.0015	0.0000	0.0002	0.0165	0.0032	0.0003	0.0158	0.0442	53.60
EB-Chem-20	0.0006	0.0001	0.0017	0.0000	0.0002	0.0086	0.0032	0.0003	0.0149	0.0402	53.50
EB-Chem-39	0.0006	0.0001	0.0013	0.0001	0.0001	0.0070	0.0037	0.0003	0.0124	0.0297	52.60
EB-Chem-40	0.0006	0.0001	0.0013	0.0000	0.0002	0.0064	0.0032	0.0003	0.0129	0.0334	51.70
EB-Chem-38	0.0006	0.0001	0.0010	0.0000	0.0001	0.0065	0.0030	0.0002	0.0118	0.0297	51.80
EB-Chem-37	0.0006	0.0001	0.0012	0.0001	0.0001	0.0064	0.0043	0.0003	0.0125	0.0337	52.50
EB-29	0.0008	0.0001	0.0014	0.0000	0.0001	0.0129	0.0019	0.0002	0.0112	0.0394	53.70
GA-37-99	0.0003	0.0001	0.0020	0.0000	0.0014	0.0101	0.0027	0.0002	0.0061	0.0155	35.50
GA-47-99	0.0004	0.0001	0.0011	0.0000	0.0010	0.0206	0.0020	0.0002	0.0087	0.0215	44.40
46-A12						0.0112			0.0226	0.0420	55.30

Appendix 2: continued

Sample #	Al2O3	Fe2O3	CaO	MgO	Na2O	K2O	TiO2	MnO	P2O5	BaO	LOI	Total
EB-Chem-41	6.75	5.89	1.33	10.95	5.41	1.40	1.04	0.11	0.44	0.03	16.2	100.0
EB-Chem-42	8.17	5.56	1.76	9.53	5.66	1.50	0.84	0.13	0.57	0.05	14.8	100.5
EB-Chem-43	7.96	6.84	2.18	9.59	5.36	1.43	1.10	0.11	0.54	0.05	13.9	100.5
EB-Chem-44	7.15	6.76	2.09	9.55	5.38	1.24	1.27	0.10	0.55	0.04	14.4	100.0
EB-Chem-45	8.04	8.23	1.96	6.66	5.12	1.13	1.24	0.11	0.19	0.03	14.7	95.2
EB-Chem-46	7.75	6.48	2.12	9.66	5.30	1.37	1.37	0.10	0.71	0.05	14.0	100.5
EB-Chem-47	8.82	4.35	1.78	9.14	5.30	1.41	0.75	0.10	0.60	0.07	12.7	95.9
EB-Chem-48	9.28	5.39	1.68	8.33	5.43	1.40	0.75	0.09	0.60	0.06	13.3	99.2
EB-61	12.00	6.63	1.69	3.70	6.28	1.48	0.89	0.07	0.14	0.07	17.0	101.0
GA-OLD-18-07	6.27	4.21	1.11	13.75	3.63	1.37	0.65	0.10	0.21	0.03	16.6	98.2
GA-OLD-19-07	6.72	5.70	2.00	12.45	3.73	1.59	0.94	0.12	0.33	0.04	16.4	100.0
GA-OLD-20-07	6.44	5.71	1.73	12.30	3.75	1.45	0.89	0.15	0.38	0.04	16.6	98.6
GA-OLD-21-07	7.00	4.68	1.54	12.10	3.96	1.70	0.77	0.12	0.40	0.04	15.8	100.5
GA-OLD-22-07	6.28	4.66	1.22	13.30	3.52	1.66	0.74	0.13	0.22	0.04	17.5	100.0
GA-OLD-23-07	6.11	4.65	1.24	13.25	3.82	1.84	0.77	0.12	0.36	0.04	15.8	98.7
GA-OLD-24-07	7.43	5.07	2.24	11.30	3.68	1.94	0.98	0.14	0.22	0.05	15.2	99.7
GA-OLD-25-07	6.87	4.51	0.64	12.20	3.82	1.73	0.73	0.12	0.17	0.03	17.3	99.2
GA-OLD-26-07	7.01	4.46	0.69	12.15	3.97	1.63	0.79	0.14	0.19	0.04	17.1	98.5
GA-OLD-27-07	6.54	4.41	1.17	12.65	4.15	1.42	0.73	0.19	0.38	0.05	17.7	99.0
GA-OLD-28-07	6.18	5.21	1.31	14.20	4.87	1.10	1.02	0.12	0.37	0.03	11.0	98.5
GA-OLD-29-07	6.81	5.37	0.75	13.10	4.81	1.08	0.91	0.12	0.16	0.02	11.5	97.3
GA-OLD-31-07	13.75	4.67	0.93	1.93	7.03	2.92	0.57	0.12	0.10	0.12	11.2	99.8
GA-OLD-36-07	6.64	4.06	0.79	12.80	4.22	1.46	0.65	0.12	0.17	0.03	17.0	100.5
GA-OLD-37-07	9.31	5.80	1.93	8.12	4.88	1.96	1.04	0.13	0.28	0.06	14.4	100.5
GA-OLD-38-07	9.29	5.78	2.37	8.01	4.75	1.84	1.04	0.13	0.39	0.06	14.2	100.0

Appendix 2: continued

Sample #	Al2O3	Fe2O3	CaO	MgO	Na2O	K2O	TiO2	MnO	P2O5	BaO	LOI	Total
GA-OLD-40-07	8.80	5.19	2.44	8.46	4.45	1.80	0.92	0.10	0.69	0.05	16.8	101.0
GA-OLD-41-07	10.15	5.84	2.47	6.87	4.78	1.93	1.02	0.13	0.48	0.06	15.4	101.5
GA-OLD-42-07	10.70	6.31	2.32	6.56	4.87	1.87	1.06	0.13	0.30	0.06	13.0	100.5
GA-OLD-43-07	10.95	5.57	2.27	5.64	5.13	1.84	1.04	0.11	0.28	0.06	12.9	97.5
GA-OLD-44-07	11.50	5.84	2.09	4.85	5.17	1.86	1.02	0.09	0.26	0.06	14.6	99.6
EB-Chem-19	7.28	5.11	1.60	12.60	4.02	2.42	0.91	0.11	0.11	0.05	11.0	99.6
EB-Chem-18	5.14	4.48	0.60	15.20	3.76	2.38	0.77	0.10	0.09	0.03	13.1	99.0
EB-Chem-17	4.62	3.98	1.31	17.05	3.71	1.88	0.67	0.11	0.17	0.05	11.4	99.2
EB-Chem-16	4.95	3.63	2.78	16.65	3.75	1.51	0.60	0.10	0.32	0.04	13.2	100.0
EB-Chem-15	5.39	4.73	1.63	16.45	3.75	0.99	0.82	0.22	0.45	0.05	11.6	99.6
EB-Chem-14	4.84	4.40	1.02	16.40	3.72	0.83	0.71	0.15	0.39	0.03	13.7	98.9
EB-Chem-13	5.73	6.25	1.28	13.40	4.00	0.93	0.95	0.12	0.33	0.03	12.9	98.8
EB-12	4.57	3.90	0.49	15.45	3.59	1.02	0.83	0.35	0.14	0.08	17.6	99.0
EB-11	4.93	3.97	0.28	14.65	3.66	0.94	0.51	0.16	0.12	0.04	19.0	99.5
EB-Chem-12	5.97	5.38	0.88	15.35	3.45	1.84	0.90	0.19	0.41	0.04	13.0	98.0
EB-Chem-11	6.08	5.58	0.70	15.90	3.40	2.09	0.99	0.18	0.25	0.04	13.5	99.6
EB-Chem-10	5.97	5.51	1.16	15.60	3.32	2.14	0.92	0.23	0.48	0.05	13.3	99.2
EB-Chem-9	6.49	5.28	0.71	15.65	3.48	2.01	0.90	0.19	0.23	0.03	12.1	99.2
EB-Chem-8	5.91	4.80	7.58	12.85	2.88	1.99	0.75	0.22	0.32	0.06	14.6	98.1
EB-Chem-7	5.25	3.76	17.60	9.05	2.60	1.47	0.66	0.21	0.38	0.06	20.1	98.0
EB-Chem-6	6.04	5.59	3.18	10.75	3.59	1.18	1.18	0.19	0.90	0.06	20.2	101.0
EB-Chem-5	8.09	4.21	2.61	9.39	4.19	1.38	0.69	0.17	0.89	0.08	16.8	99.9
EB-Chem-4	8.50	4.86	1.64	9.06	4.25	1.24	0.85	0.12	0.28	0.06	17.1	100.0
EB-2	12.60	5.52	1.71	3.05	5.76	2.05	0.73	0.13	0.15	0.09	17.4	101.0
EB-50	15.30	5.70	4.03	1.59	6.53	1.67	1.52	0.13	0.27	0.11	9.6	99.9

Appendix 2: continued

Sample #	Al2O3	Fe2O3	CaO	MgO	Na2O	K2O	TiO2	MnO	P2O5	BaO	LOI	Total
EB-Chem-36	10.10	7.42	3.16	7.10	3.88	3.07	1.41	0.21	0.44	0.12	11.7	101.0
EB-Chem-35	7.69	5.47	3.09	10.05	3.28	2.34	1.04	0.15	1.44	0.08	12.0	96.0
EB-Chem-34	6.43	2.67	0.21	15.95	3.28	0.93	0.36	0.11	0.06	0.02	14.6	96.3
EB-Chem-33	6.40	3.45	0.55	15.70	3.14	1.49	0.55	0.12	0.16	0.03	14.5	99.8
EB-Chem-32	6.33	3.92	0.75	14.25	3.06	1.79	0.69	0.14	0.24	0.04	14.8	99.1
EB-Chem-31	7.38	4.73	0.39	12.60	2.97	2.14	0.71	0.26	0.18	0.05	15.7	99.3
EB-Chem-30	7.64	5.23	0.53	12.65	3.09	2.17	0.72	0.36	0.22	0.07	15.6	99.9
EB-Chem-29	8.01	4.98	0.59	11.35	3.03	2.20	0.75	0.34	0.22	0.07	15.0	95.3
EB-Chem-28	8.54	5.37	0.41	11.20	3.08	2.56	0.77	0.19	0.16	0.05	16.2	100.5
EB-Chem-27	9.69	6.15	1.49	9.24	3.69	2.34	0.88	0.12	0.58	0.06	13.4	101.5
EB-Chem-23	8.90	6.04	0.92	9.94	3.18	2.16	0.87	0.12	0.38	0.05	14.5	98.1
EB-Chem-22	9.97	5.73	1.03	8.98	3.64	2.35	0.91	0.12	0.35	0.05	11.8	99.6
EB-Chem-21	10.05	6.10	1.00	9.37	3.60	2.05	0.91	0.11	0.30	0.05	12.5	99.7
EB-Chem-20	10.10	5.60	1.07	8.65	3.55	2.16	0.92	0.11	0.31	0.05	12.8	98.8
EB-Chem-39	11.25	6.03	3.44	5.91	4.17	2.46	1.03	0.15	0.45	0.28	11.3	99.1
EB-Chem-40	11.40	6.04	2.23	5.59	4.33	2.55	1.04	0.15	0.45	0.12	11.7	97.3
EB-Chem-38	12.35	6.13	2.70	4.17	4.65	2.50	1.05	0.12	0.42	0.12	12.0	98.1
EB-Chem-37	12.30	6.29	2.58	4.34	4.62	2.43	1.13	0.16	0.46	0.12	12.0	99.0
EB-29	13.70	6.05	1.27	2.77	5.41	2.39	0.92	0.10	0.13	0.10	13.9	100.5
GA-37-99	4.55	3.26	18.05	8.92	1.79	3.31	0.53	0.08	0.08	0.03	23.1	99.4
GA-47-99	6.05	5.69	7.50	10.75	2.20	4.54	0.74	0.08	0.08	0.02	15.9	98.0
46-A12	15.74	6.29	0.63	3.93	8.26	1.99	0.75	0.22	0.20			94.01

CURRICULUM VITAE

Emily J. Beverly

Education

Ph.D.	2012-2015	Ph.D. Candidate, Baylor University, Advisor: Steven G. Driese
M.S.	2012	Rutgers University, Paleoenvironmental and paleoclimatic reconstruction of a Pleistocene catena using paleopedology and geochemistry of lake margin paleo-Vertisols, Olduvai Gorge, Tanzania, Advisor: Gail M. Ashley.
B.A.	2008	Trinity University, Provenance Analysis of the Cretaceous Hornbrook Formation of northern California and southern Oregon, Advisor: Kathleen D. Surpless.

Professional Experience

2008-2009	Research Technologist, Department of Earth, Materials, and Planetary Science, Southwest Research Institute, San Antonio, TX

Publications

Surpless, K.D. and **Beverly, E.J.**, 2011, Understanding a critical link in Cretaceous Cordilleran paleogeography: Detailed provenance of the Hornbrook Formation, Oregon and California, GSA Bulletin (submitted).